# BIOPHYSICAL DETERMINANTS OF NOTCH SIGNALING

by

Jeongsup Shim

A dissertation submitted in partial fulfillment
of the requirements for the degree of
Doctor of Philosophy
(Biomedical Engineering)
in The University of Michigan
2009

Doctoral Committee:

Associate Professor Alan J. Hunt, Co-Chair
John B. Lowe, Genentech, Inc., Co-Chair
Professor Jennifer J. Linderman
Professor Sean Morrison

To my family

Acknowledgements

First, I would like to thank my mentor, Dr. John B. Lowe. I am grateful that he gave me the opportunity to perform my graduate work in his lab and he supported my efforts to finish my project. I followed him to relocate from Ann Arbor to Cleveland, and now to South San Francisco. These moves were very unusual for a graduate student with one mentor. However, I really enjoyed this trip, although sometimes this was challenging. From this, I have learned how to do science and how to work with other people. Also, I am grateful to my thesis committee, Dr. Alan J. Hunt, Dr. Sean J. Morrison, and Dr. Jennifer Linderman for their interest and their helpful comment for my study.

Second, I thank the past and present members of Lowe's lab, specially Bronia Petryniak, Jay Myers, David Yao, and Dr. Yunfang Man. They gave me helpful comments and suggestions on my project and had a good time in Cleveland, where my study started to bloom. Specially, Bronia has been supporting my project from Ann Arbor to Cleveland, and finally to South San Francisco. Without her help, I could not have finish my work. David Yao was a good friend who enhanced my lab life in Cleveland.

Third, I would like to thank the following people who contribute to my project: Dr. Henry T. Scheck, III and David Lorch at the University of Michigan for the use of Optical Tweezers, Dr. Nolan Holland at Cleveland State University for helping with AFM experiments, Dr. Satya Yadav at the Cleveland Clinic Foundation for the SPR training and data analysis, Dr. Lino Gonzalez at Genentech, Inc. for the helpful

suggestions regarding the use of the single chain ligands for the better SPR data analysis, which was very critical to this study, Dr. Robert S. Haltiwanger and Nadia A. Rana at Stony Brook University, Dr. Rod Keck, George (Tony) Moreno and Louisette Basa at Genentech, Inc. for the mass spectrometry analysis, Dr. Phil Hass at Genentech, Inc. for the helpful comments related to the protein purification.

Fourth, I thank Dr. Shuichi Takayama, Maria Steele, Kristin Romelhardt, and Sandra Staneff in the Department of Biomedical Engineering for their support during my graduate study.

Fifth, I would like to thank all the members of the Korean Bible Church of Ann Arbor, Korean-American Presbyterian Church of Cleveland, and San Jose Korean Presbyterian Church. I am indebted for their prayers and kind care for my family and me.

Lastly, I'd like to thank my family. My wife, Heewon witnessed my graduate study and has supported me with love and prayer. During my graduate study, I got married to her and moved together from Ann Arbor to Cleveland and later to the Bay area. During this time, my father passed away after battling with cancer for 4 months, while our son, Devin and our daughter, Ellie were born. From all of these experiences, I matured and learned what the life is and how to live. My father and mother gave me endless love, care and support. When I heard my father's death, that loss was the saddest thing in my life. If he lived now, he might be pleased and proud of his son more than anyone else. I would like to thank to my in-laws. I am indebted to their prayer and the support to finish my degree. I thank God for everything and all the spiritual people who have taught me that the man's chief end is to glorify God, and to enjoy him forever.

Table of Contents

List of Figures

List of Appendices

Appendix

List of Abbreviations

ADAM	A disintegrin and metalloprotease
AFM	Atomic Force Microscopy
APC	Antigen-presenting cell
ASCII	American Standard Code for Information Interchange
ATCC	American Type Culture Collection
BCCP	Biotin carboxyl carrier protein
BM	Bone Marrow
CHO	Chinese Hamster Ovary
CL17	Clone 17
Dll	Delta-like
DN	Double Negative
DNA	Deoxyribonucleic acid
DOS	Delta and OSM-11-like proteins
DP	Double Positive
DSL	Delta, Serrate, LAG-2 motif
ECN	Extracellular domain of Notch
EDTA	Ethylenediamine tetraactic acid
EGF	Epidermal Growth Factor
EGFP	Enhanced Green Fluorescence Protein
ELISA	Enzyme-Linked Immuno Sorbent Assay
ER	Endoplasmic Reticulum
FACS	Fluorescence-activated cell sorting
FCS	Fetal Calf Serum
Fuc	Fucose
FUT	Fucosyltransferase
FX	3,5 epimerase/4-reductase
GalNAc	N-acetylgalactosamine
GDP	Guanosine Diphosphate
GMD	GDP-mannose 4,6-dehydratase
HEK	Human Embryonic Kidney
HES	Hairy and enhancer of split
hIgG	Human Immunoglobulin G
HSC	Hematopoietic Stem Cell
ICN	Intracellular domain of Notch
LSK	Lin-,Sca1+,c-kit+
MS	Mass Spectrometry
NA	Numerial Aperature
NHS	N-hydroxysuccinimide
Notch EC	Notch extracellular domain

Notch IC	Notch intracellular domain
NRR	Negative regulatory region
NTM	Notch Transmembrane domain
Ofut1	*O*-fucosyltransferase 1
Ofut2	*O*-fucosyltransferase 2
OTs	Optical Tweezers
PCR	Polymerase Chain Reaction
PEG	Poly(ethylene) Glycol
Pofut1	Protein *O*-fucosyltransferase 1
Pofut2	Protein *O*-fucosyltransferase 2
SA	Streptavidin
SPR	Surface Plasmon Resonance
TCR	T-cell receptor
Tris	tris(hydroxymethyl)aminomethane
WLC	Worm-Like Chain Model

Abstract

Notch signaling is involved in many biological contexts such as cancer, stem cell development, and neural cell development. Because of the importance of Notch function in health and disease, the Notch signaling pathway has emerged as a potential therapeutic target.

Mammalian Notch receptors are single-pass transmembrane glycoprotein receptors, which contain 29-36 EGF like repeats. The fucosyltransferase termed Pofut1 transfers fucose to the serine or threonine residue of the *O*-fucosylation consensus sequence on some EGF domains of Notch receptors. The glycosyltransferases termed Fringe can elongate *O*-fucose moieties by adding N-acetylglucosamine, which may be subsequently modified by galactose and sialic acid. These *O*-fucosylated glycans play key roles in modulating Notch-mediated signal transduction events.

Here, we have observed how *O*-fucosylated glycan modifications modulate Notch receptor-ligand interactions using surface plasmon resonance techniques. A biphasic binding and dissociation pattern was observed, suggesting a two-state receptor-ligand interaction model characterized by initial formation of a transient receptor-ligand complex followed by a conformational change that leads to a more stable receptor-ligand complex. Primary and secondary on and off-rates for the four binding-competent Notch1-Notch ligand pairs were observed to be distinct and characteristic for each Notch ligand. The overall association constants observed when Dll-1 or Dll-4 interacted with

Fringe-modified Notch1 were significantly greater than when these ligands interacted with unmodified Notch1, with enhancement likely due to Fringe modifications of fucose moieties within EGF domains 16-36. By contrast, Fringe modification of Notch1 did not significantly modulate interactions with Jag-1 or Jag-2. Mutational analyses confirm prior observations that the *O*-fucosylation site within EGF repeat 12 dictates much, if not all of the binding between Notch1 and its ligands. Finally, we observe that Fringe modification of Dll-4 enhances its ability to bind to Notch1.

Our data reveal that the molecular basis of glycan-dependent Notch-Notch ligand binding. We propose a two-state binding model with triple stranded structure for Notch-Notch ligand complex arrangement. Here, *O*-fucosylation and Fringe modification of Notch receptors play a key role in both the binding and the conformational change.

Chapter 1

Introduction

Carbohydrates are inevitable components for life. They are involved in the storage and transport of energy and in the immunity, fertilization, pathogenesis, blood clotting, and development [1].

Monosaccharides are the basic units of carbohydrates and the building blocks of bi- and polysaccharides. Free monosacchardes can exist in open chain or ring forms. Ring forms of the monosaccharides can be linked together via glycosidic bonds to form polysaccharides or oligosaccharides (or glycans).

Mammalian cells synthesize various glycans which are covalently linked to proteins and/or lipids [2]. The surfaces of most types of cells are heavily coated with these glycans, giving rise to the so-called glycocalyx (Figure 1-1). The glycocalyx is composed of the oligosaccharide side chains of glycolipids and integral membrane glycoproteins and the polysaccharide chains on integral membrane proteoglycans. A glycoprotein is a glycoconjugate containing usually *N*- or *O*-glycans which are covalently linked to a polypetide backbone [3]. The glycosaminoglycans are present as free polysaccharides or as part of proteoglycans. A glycosphingolipid (often called glycolipid) is a polysaccharide usually attached via glucose or galactose to the terminal hydroxyl group of the lipid moiety.

The common classes of glycans are defined according to the nature of the linkage

(core) regions to protein or lipid [1]. N-glycans (N-(Asn)-linked oligosaccharides) are polysaccharides covalently linked to an asparagine residue of the consensus sequence Asn-X-Ser.Thr, where X can be any amino acid besides Pro and Asp. N-glycans can be generally subdivided into three main classes: high-mannose type, complex type, and hybrid type. *O*-glycans (*O*-(Ser/Thr)-linked oligosaccharides) are typically connected via N-acetylgalactosamine (GalNAc) to a serine or threonine residue. Other types of *O*-linked glycans exist such as *O*-GlcNAc, *O*-mannose, *O*-glucose, and *O*-fucose.

Several human disease states are charaterized by changes in glycan biosynthesis and degradation that can be of diagnostic and/or therapeutic significance: Leukocyte adhesion deficiency II (LADII) [4] , carbohydrate-deficiency glycoprotein syndromes (CDGS) [5], mucopolysaccharidosis (MPS) [6], congenital dyserythropietic anemia type II (CDAII/HEMPAS) [7, 8], and galactosemia [9]. In the tumor environment, changes in glycosylation are associated with the pathogenesis of cancer, and are implicated in the tumor progression, including tumor cell proliferation, dissociation and invasion, adhesion and metastasis, and angiogenesis [10].

Although glycans play an important role in a variety of biological events, it has been difficult to elucidate the structure and the function of glycans in the living system due to the complexity and diversity of glycans and the lack of tools [1]. Glycans may be one of the most complex entities in nature. The complexity of the "glycome" exceeds the complexity of the proteome as a result of the enormous structural diversity of glycans and is further complicated by the combination and interaction of carbohydrates with each other and with proteins. Recently, new technologies to explore the structure of glycan have opened up a new frontier for glycomics and glycobiology [11, 12] and the

importance of glycobiology has been recognized in biotechnology and medicine [13-15].

Fucosylated Glycans

L-fucose (6-deoxy-L-galactose) is a monosaccharide that is commonly found in many glycan structures in mammals. Lack of a hydroxyl group on the carbon at the 6-positon (C-6) and the L-configuration distinguish fucose from other six-carbon sugars present in mammalian cells.

Various fucosylated glycan structures have been identified. Fucosylated glycans are synthesized by fucosyltransferases in the Golgi or ER (Figure 1-2). Thus far, thirteen fucosyltransferases have been identified in mammals. The *FUT1* and *FUT2* loci encocde $\alpha(1,2)$-fucosyltransferases [16, 17]. The *FUT3* locus encodes an $\alpha(1,4)$-fucosyltransferases and the *FUT4-FUT7* and *FUT9* loci encode $\alpha(1,3)$-fucosyltransferases responsible for synthesis of the Lewis[x] and sialyl Lewis[x] antigens [18]. The *FUT8* locus encodes an $\alpha(1,6)$-fucosyltransferase that adds fucose to asparagine-linked GlcNAc moieties [19]. The *Pofut1* and *Pofut2* loci encode *O*-fucosylatransferases that add fucose directly to serine/threonine residue of only a few proteins. Pofut1 modifies Epidermal Growth Factor-like (EGF) repeats of Notch receptors, Notch ligands, and Cripto [20, 21] and Pofut2 modifies thrombospondin type 1 repeats [22]. The large number of fucosyltransferases and the structural diversity of their products imply an important role for fucose in biology. It has been suggested that Pofut1 and Pofut2 reside in ER [23], although an ER-specific fucose transporter gene has not yet been identified. *FUT10* and *FUT11* are the putative $\alpha(1,3)$-fucosyltransferase loci, which have been identified in the human genome by comparison with fucosylatransferase

3

sequences in the *Drosophila* genome [24]. However, no enzymatic activity has yet been assigned to these hypothetical proteins.

GDP-fucose is used as a donor substrate by all fucosyltransferases in the synthesis of fucose-containing glycoconjugates [25]. Two pathways have been known to synthesize GDP-fucose in the cytosol of mammalian cells. These are termed the de novo pathway and the salvage pathway (Figure 1-3) [26]. The de novo pathway utilizes two enzymes, GDP-mannose 4,6-dehydratease (GMD) and the FX protein (GDP-4-keto-6-deoxy-D-mannose-3,5-epimerase-4-reductase) to convert GDP-mannose to GDP-fucose [27-29]. GDP-fucose is then transported into Golgi lumen or ER where it is utilized as a fucosyltransferase substrate. Smith *et al.* [30] created a mouse lacking the *FX* locus (FX$^{-/-}$ mice). These mice lack all forms of fucosylation and do not survive long after birth unless fucose is added to their diet. A salvage pathway that elaborates GDP-fucose [25] allows GDP-fucose biosynthesis to be rescued by exogenous fucose, thereby restoring fucosylation.

Roles for fucosylated glycans have been investigated in a variety of biological contexts [31, 32]. Well-studied fucosylated glycans include the molecules of the ABO and Lewis blood group systems [33], host-microbe interactions [34, 35], and selectin dependent leukocyte adhesion [36-41]. In the glycan structures relevant to these systems, fucose mainly exists as a terminal modification of glycan structures. Recently, glycosyltransferases capable of adding sugars to *O*-fucose have been found. These are termed the Fringe family of enzymes, which act on fucose that modifies some EGF repeats [21, 42] and one or more β(1,3)-glucosyltransferases which act on fucose moieties that modify thrombospondin type 1 repeats [43]. *O*-fucosylated glycans are

4

involved in cell signaling events during a variety of development processes [21, 42]. Notch receptors, Notch ligands, the Cripto receptors, and urokinase type plasminogen activator are glycoprotein receptors that have *O*-fucosylated glycans critical to development [20, 22]. Especially, Notch receptors are of interest because inactivation of *O*-fucose modulator, Pofut1 results in a failure of embryonic development, and dysfunction of Notch signaling [44].

Glycan-dependent Notch Signaling

Notch receptors are single-pass transmembrane glycoprotein receptors essential to cell fate determination in a wide array of developmental processes [45-47]. Inactivation of the mouse *Notch1* gene did not cause gross developmental anomalies, but did yield delayed and disorganized somitogenesis that resulted in embryonic lethality around day 10 of gestation [48-50]. Defects in Notch function caused by mutations in genes encoding Notch receptors or their ligands cause or are strongly associated with a variety of diseases [51] such as several forms of cancer [52-54] including T cell acute lymphoblastic leukemia (T-ALL) [55], tumor angiogenesis [56], Cerebral Autosomal Dominant Arteriopathy with Sub-cortical Infarcts and Leukoencephalopathy (CADASIL) [57, 58], multiple sclerosis [59], spondylocostal dysostosis (SCD) [60], Alagille syndrome [61], and congenital heart defects [62]. Because of the importance of Notch function in health and disease, Notch signaling pathway has emerged as a potential therapeutic target [63, 64].

Notch was originally discovered in *Drosophila*. Four homologues have now been identified in mammals [46].   These are termed Notch1 (N1), Notch2 (N2), Notch3 (N3),

5

and Notch4 (N4) (Figure 1-4). Notch receptors are synthesized in ER, where Notch is *O*-fucosylated. Further, Notch receptors are proteolytically processed during transport to the cell surface by a furin-like protease in Golgi apparatus (at site S1), producing an extracellular Notch (ECN) subunit and a Notch transmembrane (NTM) subunit. These two subunits, which remain non-covalently associated, constitute the mature heterodimeric cell-surface receptor.

Notch receptors are activated when the ECD interacts with ligands on adjacent cells. Notch ligands were first identified in *Drosophila* and are called Delta and Serrate. Multiple homologues of each are present in mammals where the Serrate homologues are called Jagged. Five Notch ligands have now been identified in mammals. These are termed Jagged1, Jagged2, Delta-like1, Delta-like3, and Delta-like4 (Figure 1-4). Each of the ligands is a single-pass transmembrane protein with a conserved N-terminal Delta, Serrate, LAG-2 (DSL) motif essential for binding to Notch. Jagged contains a cysteine-rich region, but the exact mechanism of how the cysteine-rich region modulates Notch signaling is not known, although it was suggested that this region is required for activation of Notch signaling in *Xenopus* primary neurogenesis [65].

Activation by ligand triggers a series of proteolytic cleavages of the NTM that release the ICN from the membrane. The NTM subunit is released by at least two sequential proteolytic cleavages (at site S2 and S3). The ICN then translocates to the cell nucleus, ultimately resulting in transcriptional regulation of developmental control genes such as Hes1 (Figure 1-5).

Notch receptors are heavily glycosylated with *N*-glycans [66, 67] and *O*-glycans such as *O*-fucose [21, 42, 44, 68], *O*-glucose [69-71], and possibly *O*-GlcNAc [72]. *O*-

glucosylation and *O*-fucosylation regulate Notch folding, trafficking, and signaling although these post-translational modifications are very unusual [25, 44]. *O*-glucosylation of Notch receptor was first discovered in a biochemical study of mouse Notch1 [71]. *O*-glucose attaches to serine between the first and second cysteine residues of EGF repeats within the consensus sequence C_1XSXPC_2 [70, 71]. The *O*-glucosylated glycan forms the trisaccharide EGF-*O*-α1Glcβ1,3Xylβ1,3Xyl [71]. However, the biological role of *O*-glucosylation on Notch receptors was not known until recently. Drosophila gene, *rumi*, when mutated, yields a Notch loss of function phenotype, and has been found to be a protein *O*-glucosyltransferase [69]. Although loss of *rumi* does not reduce cell surface Notch expression or binding of Notch to Delta, Notch signaling was inhibited due to the loss of the S2 proteolytic cleavage, which is essential for Notch activation. The biological relevance of *rumi* to mammalian systems remains to be determined.

O-fucosylation of EGF repeats is catalyzed by *Pofut1*. *Pofut1* adds GDP-fucose to specific serine or threonine residues on certain EGF-like repeats, including some found within Notch receptors. *Pofut1* is thought to be essential for Notch function [73]. The recent demonstration that *Pofut1* is localized to the endoplasmic reticulum (ER), where it may function in quality control or possibly even as a molecular chaperone raises the possibility that specific *O*-fucosylation sites may be necessary for the processing and maturation of the Notch receptor [23, 74].

The glycosylatransferases of the Fringe family modify *O*-linked fucose with GlcNAc. The *Fringe* locus was originally identified during a *Drosophila* mutant screen for genes involved in dorsal-ventral boundary formation during wing development.

Drosophila Fringe (Dfng) and its mammalian homologues, Radical (Rfng), Lunatic (Lfing), and Manic Fringe (Mfng), play key roles in developmental processes by modifying some *O*-fucosylated glycan structures [75] and may decorate the different sites within Notch EGF repeats [76, 77]. They subsequently play different roles in the physiological Notch signaling [78]. Fringe catalyses elongation of *O*-linked fucose on EGF repeats by the addition of a β1,3-GlcNAc, which is required for Notch signaling in mammalian cells [79]. Subsequent steps are addition of a β1,4-Gal followed by addition of an α2,3-sialic acid moiety. This glycosylation of the extracelluar Notch (ECN) subunit of Notch with Sia-α2,3-Gal-β1,4-GlcNAc-β1,3-α1-*O*-Ser/Thr, takes place during maturation in the Golgi apparatus (Figure 1-6). A function of the secreted form of Fringe has not yet been assigned [80].

It has been reported that controlled post-translational variation of the glycosylation patterns of ECN subunits by Fringe glycosyltransferases can alter the responsiveness of Notch receptors to different ligands [81]. For example, Fringe differentially modulates Jagged1 and Delta1 signaling through the Notch receptor [82-84]. Mechanisms to account for this observation remained to be defined.

There exist some discrepancies regarding the role of the Fringe enzymes and their cognate glycans in ligand binding. It remains unclear whether Fringe molecules and their cognate glycans directly modulate the binding affinity of ligands to Notch, and/or other aspects of the ligand-receptor interaction (i.e by changing the conformation of Notch, or by causing Notch receptor clustering or repulsion in the plane of the cell membrane). To more precisely reveal the influence of Fringe on the receptor-ligand binding, the characteristics of the binding properties between Notch and its ligands should be

quantified as a function of whether Notch is modified by each of the Fringe enzymes.

Evaluation of the role of *O*-fucose at various sites is essential to dissect the mechanism by which these sugars affect Notch function. Although multiple EGF domains are thought to be involved in Notch binding to the ligands, the ligand binding region (EGF 11-12) and the *Abruptex* region (EGF 24-29) are of interest for Notch binding and signaling [85, 86]. For example, there is evidence in *Drosophila* that ligand interaction with EGF 24-29 in the *Abruptex* region is required for Notch signaling. Mutation of distinct *O*-fucosylation sites within the binding region or the *Abruptex* region results in changes in Notch binding and signaling. Mutation of the *O*-fucosylation site in Notch1 EGF repeat 12 abrogated Notch downstream signaling, while mutation of the *O*-fucosylation site in Notch EGF 26 enhanced Notch signaling [87]. Moreover, three *O*-fucosylation sites in EGF 12, 26, and 27 are highly conserved in all known Notch homologues within 36 EGF repeats. This observation suggests that these three sites are biologically relevant *O*-fucosylation sites for Notch-ligand binding and signaling.

In mammalian Notch signaling, mutation of the *O*-fucosylation site in EGF repeat 12 of Notch1 resulted in loss of signaling by Delta1 and Jagged1, while mutation of the *O*-fucosylation site in EGF repeat 26 resulted in hyperactive signaling in response to Delta1 and Jagged1 interaction. Mutation of the *O*-fucosylation site in EGF repeat 27 resulted in faulty trafficking of the Notch receptor to the cell surface and decreased S1 processing of the receptor [87]. However, it is not clear why the *O*-fucosylation site in EGF 26 enhances the Notch signaling.

Biophysical Microenvironment in Notch Signaling

The biophysical "microenvironment" where Notch and its ligands contribute to Notch signaling, including an external pulling force generated by trans-endocytosis of the extracellular domain of Notch, and a physical configuration formed by clustering of Notch and its ligands have been implicated in controlling the strength of Notch signals. Specifically, it has been reported that endocytosis of Notch ligands is required for Notch signaling [88-90]. Two broad models have been suggested to elucidate the contribution of endocytosis in Notch activation [91]. The first model proposes that endocytosis facilitates S2 cleavage and then removes the ECN, or vice versa. In this case, endocytosis contributes an external pulling force to pull the ECN "away from" the surface of the receiving cell. The second model proposes that a Notch ligand undergoes endocytosis and the re-trafficking to the cell surface, where it is presented as the active and commonly clustered form of the ligand. However, is it not yet clear whether either mechanism contributes to Notch activation.

It has been reported that Notch is not activated by either monomeric or dimeric ligand in solution, whereas Notch signaling is induced when the ligands are immobilized or pre-clustered [92]. Also, it has been observed that the density of the Notch ligand Delta1 determines development of B and T cell precursors from hematopoietic stem cells [93]. Studies with *Drosophila* have demonstrated that the biological consequence of Notch signaling depends on the strength of the Notch signal. For example, half the wild-type level of Notch gene dosage is insufficient to properly specify the dorsoventral margin of a wing, giving rise to the eponymous "notched wing" phenotype [94]. These

results imply that a critical threshold of Notch signaling is required for inducing different cell-fate outcomes.

It is not yet known if the density of Notch ligands (perhaps controlled by endocytosis) modulate the cell surface clustering of Notch receptors and thus modulate Notch signal transduction strength. Similarly, it is not known if Notch molecules are evenly distributed over the surface of the cell, or aggregated at distinct positions on the cell surface, perhaps as a function of the state of *O*-glycosylation of Notch receptors, which could in turn modulate the strength of Notch signaling in response to Notch ligands.

A consideration of the interactions between cell surface glycans and cell surface lectins [95, 96] suggests the possibility that Notch signaling may be facilitated by *O*-fucose-linked glycan-dependent control of receptor clustering.

Techniques to Study the Glycan Structure and Protein-Glycan Interactions

Mass Spectrometry is a powerful tool in the study of glycan structure because of its sensitivity of detection and ability to analyze complex mixtures of glycans derived from a variety of organisms and cell lines [11, 97]. Mass spectrometry is an analytical technique that identifies the chemical composition of a compound or sample on the basis of the mass-to-charge ratio of charged particles. A mass spectrometer creates charged particles (ions) from molecules. It then analyzes those ions to provide information about the molecular weight of the compound and its chemical structure. The three essential functions of a mass spectrometry, and the associated components, are the ionizer, the ion

analyzer, and the detector. There are many types of mass spectrometry techniques and sample introduction techniques that allow a wide range of analyses. The Haltiwanger group has successfully used MS analysis to identify *O*-linked modifications on EGF like repeats of Notch receptor [97-99], where the glycan structure and the peptide sequence modified with *O*-fucose in Notch receptors were identified from the LC-MS/MS spectrum. Using MS, they identified only *N*-acetylglucosamine added onto Notch in the presence of Fringe in *Drosophila* S2 cells. This result argues against models in which subsequent modifications after Fringe is required for the Notch binding and signaling and instead establish that the simple addition of GlcNAc is necessary and sufficient for *Drosophila* Notch-ligand binding [99].

In my thesis work, I have used MS to identify the glycan structure of Notch1 receptor with various glycosylation status.

To study the protein-glycan binding, several methods have been used [100, 101], including X-ray crystallography, NMR spectoscopy, equilibrium dialysis, affinity chromatography, titration calorimetry, ELISA-type assays, IC_{50}-hapten inhibition, precipitation, electrophoresis, optical tweezers (OTs), atomic force microscopy (AFM) and surface plasmon resonance (SPR). In my thesis work, I have used OTs, AFM, and SPR to investigate glycan mediated Notch-Notch ligand binding events.

OTs use the optical trap in the optical microscope with high numerical aperture (NA) to exert very small forces (0–100 pN) against molecules or materials interacting weakly with the bead (Figure 1-7). The bead is visualized in the optical trap, and the substrate or a second bead to which it is bound is moved relative to the trap position. By

varying the force exerted on the optically trapped bead, one can determine the force necessary to break the bonds. Although force-distance profiles cannot be measured accurately using OT, OTs—because of their sensitivity—have been used to measure the force-extension profiles of soft, entropic springs such as titin [102], as well as the force-velocity relationships of molecular motors [103-108].

AFM uses a micro-fabricated cantilever with a very low spring constant (>1 pN/nm) (Figure 1-7). This instrument has been used extensively to image soft biological materials with a lateral resolution of ±1 nm [109]. For the force measurement of protein-protein binding, proteins of interest are coated on the cantilever tip and the surface of mica or glass as well. The cantilever tip is brought into the surface and makes contact. After this contact, the cantilever is retracted to break the bond. During this event, the position of a laser beam reflected off the cantilever surface tracks the relative movements of the probe within ±0.1 nm and records the spring deflection. With the known spring constant of the cantilever, the rupture force can be calculated by Hooke's law ($F=kx$). Recently, AFM has been combined with various visualizing techniques such as time-resolved fluorescence microscopy [110] to image the lateral structure of different lipid bilayers and their morphological changes as a function of time and combined OTs and AFM [111] to probe fluorescence-labeled receptor clusters in the cell membrane via force spectroscopy using antibody-functionalized tips.

SPR is a powerful tool to observe the protein-protein binding. As shown in Figure 1-8, at an interface between two transparent media of different refractive index (glass and water), light coming from the side of higher refractive index is partly reflected and partly

13

refracted. Above a certain critical angle of incidence, no light is refracted across the interface, and total internal reflection is observed. While incident light is totally reflected the electromagnetic field component penetrates a short (tens of nanometers) distance into a medium of a lower refractive index, creating an exponentially attenuating evanescent wave. If the interface between the media is coated with a thin layer of metal (gold), and light is monochromatic and p-polarized, the intensity of the reflected light is reduced at a specific incident angle producing a sharp shadow (called surface plasmon resonance) due to the resonance energy transfer between the evanescent wave and surface plasmons. The resonance conditions are influenced by the material adsorbed onto the thin metal film. A satisfactory linear relationship is found between resonance energy and mass concentration of biochemically relevant molecules such as proteins, sugars and DNA. The SPR signal which is expressed in resonance units is therefore a measure of mass concentration at the sensor chip surface. This means that the analyte and ligand association and dissociation can be observed and ultimately rate constants as well as equilibrium constants can be calculated.

SPR experiments offer several advantages for the verification and study of protein–protein interactions. The main advantages are that very small amounts of sample are needed (mg or sub-mg may suffice), and that no labeling is required. In addition, the method can provide information not only on affinities but also on the rates of association and dissociation with very high resolution in real time, which can be equally important in biology.

Protein *O*-fucosyltransferase 1 and Fringe modulate ligand binding and Notch signaling [21, 44]. The role of *O*-fucose and the Fringe action in *O*-fucosylation sites has been extensively investigated [73, 87, 112]. Although it has been known that Fringe differentially modulates Jagged/Serrate and Delta signaling through the Notch receptor by increasing Delta signaling and reducing Jagged/Serrate signaling [82], it remains unclear how *O*-linked glycan structures change the Notch-ligand binding affinity and/or kinetics. Chapter 2 describes the construction and characterization of reagents including recombinant cDNA and proteins that I have used to characterize Notch-ligand binding affinity and kinetics. Chapter 3 describes the advantages and disadvantages of the usage of OTs to study Notch-ligand binding. Chapter 4 summarizes experiments where I probed ligand binding forces between Notch and its ligands at a single molecule level using AFM to investigate how the glycans influence the interaction of Notch1 with its ligands. Chapter 5 will summarize my experiments using SPR to characterize the kinetics of Notch-ligand interactions, as a function of the state of glycosylation of both Notch and Notch ligands, and as a function of mutations at key *O*-fucosylation sites. Chapter 6 will summarize my conclusions from these studies, will place these in the context of proposals about Notch-ligand interactions from the literature, and will provide a perspective on future experimental directions that are suggested from our studies.

A

glycocalyx   cytosol   nucleus   plasma membrane

200 nm

B

transmembrane glycoprotein   adsorbed glycoprotein   transmembrane proteoglycan

● = sugar residue

cell coat (glycocalyx)

glycolipid

lipid bilayer

CYTOSOL
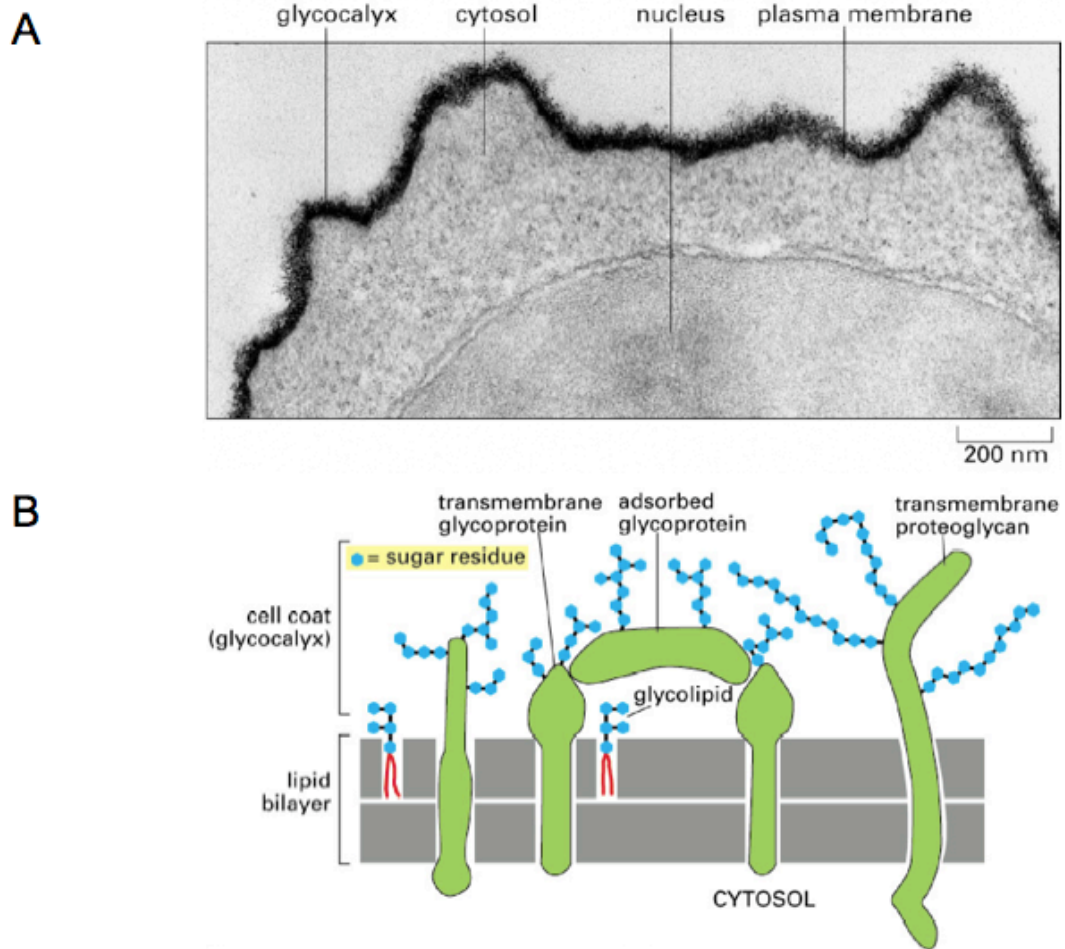
Figure 1-1. Glycocalyx and simplified diagram of glycocalyx. A. Scanning electron microscopic analysis of the surface of a lymphocyte stained with ruthenium red. B. The glycocalyx is made up of the oligosaccharide side chains of glycolipids and integral membrane glycoproteins and the the polysaccharide chains on integral membrane proteoglycans. (Adapted from Molecular Biology of the Cell [2])

Figure 1-2. Fucosylated glycans in mammals. Structures of selected fucosylated glycans are shown here, N=number of genes. (From Dr. John Lowe)
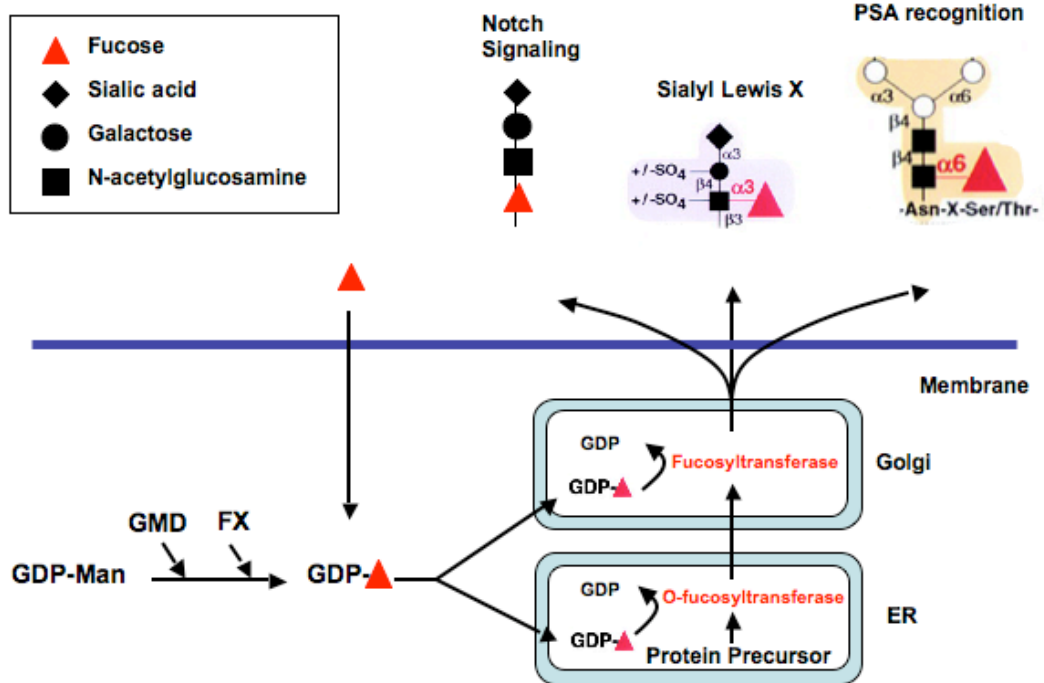
Figure 1-3. Fucosylation pathways in mammals. Two different cytosolic pathways lead to the formation of GDP–fucose. The constitutively active *de novo* pathway converts GDP–mannose into GDP–fucose via oxidation, epimerization, and reduction catalyzed by two enzymes (GMD and FX). The salvage pathway initiates with free fucose, delivered to the cytosol from extracellular sources (shown) or from intracellular (lysosomal) sources (not depicted). GDP–fucose from this pathway is then transported into the Golgi lumen or ER. Most of the fucosyltransferases are resident in Golgi, while *O*-fucosyltransferases in ER. Fucosylation with other glycosylation events lead to the synthesis of cell surface glycoconjugates with structures (highlighted in color) that contribute to Notch signaling [21], selectin recognition [113], or to binding by pea lectin (PSA). Modified from Fig. 1 in [30].
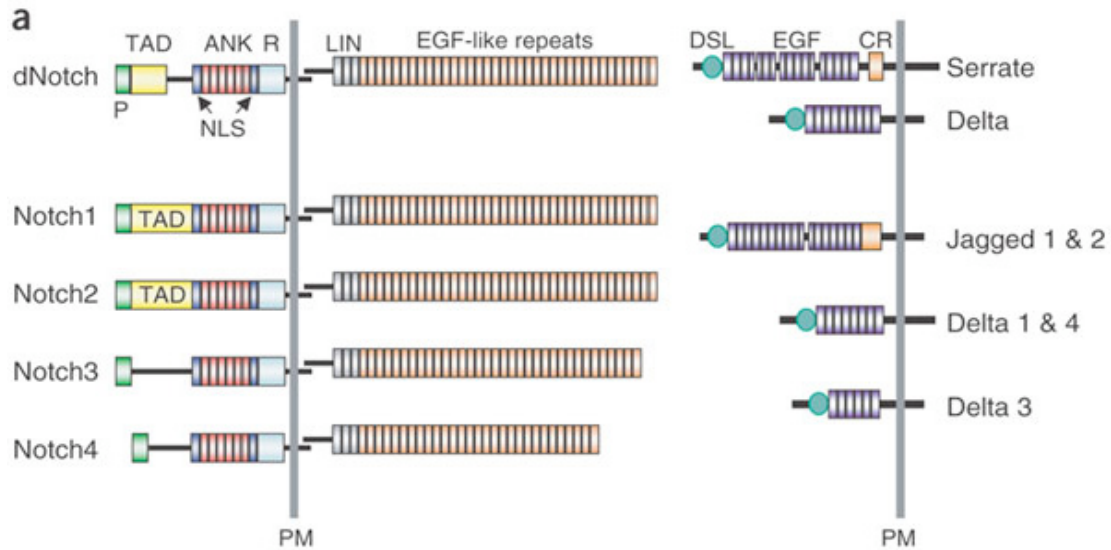
Figure 1-4. Notch receptor and ligands. The *Drosophila* genome encodes one Notch receptor (dNotch), whereas the mammalian genome encodes four (Notch1−Notch4). The extracellular domains contain EGF-like repeats (36 in dNotch, Notch1 and Notch2; 34 in Notch3; 29 in Notch4) associated with ligand binding and three cysteine-rich Notch/LIN12 repeats (LIN) that prevent ligand-independent signaling. The cytoplasmic portion contains two protein-protein interaction domains, the RAM domain (R), six ankyrin (ANK) repeats, two nuclear localization signals (NLS), a transactivation domain (TAD, absent from Notch3 and Notch4) and a PEST sequence (P). dNotch can be activated by two transmembrane-bound ligands, Serrate and Delta, whereas the mammalian Notch receptors (Notch1−Notch4) are activated by five ligands (Jagged1 and Jagged2, homologs of Serrate; and Delta1, Delta3 and Delta4, homologs of Delta). The common structural feature of Notch ligands is an N-terminal domain, DSL (Delta, Serrate and Lag). A cysteine-rich (CR) domain is located downstream of the EGF-like repeats in Serrate, Jagged1 and Jagged2. PM, plasma membrane. (Adapted from Radtke et al., Nat Immunol, 2004)
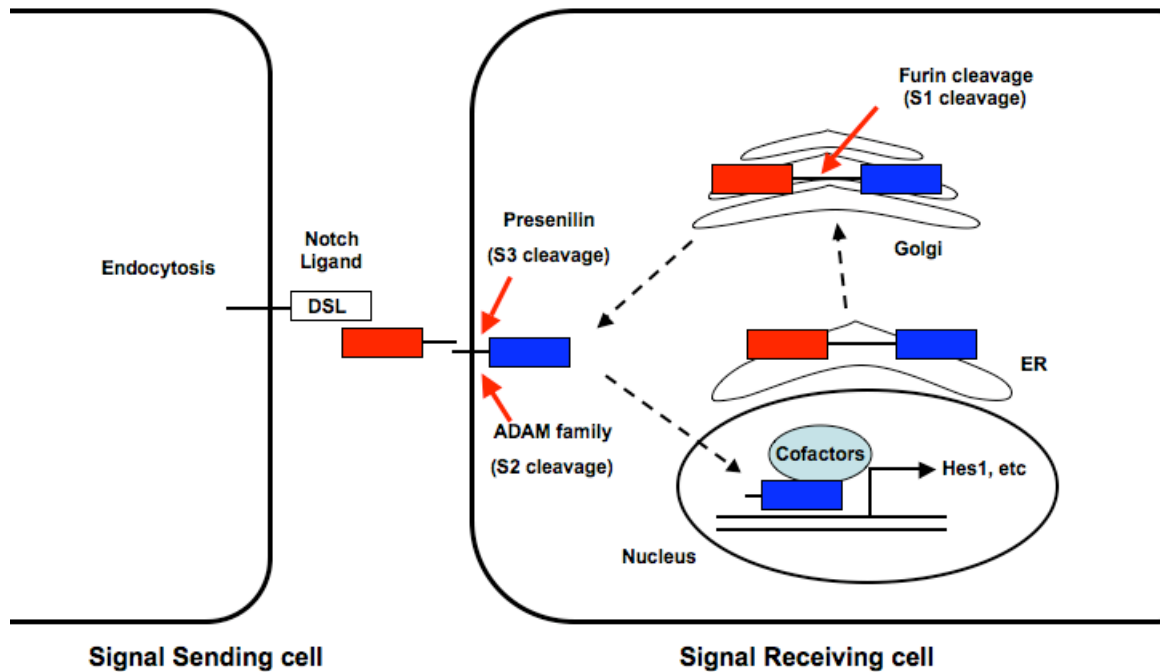
Figure 1-5. Central biochemical events in Notch signaling. Notch receptors are synthesized in ER, where Notch is *O*-fucosylated. Further, Notch receptors are proteolytically processed during transport to the cell surface by a furin-like protease in Golgi apparatus (at site S1), producing an extracellular Notch (ECN) subunit and a Notch transmembrane (NTM) subunit. Notch receptors are activated when the ECD interacts with DSL ligands on adjacent cells. Activation by ligand triggers a series of proteolytic cleavages of the NTM that release the ICN from the membrane. Endocytosis is required in this step. The NTM subunit is released by at least two sequential proteolytic cleavages (at site S2 and S3). The ICN then translocates to the cell nucleus, ultimately resulting in regulation of developmental control genes such as Hes1.
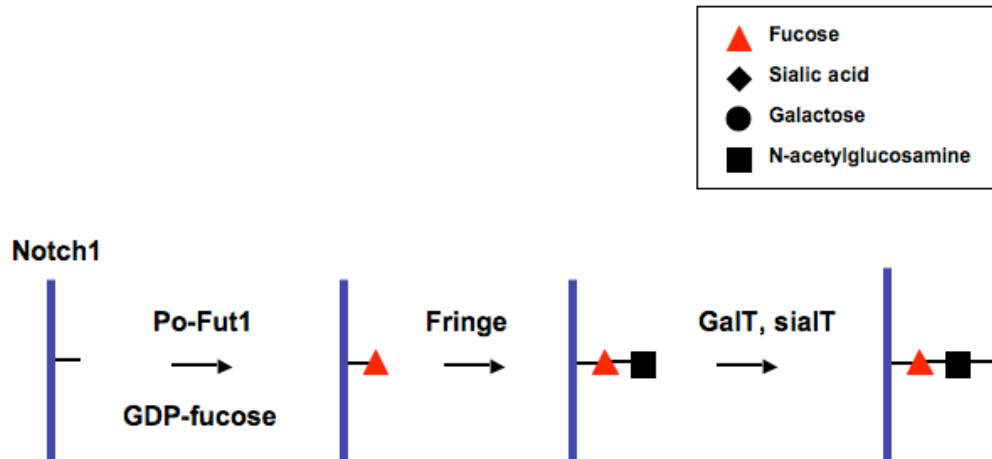
Figure 1-6. _O_-fucosylated glycan in Notch receptor. In mammals, _Pofut1_ adds GDP-fucose on _O_-fucosylation sites of Notch EGF repeats containing _O_-fucosylation consensus sequence. Fringe catalyses elongation of _O_-linked fucose (triangle) on EGF repeats by the addition of β 1,3-GlcNAc (square). Subsequent steps are addition of a β 1,4-galactose (circle) followed by addition of an α 2,3-sialic acid (diamond), through the actions of specific β1,4galactosyltransferase and α2,3sialyltransferase activities .
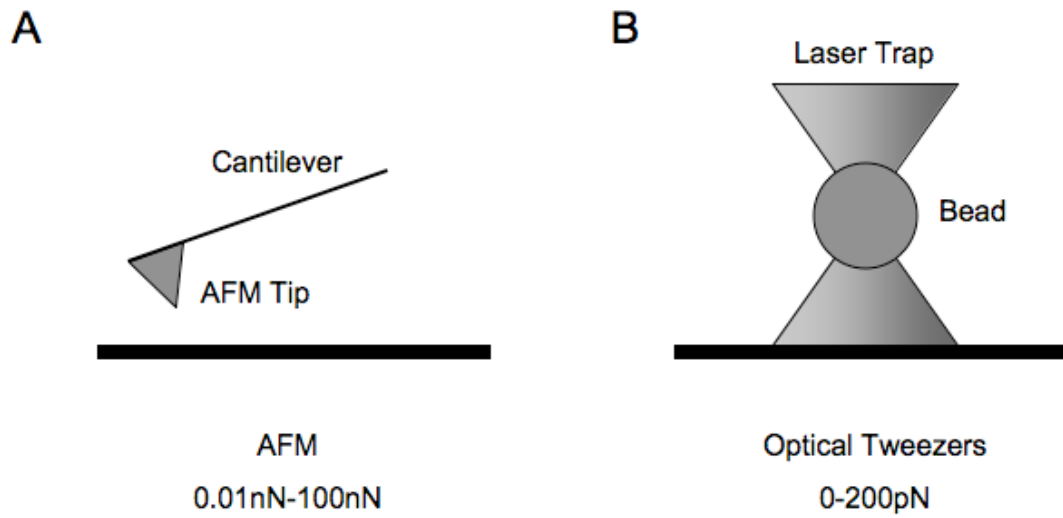
Figure 1-7. Force probes. (A) The atomic force microscope, showing the probe tip attached to the cantilever force transducer. (B) Optical tweezers. The bead is held in the optical trap, and the radiation pressure exerted on the bead opposes adhesive contacts between materials on the bead and surface.
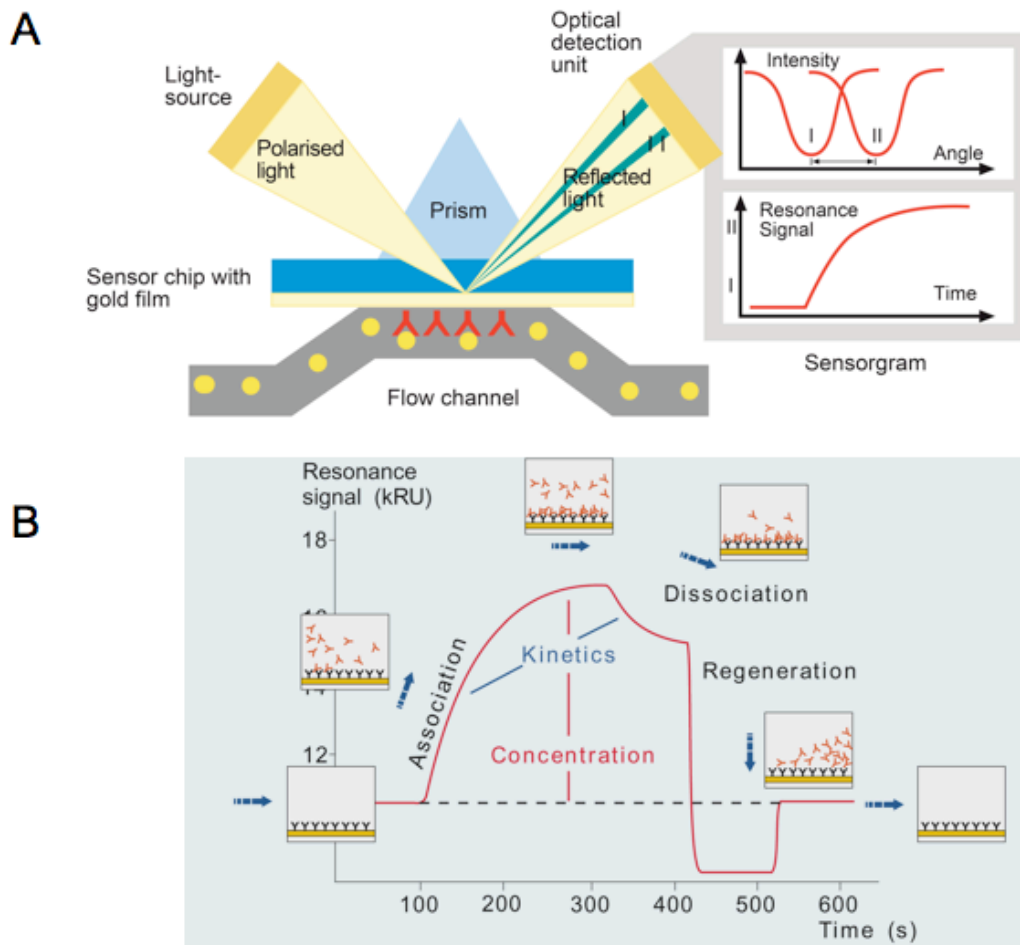
Figure 1-8. The basic principles of SPR analysis. (A) SPR uses a physical phenomenon known as total internal reflection. As light from the light source shines on the sensor chip, it is reflected at a specific angle (angle I). The identity of the transmitted angle depends on the refractive index of the material close to the non-illuminated side of the gold surface, where the binding reaction takes place. As an analyte is injected into the flow cell and binds to ligand on the surface, it causes a change in refractive index. Such a change will result in a shift in the angle I to angle II. The change in angle is recorded by the detector (top right graph) and is displayed on a computer screen in the form of a sensogram (bottom right graph). (B) A sensogram is a graphic representation of the signal generated during a binding cycle. Initially, there is no protein bound to the immobilized ligand surface and the signal is at baseline. As an analyte is injected over the surface, protein molecules will interact with the ligand, yielding the association rate of the complex. At the end of the injection, buffer flows over the surface to provide the dissociation rate of the complex. A regeneration reagent is used to remove any protein that remains bound after the dissociation step to bring the signal back to baseline. At this point another binding reaction can be initiated. (Adapted from Biacore, Inc. Website - www.biacore.com)

Chapter 2

Construction and Characterization of Reagents

Introduction

Notch receptors are glycoproteins which are heavily glycosylated with *O*-fucose [21, 42, 68], *O*-glucose [69, 70], *N*-glycans [23, 114], and possibly *O*-GlcNAc [72]. *O*-fucose is added to the *O*-fucosylation site of some EGF repeats of Notch receptors by *Pofut1* in ER and *O*-fucose is extended with GlcNAc by Fringe. This *O*-fucose-GlcNAc is elongated more by galactose and sialic acid. *O*-glucose is extended by two xyloses [115]. The structure of *N*-glycan that modifies Notch receptors is not well studied, and little is known about the *O*-GlcNAc modification of Notch family members, beyond the fact that this modification is present.

O-fucosylation and Fringe modification of mouse Notch1 receptors are of interest because many *in vivo* and in vitro experiments suggest that *O*-fucosylation and subsequent modification is critical in Notch signaling. To study the role of *O*-fucosylated glycans on Notch receptors, it has proven useful to arrange to be able to precisely control *O*-fucosylation of Notch. Two approaches have been used to control *O*-fucosylation of Notch in mammalian cells. One is to control the synthesis of the fucosyltransferase

substrate GDP-fucose and another is to knock out the fucosyltransferase, including especially *Pofut1*.

(i) Control of global GDP-fucose synthesis

Two pathways for the synthesis of GDP-fucose have been described in mammalian cells. The constitutively active de novo biosynthetic pathway converts GDP-mannose into GDP-fucose via oxidation, epimerization, and reduction catalyzed by two enzymes (GMD and FX) (Figure 1-3, [25]). The salvage pathway initiates with free fucose, delivered to the cytosol from extracellular sources or from intracellular (lysosomal) sources (not depicted in Figure 1-3). GDP-fucose from this pathway is then transported into the Golgi lumen or ER for the further process.

Several fucosylation deficient cell lines have been established: Lec13 cell lines and CL17 cell lines. GMD enzymes are mutated in Lec13 cells [28, 116, 117] and FX genes mutated in CL17 cells [118]. In these two cell lines, the *de novo* fucosylation pathway is deficient, but the salvage pathway is intact. Therefore, fucosylation can be controlled by adding exogenous fucose to the culture medium, which then enables GDP-fucose synthesis through the salvage pathway.

(ii) *Pofut1* knock-out

Pofut1 transfers *O*-fucose to EGF repeats of Notch in the ER [119]. To study the role of *O*-fucose in Notch signaling, the *Pofut1* locus has been genetically deleted. Mouse embryos lacking Pofut1 die at midgestation, and exhibit severe defects in somitogenesis,

vasculogenesis, cardiogenesis, and neurogenesis [44]. This phenotype is similar to Notch signaling deficient phenotype in mouse [48, 49, 120].

Drosophila Ofut1 is proposed to act as both a chaperone to promote the Notch receptor folding and a protein *O*-fucosyltransferase to add fucose in EGF repeats of Notch receptors [74]. By contrast, it has been reported that mammalian Notch receptors are expressed at wild type levels on the cell surface in the absence of Pofut1 and *O*-fucose, but exhibit reduced binding of Notch ligands and reduced ligand-induced Notch signaling [73]. The apparent discrepancy between the consequences of Ofut1 deficiency in Drosophila and in mammals remains unresolved, and whether mammalian Pofut1 contributes to Notch protein folding and expression is still controversial.

This Chapter will summarize the soluble Notch1 and Notch ligands that were used in Notch-ligand binding experiments described in later chapters. Notch1 receptors were chosen among four Notch receptors because of the importance of Notch1 receptors in many physiological situations including T cell commitment in vivo [121, 122]. This Chapter will also summarize experiments that were done to characterize Lec13, CL17 and CL17/Lfng cells, and their ability to support O-fucosylation of mNotch1. Finally, this Chapter will report on the results of MS analysis done to analyze the glycan structure of soluble mNotch1 expressed from CL17 cells.

Methods

Bir A enzyme cloning- The *BirA* locus (Gene Bank Number M10123) was cloned with the primers (5'-CCC AAG CTT AAG GAT AAC ACC GTG CCA CTG AAA TTG ATT G-

3' and 5'-GCA GAT ATC TTA TTT TTC TGC ACT ACG CAG GGA TAT TTC ACC-3') from genomic DNA of *E. coli* XL10 strain. 10ul of 10mM MgCl$_2$ was additionally added to the *pfu* turbo PCR reaction (Invitrogen) to optimize the PCR reaction for the genomic DNA. The *BirA* locus was inserted using the *HindIII* and *EcoRV* restriction sites into pSecTag2/HygroB expression vector (Invitrogen). This vector includes a c-Myc epitope and a polyhistidine tag "downstream" from the site where the *BirA* locus was cloned. However, the BirA insert was constructed to include a stop codon at its 3' end, so the c-Myc epitope and polyhistidine tag which are included in pSecTag2/HygroB will not be expressed. BirA expressed by the pSecTag/HygroB-based vector was expressed with an amino-terminal Ig κ-chain leader sequence, which allowed it to biotinylate membrane and secreted proteins in mammalian hosts when those proteins include a BirA recognition motif [123].

Site-specific mono-biotinylation system- Soluble Notch1 and Notch ligands were fused with c-Myc tag and biotinylation tag (bioin-tag). The c-Myc tag sequence used in this study was EQKLISEEDL and biotin tag sequence is AGGLNDIFEAQKIEWHEDTGGS. The overall sequence is EQKLISEEDL (c-Myc)-TGG-AGG LND IFE AQK IEW HED TGG S (biotin tag)–TAA (stop codon). This sequence was cloned between the BamHI and XbaI sites of the vector. The primers used for the tag are 5'-/Phos/GAT CCC GAA CAA AAA CTC ATC TCA GAA GAG GAT CTG ACT GGC GGA GCT GGC GGA CTT AAT GAT ATT TTT GAA GCC CAG AAG ATT GAA TGG CAT GAA GAC ACT GGT GGC TCT TAA T-3' and 5'-/Phos/CTA GAT TAA GAG CCA CCA GTG TCT TCA TGC CAT TCA ATC TTC TGG GCT TCA AAA ATA TCA TTA AGT CCG

CCA GCT CCG CCA GTC AGA TCC TCT TCT GAG ATG AGT TTT TGT TCG G-3'.

These two primers were annealed to make a double stranded DNA fragment. 5μl of 5' primer (5μg), 5μl of 3' primer (5μg), 8μl of water, and 2μl of 10x annealing (1M NaCl, 0.1M Tris-HCl (pH 7.8), 1mM EDTA) buffer were mixed and heated in boiling water for 5 minutes. The mixture then cooled to room temperature overnight.

To test this site-specific mono-biotinylation system, the extracelluar domain of DLL1 (M^1-H^{535}) was appended to the c-Myc-biotin tag in pcDNA1. For the control, lysine target for biotinylation in the biotin tag sequence was mutated to an alanine residue to assess the monospecificity of the biotinylation system.

Generation of soluble form of mouse Notch1- Soluble mNotch1 fragments comprised of EGF 1 through 15 (M^1-E^{606}) or EGF 1 through 36 (M^1-T^{1633}) were generated from full-length mNotch1 (Gene Bank Number NM 008714) by PCR. These fragments were fused in-frame to a c-Myc tag sequence and the biotin-tag sequence in expression vectors pcDNA1 (Invitrogen) to make soluble mNotch1 with EGF 1 to15   (Notch1(15)-c-Myc-biotin-tag) and with EGF 1 to 36 (Notch1-c-Myc-biotin-tag).

3xFlag was cloned from p3xFlag-CMV-8 (Invitrogen) with the primers, 5'-CCG CTC GAG CCG TCA GAA TTA ATT CAC CAT GTC TGC ACT TC-3' and 5'-GAT CTA TCG ATG AAT TCG CGG CCG CAA G-3', creating XhoI and NotI restriction sites. This 3xFlag sequence has its own signal peptide from the original vector, allowing the removal of the signal peptide from the wild type mNotch1 sequence. By mutagenesis, a NotI restriction site was generated between the DNA sequence corresponding to amino acid residues G^{52} and G^{59}. After removing the DNA segment corresponding to the signal

peptide from the wild type mNotch1 between the XhoI and NotI sites, the 3xFlag tag sequence was fused in-frame to the N-terminus of mNotch1 to create the 3xFlag-Notch1(36)-c-Myc-biotin tag sequence.

For mass spectroscopy analysis, c-Myc and polyhistidine (6xHis) tags were fused to soluble mNotch1 with EGF 1 to 15 (Notch1(15)-myc-His$_6$) in pcDNA1.

Generation of soluble forms of mouse Notch ligands- Sequences encoding the transmembrane and cytoplasmic domain were deleted from full length mouse Notch ligands; Delta-like-1 (Gene Bank Number 007865), Delta-like-3 (Gene Bank Number 007866), Delta-like-4 (Gene Bank Number 019454), Jagged-1 (Gene Bank Number NM013822), and Jagged-2 (Gene Bank Number 010588). A c-Myc tag sequence and a polyhistidine sequence were fused in-frame to cDNAs encoding the extracellular domains of each of the Notch ligands (Dll-1 (M^1-H^{535}), Dll-3 (M^1-R^{468}), Dll-4 (M^1-P^{521}), Jag-1 (M^1-L^{1062}), and Jag-2 (M^1-T^{1068})) in expression vectors pcDNA1 (Invitrogen).

Dll-1-hIgG, Dll-4-hIgG, and Jag-1-hIgG fusion proteins were also constructed. A cell line stably transfected with a Jag-2-hIgG fusion protein was obtained as a gift from Dr. Bluel (Max-Planck Institute) [124]. As a negative control, a Dll4 fusion protein was constructed in which the DLS domain was inactivated by mutation, as described by Glittenberg et al [125]. Five residues with the DSL domain (KKRDD) were substituted with AAAAA. In brief, two fragments were constructed independently with the primer pairs DSL1 (5'-TTC TCG AGG CCA CCA TGA CGC CTG CGT CCC GGA GCG CCT G-3'; 5'-TTG AAT TCA GCA GCA GCA GCA GCG CAT AGG CGA GAA CAG CTC TCT CCA TAG TAG TTG-3') or DSL2 (5'-TTG AAT TCG GAC ATT ATG AGT GCC

AGC CAG ATG GCA GCC TG-3'; 5'-CGG GAT CCG GAA ACT CGC AGC GGC TGC CCA CAA AGC C-3') and digested with Xho1-EcoRI and EcoRI-BamH1, respectively. The fragments were fused together into c-Myc-His$_6$/pcDNA1 vector.

Generation of mutations in mouse Notch1- ll mutations in the expression vector used to generate recombinant soluble mNotch1 molecules were created using PCR-mediated site-directed mutagenesis with Notch1(36)-c-Myc-biotin tag in pcDNA1 as template. The mutagenesis primers were designed to generate mutations in *O*-fucosylation sites (serine/threonine to alanine) based on *O*-fucosylation consensus sequence, The mutagenic oligonucleotides used were 5'-CCA TGT CAG AAT GAT GCC GCT TGC CTG GAC CAG ATT G-3' for EGF 12, 5'-CTG CTT CAA TGG TGG TGC CTG TGT GGA TGG TAT CAA C-3' for EGF26, and 5'-CTG TCT GCA CGG TGG TGC CTG CCA AGA CAG CTA TG-3' for EGF27.   All mutations were confirmed by DNA sequencing.

Generation of Fringe expression vector- cDNAs expressing *Lfng* (Gene Bank Number NM 008494), *Mfng* (Gene Bank Number NM 00859), and *Rfng* gene (Gene Bank Number NM 009053) were subcloned into plasmid pZeoSV (Invitrogen) which is a constitutive mammalian expression vector encoding a resistant gene to the antibiotic Zeocin.

Stable transfection of lunatic fringe- To create a CHO cell line that stably expresses Lfng, the coding sequence of a Lfng cDNA was cloned proximal to the to sequence corresponding to c-Myc-His$_6$ in pcDNA1 used for soluble mNotch1 cDNA constructs.

Cloned Lfng fragment was constructed with primer pairs (5'-TTT AAG CTT GCC ACC ATG CTC CAG CGG TGC GGC CGG CGC C-3' and 5'GGA AGA TCT CCG AAG ATG GCG GAG CGA GGA CAC CAG GGT GTG TCT G-3').

The expression vector encoding Lfng (Lfng-myc-His$_6$/pcDNA1) was co-transfected into CL17 with pPUR (purimycin resistant gene) to achieve stable transfection. Puromycin resistant clones were selected for two weeks with 5μg/ml of puromycin. Lfng [30]expressing CL17 was obtained by probing his-tag fused to Lfng by western blotting.

Expression of soluble mouse Notch1 and Notch ligands- An FX null CHO cell line (CL17 cells) or a GMD null CHO cell line (Lec13 cells) was used to control the fucosylation of mNotch1, and Notch ligands, by modulating the synthesis of GDP-fucose using exogenous fucose in the culture media .

Expression vectors encoding the soluble mNotch1 or mNotch ligands (10μg/10cm dish) and BirA (1μg/10cm dish) were transiently transfected into CL17 cell lines with Lipofectamine 2000 using the manufacturer's protocol. The next day, the cells were transferred to 3x15cm dishes and the media was changed to the serum-free media (CD-CHO-A, Gibco) with 1% serum and 100μM biotin. To generate fucosylated proteins, 1mM fucose was added to the media. After 5 days, the supernatant was collected for the protein purification.

Expression of soluble Notch ligands- Expression vectors encoding the soluble Notch ligands (10μg/10cm dish) and BirA (1μg/10cm dish) were transiently transfected into

HEK 293T cell lines with Lipofectamine 2000 using the manufacturer's protocol. The next day, the cells were transferred to 1x15cm dishes and the media was changed to serum-free media (Hyclone). After 5 days, the supernatant was collected for protein purification.

Protein Purification- The collected cell culture supernatants were concentrated to 5ml using a Centricon-70 Filter unit (Millipore, MWCO 10K) and were brought up to 15ml with binding buffer (20mM Tris, 500mM NaCl, 20mM Imidazole). 1ml of Ni-NTA agarose beads (Invitrogen) were washed and added to the supernatant. Beads were washed 3 times with 8ml of the binding buffer. The beads were centrifuged at 1000g for 1 minute. Protein was eluted with elution buffer (20mM Tris, 500mM NaCl, 250mM Imidazole). Eluted protein was dialyzed 3 times with Dialysis Cassette (Pierce, MWCO 10K) in 10mM Hepes, 150mM NaCl, 1mM $CaCl_2$. Purified proteins were analyzed by silver staining and western blotting. Protein concentration was quantified by BCA method or OD280 measurement.

Surface expression of mouse Notch1 receptors in 3xFlag-Notch1/Lec13 cells using EDTA dissociation method- 3xFlag-Notch1/Lec13 and pcDNA1/Lec13 were suspended in $1x10^6$ cells. Cells were washed twice with ice cold HBSS with Ca^{2+} and Mg^{2+} followed by centrifugation and then wash with 1ml ice cold HBSS without Ca^{2+} and Mg^{2+}. Cells were pelleted by centrifugation at 400xg for 7 min and supernatant was discarded. Cells were re-suspended with 60 µl of 0.5mM EGTA in TBS pH 7.5 followed by incubation at 37°C for 15 min. EDTA treated cells were centrifuged 1 time at 400xg for 7 min.

Supernatants were transfered to clean 1.5 ml eppendorff tubes and spun again at 800xg for 7min. Clarified supernatant was transfered to fresh tubes containing 1μl of BSA at concentration 1mg/ml and 1ml of complete protease inhibitor with EDTA (Roche) 60x solution. Finally, EDTA supernatants containing EDTA labial cell protein were aliquot and snap frozen on dry ice.

Cell pellets were subjected to lysis with 60μl of RIPA buffer containing complete protease inhibitor cocktail. Total cell protein was separated from DNA by centrifugation at 4°C for 30 min at 14K. Aliquots of whole cell protein extracts were snap frozen on dry ice and were stored at -80°C.

For cell surface expression of mNotch1 total cell extract was examined for protein concentration with micro BCA protein assay kit (Pierce). Total cell extract 30μg/line or an equivalent of EDTA released protein were separated on 4-12% NuPAGE (Invitrogen) using MOPS electrophoresis buffer. Gels were transferred to PVDF blotting membrane. After 8hr of blocking with 5% non-fat dry milk, membranes were washed and probed with hamster anti human Notch1 8G10 antibody (Santa Cruz) at 1:200 dilution over night at 4°C. Detection antibody, goat anti hamster-HRP was used for 2hr at RT. After 5 washes, each blot was developed with ECL detection system (Amersham).

Surface expression of mouse Notch1 receptors in 3xFlag-Notch1/Lec13 cells using flow cytometry- 3xFlag-Notch1/Lec13 or pcDNA1/Lec13 were cultured in alpha-MEM with 10% dialyzed FCS without fucose at 37°C with 5% CO_2 for the routine maintenance. For fucose-dependent expression study of cell surface Notch1 and fucosylated glycoproteins, cells were cultured in duplicate plates. Fucose was added to one plate at 1mM for 48 hr

before staining on alpha-MEM cultured cells. Next day cells were trypsinized followed by centrifugation at 1200 RPM for 5 min. Cell pellets were re-suspended in CD-CHO-A media (Gibco) and were counted and centrifuged again followed by preparing cell suspension at concentration 0.5×10^6 in CD-CHO-A with or without 1mM Fucose. 2 ml of the cell suspension was plated in 35 mm tissue culture untreated dishes.

3xFlag-Notch1/Lec13 or pcDNA1/Lec13 cells cultured with or without fucose were passed through 40µM cell strainer. Antibody staining of the cells was carried out in V-bottom 96 well plates on ice. Cells were re-suspended in the staining media at 1×10^6 /ml and were dispensed into V-bottom 96 well plate (0.2×10^6 per well). Dispensed cells were centrifuged and cell pellets were re-suspended in the staining media (HBSS with 2mM $CaCl_2$, 1mg/ml BSA, and 0.1% NaN3) with 1: 200 dilution of Biotinylated anti-Flag or biotinylated control antibody (mouse IgG1) and FITC conjugate-PSA lectin at 1:800 or control PSA/100mM Mannose. After 30 minutes incubation cells were centrifuged followed by two washes and staining with Strepavidin-PE-conjugate at 1:400 for 20 minutes. PE conjugate of anti-Notch1 antibody was used at dilution 1:100. After final step of staining protocol, cells were washed twice with the staining media and were subjected to flow cytometry analysis on BD FACS with Cell Quest Software.

Mass Spectrometry Analysis- Mass spectral analysis of *O*-fucosylation sites was performed essentially as described [98, 99]. Briefly, 1 µg of N1(15)-IgG expressed in CL17 cells with or without fucose was reduced and alkylated, separated by SDS-PAGE, and subjected to in-gel tryptic digestion. The resulting peptides were analyzed by LC-MS/MS on an Agilent XCT Ion Trap mass spectrometer. Glycosylated peptides were

identified by searching MS/MS data for neutral losses of the GlcNAc-fucose disaccharide (349.1 Da). Loss of the disaccharide gave a characteristic fragmentation pattern allowing rapid identification of glycopeptides. The mass of the unglycosylated peptide was then matched to predicted masses of tryptic peptides from Notch containing the *O*-fucosylation consensus sequence:C^2XXXX(S/T)C^3, where C^2 and C^3 are the second and third conserved cysteines of an EGF domain. Once glycopeptides were identified, additional searches of the MS/MS data for the unmodified peptides were performed (Extracted Ion Searches). The extracted ion searches take advantage of the fact that glycosidic linkages are more labile than peptide bonds upon collision-induced dissociation (CID), and hence the major product ion from fragmentation of a glycopeptide is the unglycosylated peptide. Using this method, peptides bearing different forms of the *O*-fucosylated glycans (*e.g.* mono- or disaccharide) were found. No glycopeptides with tri- or tetrasaccharide forms of *O*-fucose were identified, nor, aside from *O*-glucose glycans (to be reported elsewhere) were any other modifications of *O*-fucose bearing peptides identified.

Results

Specificity of mono-biotinylation

To immobilize the proteins to a surface, as a means to enable measurement of protein-protein interactions, several methods have been suggested. Because streptavidin-biotin bond is the strongest known protein-mediated bond in nature, systems based on the strepavidin-biotin have been extensively used in the force-related study such as AFM [126, 127].

In the streptavidin-biotin system, one protein of interest is first biotinylated and then bound to streptavidin on a surface. A common biotinylation method uses amine coupling with NHS. This method biotinylates all lysines in a target protein.

In our in vitro binding studies, we wished to mimic the orientation of Notch and its ligands as presented, respectively, on the receiving cell and the sending cell. We were thus concerned about the "orientation" of the immobilized protein as it is bound to the solid surface, and thus sought to achieve site-specific biotinylation that would tether the COOH-terminal end of the protein to the solid surface. We thus developed a site-specific mono-biotinylation system as shown in Figure 2-2 and as outlined in Chapman-Smith and Cronan [128, 129]. This system uses the BirA enzyme to add biotin to lysine in the specific sequence. The *E. coli* biotin holoenzyme synthetase, BirA, catalyzes transfer of biotin to the epsilon amino group of a specific lysine residue of the biotin carboxyl carrier protein (BCCP) subunit of acetyl-CoA carboxylase. A 23 residue peptide has been defined as supporting the minimal substrate requirements for BirA-catalyzed biotinylation in vivo although the sequence of the peptide bears little resemblance to the biotinylated sequence in BCCP [130].   This the *in vivo* biotinylation system allows site-specific biotinylation without any exogenous reagents and eliminates possible inactivation of the protein of interest by nonspecific biotinylation that is typically achieved in vitro using chemical or enzymatic means. In order to biotinylate secreted proteins from mammalian cells, BirA needs to be present in the secretory pathway [123]. To achieve this, BirA was inserted into a mammalian expression vector designed to target the protein to the endoplasmic reticulum by fusion into the Igκ immunoglobulin secretory leader.

36

To evaluate the activity and specificity of this site-specific mono-biotinylation system, the secreted BirA (pSecBirA) was co-transfected into the HEK 293T cell lines along with the Dll-1-cmyc-biotin tag or a mutant of Dll-1-cmyc-biotin tag designed to be deficient in the BirA-dependent mono-biotinylation process (Figure 2-3A). In this mutant, the lysine that is the substrate for biotinylation within the biotinylation recognition site has been changed to alanine. The supernatants of these transfected cells were harvested and probed by Western blotting (Figure 2-3B). The wild type recombinant Dll-1-myc-biotin tag molecule is expressed as mono-biotinylated form, whereas the mutant is expressed but not biotinylated. These data indicate that the in vivo biotinylation system allows us to generate site-specific mono-biotinylated proteins.

Characterization of Lec13, CL17, and CL17/Lfng cell lines

FACS analysis with CSLEX-1, Northern blot analysis of FX transcript expression and western blotting analysis of FX protein expression had been used to characterize the CL17 cells in the previous study [118]. CL17 cells were generated from CHO-Tag cells, which stably express mouse polyoma large T antigen (TAg), with a cDNA encoding human fucosyltransferase III (FT3), an enzyme that directs synthesis of many $\alpha(1,3)$-fucosylated glycans including the sialyl Lewis^X epitope recognized by the monoclonal antibody CSLEX-1. CL17 cells lack the expression of sLe^X moiety when cultured in standard medium, as assessed by flow cytometry and staining with CSLEX-1. However, cells restored the capability of binding of CSLEX-1 in the presence of exogenous fucose, indicating that the fucose salvage pathway is intact in CL17 and thereby fucosylation defect is localized to the de novo pathway. Although the higher FX transcriptional level

was observed in CL17 cells, no detectable level of FX proteins was observed in western blotting. By sequencing the coding region of the FX cDNA from CL17 cells, insertion of a single G:C basepair at nucleotide position 838 was identified. This frameshift mutation would be expected to induce protein misfolding, which could lead to degradation during the protein synthesis process. It was confirmed that GDP-fucose was not synthesized in CL17 cells by paper chromatography.

In this work, the fucosylation-deficient cell lines, Lec13, CL17, and CL17/Lfng cells are further characterized by analyzing the fucosylated glycans. Two methods were used to characterize the fucosylated glycans: fucose specific antibody binding and Notch ligand (Dll-4) binding to Notch receptors containing fucosylated glycans.

CSLEX-1 and PSA staining to Lec13, CL17, and CL17/Lfng cells were performed to observe whether fucosylated glycan was present on the cell surface (Figure 2-4A and B). CSLEX-1 binds to CL17+fucose and CL17/Lfng+fucose, while no detectable level was observed from Lec13-fucose, Lec13+fucose, CL17-fucose, and CL17/Lfng-fucose. This result indicates that Lec13 does not have the full FT activity for the synthesis of sialyl Lewis^X epitope and in both cells, sialyl Lewis^X epitope is not fully produced in the culture without fucose. PSA binds to all three cell lines in the presence of fucose, while low level of binding was observed from the culture without fucose. These data suggest that Lec13, CL17, and CL17/Lfng cells are the fucosylation deficient in culture without fucose and can be used to control fucosylation. However, it is possible that a very low concentration of GDP-fucose is present in these three cell lines.

Dll-4 binding to Lec13 and CL17 was carried out using flow cytometry to see whether the exogenous fucose alters the binding to Notch receptors (Figure 2-4C).

Culture in the absence of exogenous fucose resulted in decreased binding to Dll-4, while Dll-4 binding to cells was enhanced with fucose in culture. These data suggest that the fucose may modulate Notch and Dll-4 binding, in part by regulating the surface expression of Notch receptors or by changing the affinity of Notch receptors to Dll-4, or both.

Surface Expression of mouse Notch1 receptors

To address the possibility that loss of fucosylation decreases the surface expression of Notch receptors, EDTA dissociation and FACS analysis were performed (Figure 2-5). Because of lack of anti-Notch antibody, 3xFlag tagged mouse Notch1 receptors was stably transfected in fucosylation deficient Lec13 cells. Since the Notch receptor is a heterodimer associated with a calcum-dependent ionic bond, therefore the ECD can be dissociated with EDTA treatment. To observe the expression of 3xFlag-Notch1 receptors inside the cells, whole cell extracts were probed with anti-mouse Notch antibody (8G10). The same amount of 3xFlag Notch1 was detected and no band was seen in vector control. However, a lesser amount of 3xFlag Notch1 was detected in the culture without fucose compared to the culture with fucose. This data demonstrate that loss of fucosylation decreases the surface expression of Notch1 receptors.

To directly observe Notch1 receptors on the cell surface, FACS analysis was carried out with anti-Flag antibody to detect Flag tag on Notch1 receptors Figure 2-6. To monitor the fucosylated glycans on 3xFlag-Notch1 receptors in Lec13 cells, PSA staining was performed. We observed that PSA binding is restored in the presence of fucose, while PSA binding is significantly reduced in the absence of fucose. To detect the surface

expression of 3xFlag-Notch1, anti-Flag staining was done. Notch1 was expressed when cultured in the presence of fucose, while the surface expression of Notch1 was significantly reduced in the absence of fucose. Together, loss of fucosylation reduces the surface expression of Notch receptors.

Mass Spectrometry Analysis of mouse Notch1

Our results left open the possibility that very low level of fucose is present in the fucosylated glycans on Lec13 and CL17 cell in the fucose depleted culture. To address this possibility, we analyzed tryptic peptides derived from mouse Notch1 by tandem mass spectrometry (LC-MS/MS). To investigate the *O*-fucosylation on the EGF repeats of mouse Notch1 receptors, two soluble mouse Notch1 peptides expressed from CL17 were analyzed: Notch1(15)-hIgG-fucose and Notch1(15)-hIgG+fucose.

Figure 2-7 shows spectra from Notch1(15)-hIgG+fucose. In Figure 2-7A, both the MS (*top panel*) and MS/MS (*bottom panel*) spectra show the ion from EGF3 containing an *O*-fucosylation site. The *top panel* shows that the MS spectrum contains the *O*-fucosylated peptide (*m/z* 866.5) that corresponds to the doubly charged form of a peptide modified with an *O*-fucose monosaccharide. The MS/MS spectrum of the CID-induced fragmentation of this ion is shown in the *bottom panel*. Fragmentation leads to the loss of a dHex (fucose) (resulting in *m/z* 793.5 ion). Because the glycosidic linkages are significantly more susceptible to CID than peptide bonds, the major product of fragmentation is the deglycosylated peptide [99]. The ion at m/z 866.5 corresponds to the predicted mass for the doubly charged form of a tryptic peptide containing an *O*-fucosylation consensus sequence from EGF 3: [113]NGGTCDLLTLTEYK[126]. These data

confirm the presence of the peptide bearing *O*-fucose. Figure 2-7B shows a search of the entire chromatogram for the amount of this ion (*m/z* 866.5) compared to the same peptide without the *O*-fucose (*m/z* 793.5). While the ion corresponding to the *O*-fucosylated peptide (plotted in red) can be easily seen, the naked peptide (plotted in black) cannot. Thus, in this sample, this peptide appears to be fully glycosylated.

Figure 2-8 contains the spectra from Notch1(15)-fucose generated in CL17 cells without fucose. Figure 2-8A shows MS (*top panel*) and MS/MS spectra (*middle and bottom panel*) of the same peptide from EGF3. The *middle panel* is the MS/MS spectrum of the *O*-fucosylated peptide (*m/z* 866.5), and the *bottom panel* is the MS/MS spectrum of the naked peptide (*m/z* 793.5). Figure 2-8B shows a search of the chromatograms for the relative amounts of these two peptides. Again, the most abundant species is the *O*-fucosylated peptide (in red), while a small amount of naked peptide (in black) can be seen. The bottom line is that the majority of what we see in both samples is the *O*-fucosylated peptide. There is a small increase in non-fucosylated peptide in the Notch1(15)-fucose sample.

Taken together, this result demonstrates that CL17 cells have low level of GDP-fucose in the culture medium (0.5-1% serum) in the absence of fucose and may modify the fucosylated glycans of glycoproteins such as Notch1 receptors.

Discussion

To study glycan-dependent Notch binding and signaling, precise control of glycosylation is critical. Using fucosylation-deficient CL17 cells, soluble mouse Notch1 receptors with different glycosylation statuses were obtained and the fucosylated glycan structure was analyzed by MS. With MS analysis, some level of fucose was found in

soluble mNotch1 secreted from CL17 cells cultured in the absence of fucose, while soluble mNotch1 synthesized by cells grown in the presence of fucose was fully fucosylated.

There are several ways to explain how fucose can occur in EGF repeats of Notch1 expressed in CL17 without exogenous fucose. We raise five possibilities; (1) free fucose may exist in serum, (2) fucosylated protein may exist in serum and may be endocytosed and catabolized by cells to release fucose, which can then feed the salvage pathway, (3) mutated GMD or FX may have enzyme activity to some extent, (4) Pofut1 may have a high affinity compared to other fucosyltransferases and may use very low levels of GDP-fucose presence in the absence of exogenous fucose, (5) an unknown GDP-fucose synthetic pathway may exist that is distinct from the *de novo* pathway and the salvage pathways.

To test hypothesis (1) and (2), SPR analysis was performed for mNotch1 grown with regular serum and dialyzed serum (free fucose might be removed by dialysis.). SPR analysis shows that mNotch1 from both serums does not bind to Dll-4 (data not shown). This indicates that free fucose in the serum (if any) has no effect on Notch binding to ligand, although mass spectrometry needs to be completed on both samples to help support this conclusion.

Serum can contain fucose as the free form and/or the fucosylated form on the proteins. The free form of fucose can be removed by dialysis. However, the fucosylated form on the glycoprotein in serum is not possible to remove by dialysis. We propose that fucosylated proteins in serum maybe the only external source of fucose.

To quantify the fucosylation level of Lec13 and CL17 cells, soluble mNotch1 was collected from both cell lines and we carried out a SPR binding experiment with Dll-4. Although Lec13 cells have a very low expression level of soluble mNotch1 in the absence of fucose, the binding kinetics and affinity of mNotch1 from Lec13 are identical with those of mNotch1 from CL17 (data not shown). These data suggested that Lec13 and CL17 have a very low level of GDP-fucose as suggested in Kanda et al. [131]. In Lec13 cells, 3% of GDP-fucose was found in cytoplasm compared to wild type CHO cells even though these cells were grown in dialyzed serum [131]. Later, the Satoh group reported that they established fucose-free cell lines [132], but fucosylation of Notch receptor was not tested. In addition, granulocytes from FX(-/-) mice had very low level of PSA binding, while no binding was observed to E-selectin and P-selectin binding [30]. It demonstrated that each FT has a different affinity in the extremely low concentration of GDP-fucose in the cytoplasm. Pofut1 may have a very high affinity for GDP-fucose, compared to other FTs, and may be able to fucosylated Notch even in the presence of very low concentrations of GDP-fucose. This is relevant because Drosophila Ofut1 has a chaperone activity and mammalian Pofut1 is resident in the ER [23], the place of protein synthesis. For proper folding, one or more specific *O*-fucosylation sites may serve as the "regulatory checkpoint" for the processing of Notch receptors. However, the affinity of Pofut1 to each EGF repeats of Notch and the *O*-fucosylation sites that serve as the "regulatory checkpoint" need to be unveiled.

An unknown fucosylation pathway can be involved in the processing of the Notch proteins. In GMD mutated CHO/DS44 cells, no detectable intracellular GDP-fucose was

observed using a sensitive HPLC-based detection system [131]. Therefore, the existence of an unknown fucosylation pathway is unlikely.

Together, expression of Notch receptor is susceptible to the concentration of GDP-fucose in the cytoplasm. This implies that Lec13 and CL17 have the capability to transfer GDP-fucose to the EGF repeats of Notch receptors with very high affinity in an extremely low concentration of GDP-fucose and in the extremity, Notch receptors would not be expressed in the cultures with absolutely no GDP-fucose, at least, in mammalian CHO cell lines.

This possibility provides a new opportunity to re-examine two strategies to control Notch fucosylation: control of global GDP-fucose synthesis and knockout of the *Pofut1 locus*. Murine ES cells lacking Pofut1 have wild type levels of cell surface Notch receptors. However, *Pofut1*$^{-/-}$ ES cells do not bind Notch ligands or exhibit Notch signaling [73]. This result demonstrates that Notch receptors can be processed without or, at least with very low Pofut1 in the presence of GDP-fucose. In contrary, how does Pofut1 process the Notch receptors in the absence of GDP-fucose? Would Notch receptors be expressed in *Pofut1*$^{-/-}$ cells, which contain normal levels of GDP-fucose? Functionally, these two strategies are not identical: Pofut1 without GDP-fucose and no Pofut1 with GDP-fucose. Taken together, we propose that Pofut1 may malfunction without GDP-fucose and induce the mis-folding of Notch receptors.

In this Chapter, we developed the soluble mNotch1 expression system using fucosylation-deficient CL17 cells. Also, we assayed the fucosylated glycan and the fucosylated proteins on CL17 cells by flow cytometry and characterized the glycan structure of soluble mNotch1 by MS analysis. Because we found some level of

fucosylation of Notch1 receptors in CL17 grown in culture without fucose, Notch1-fucose denotes Notch1+fucose^{Low} in this thesis, while Notch1+fucose and Notch+fucose+Lfng would have wild-type glycosylation.

Notes to Chapter 2

[1] Acknowledgements: We thank Nadia A. Rana and Dr. Robert B. Haltiwanger for the mass spectrometry analysis.

[2] Attribution of data: Bronislawa Petyriak performed the experiments depicted in Figure 2-4, Figure 2-5, and Figure 2-6. Nadia A. Rana and Dr. Robert B. Haltiwanger performed the mass spectrometry analysis depicted in Figure 2-7 and Figure 2-8.

Table 2-1. cDNA constructs of soluble mouse Notch1 and Notch ligands

DNA	N-terminal Tag	C-terminal Tag	vector
Notch1(15)	-	c-myc-biotin-tag	pcDNA1
Notch1(15)	-	c-myc-His$_6$	pcDNA1
Notch1(15)	-	IgG	pcDNA1
Notch1(36)	-	c-myc-biotin-tag	pcDNA1
Notch1(36)	3xFlag	c-myc-biotin-tag	pcDNA1
Notch1(12f)	-	c-myc-biotin-tag	pcDNA1
Notch1(24f)	-	c-myc-biotin-tag	pcDNA1
Notch1(26f)	-	c-myc-biotin-tag	pcDNA1
Notch1(27f)	-	c-myc-biotin-tag	pcDNA1
Dll-1	-	IgG	pcDNA1
Dll-1	-	c-myc-His$_6$	pcDNA1
Dll-1	-	c-myc-biotin-tag	pcDNA1
Dll-1	-	c-myc-biotin-tag (K→A)	pcDNA1
Dll-3	-	IgG	pcDNA1
Dll-3	-	c-myc-His$_6$	pcDNA1
Dll-3	-	IgG	pcDNA1
Dll-4	-	c-myc-His$_6$	pcDNA1
Dll-4 (*DSL)	-	c-myc-His$_6$	pcDNA1
Jag-1	-	IgG	pcDNA1
Jag-1	-	c-myc-His$_6$	pcDNA1
Jag-2	-	c-myc-His$_6$	pcDNA1
Lfng	-	c-myc-His$_6$	pcDNA1
Lfng	-	-	pZeoSV
Mfng	-	-	pZeoSV
Rfng	-	-	pZeoSV
BirA	-	-	pSecTag2B
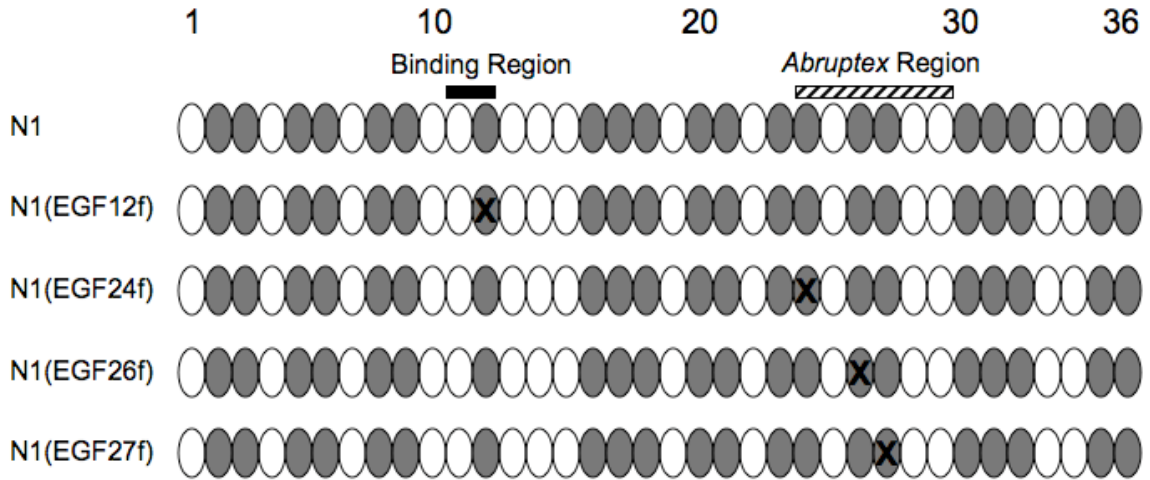
Figure 2-1. Mouse Notch1 mutant constructs. This schematic shows mutants of mouse Notch1 receptors used in this study. One oval means one EGF repeat. Map showing the EGF domains that are mutated (indicated by *X*) in each of the mouse Notch1 *O*-fucosylation site mutant constructs. *O*-fucosylation sites in EGF 12, 24, 26, and 27 were mutated to observe the distinct role of individual *O*-fucosylation site in Notch binding and signaling. Gray oval is the potential *O*-fucosylation sites on mouse Notch1 EGF repeats based on the broader consensus sequence ($C^2X_{4-5}\underline{S/T}C^3$). EGF11-12 are the binding region and EGF24-29 *Abruptex* region.
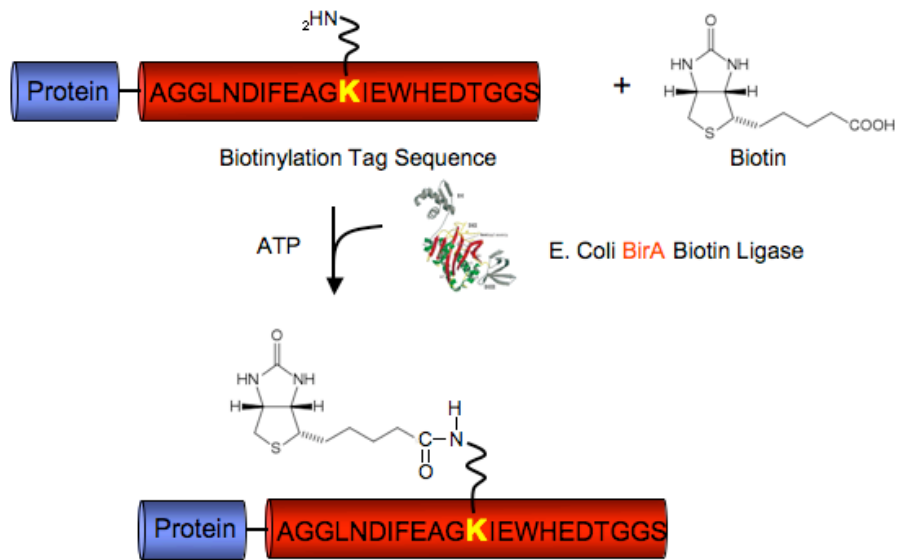
Figure 2-2. Site-specific mono-biotinylation system. *E. coli* BirA biotin ligase adds biotin to lysine of the biotinylation tag sequence (AGGLNDIFEAGKIEWHEDTGGS) with ATP.
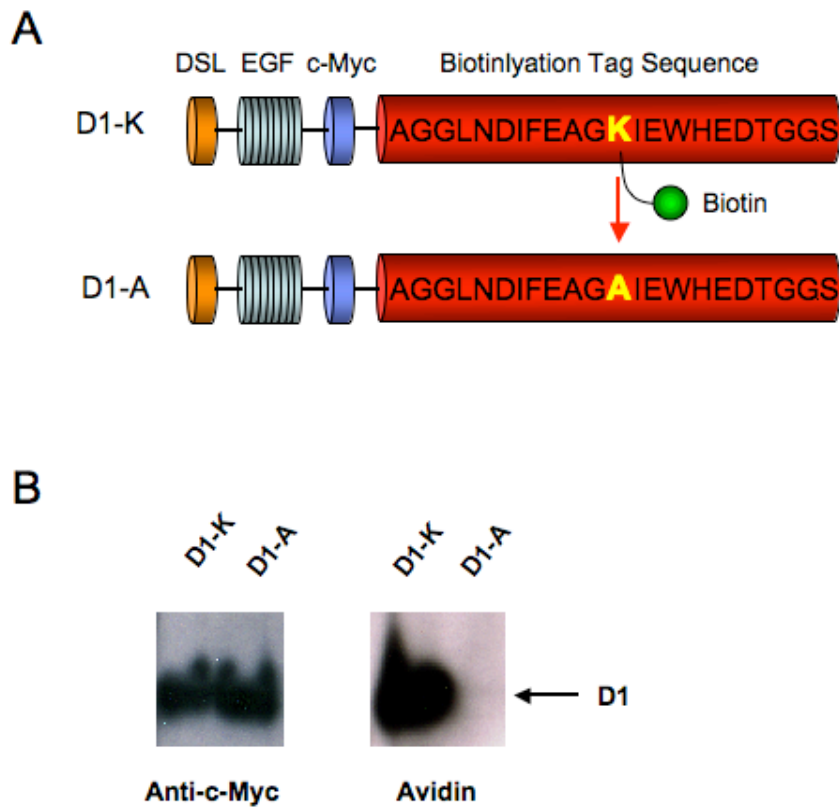
Figure 2-3. Verification of site-specific mono-biotinylation system. A. Biotinylation tag sequence was fused to the extracellular domain of Dll-1 with c-myc tag (D1-K). For the negative control, lysine in the biotinylation tag sequence is mutated to alanine (D1-A). B. D1-K and D1-A were co-transfected with BirA into HEK 293T cells. Next day, soluble biotin was added to the culture media for the in vivo biotinylation. D1-K and D1-A were probed with anti-cmyc antibody, indicating that both proteins were expressed from the cells. However, only D1-K was detected with avidin-HRP, while D1-A was not.
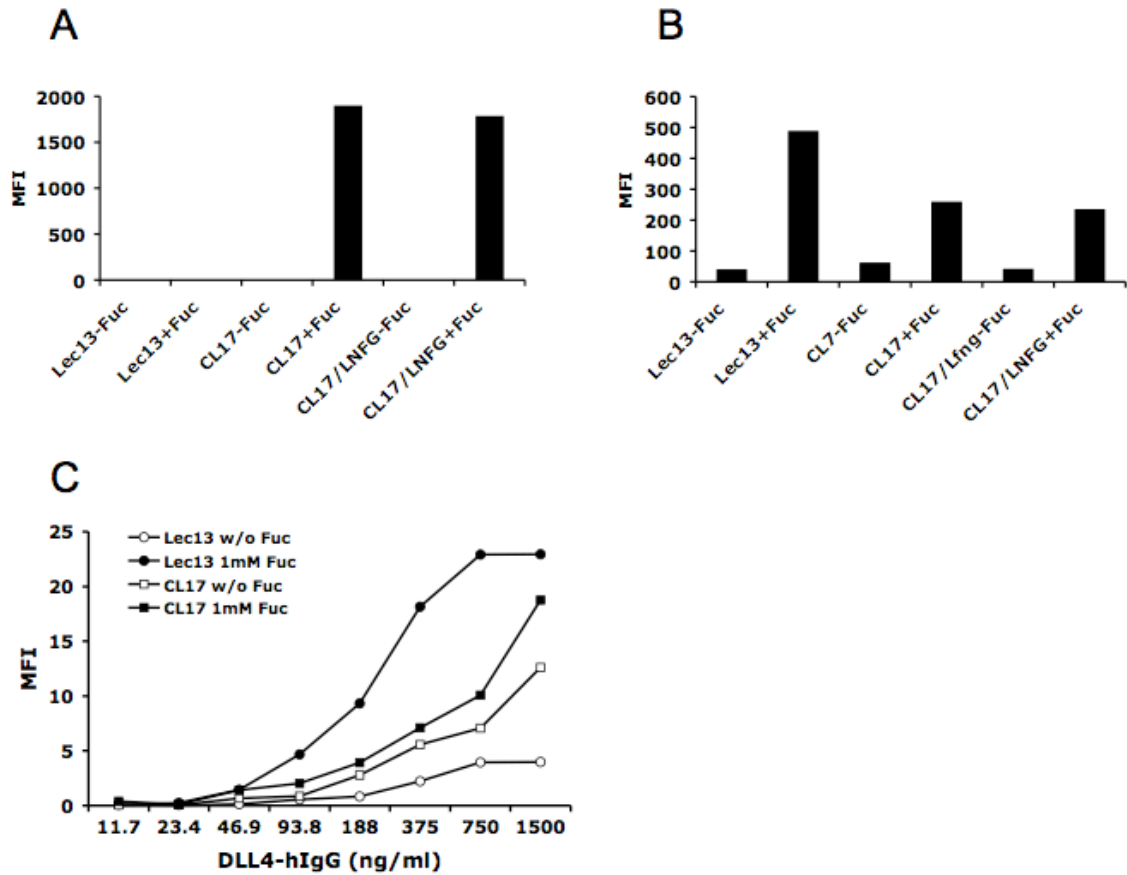
Figure 2-4. Characterization of Lec13 and CL17 cells. A. Staining of CSLEX-1 to Lec13, CL17, and CL17/Lfng cells. No detectable binding was observed in Lec13-fuc, Lec13+fuc, CL17-fuc, and CL17/Lfng-fuc, while CL17+fuc and CL17/Lfng+fuc have the capability of binding to CSLEX-1, indicating CL17 cells express sLe^X in the presence of fucose. B. Binding of PSA to Lec13, CL17 and CL17/Lfng cells. Low level binding was observed in Lec13-fuc, CL17-fuc, and CL17/Lfng-fuc, while Lec13+fuc, CL17+fuc and CL17/Lfng+fuc have the capability of binding to PSA, indicating that Lec13, CL17, and CL17/Lfng cells bind PSA in the presence of fucose. C. Titration of Dll-4-hIgG binding to Lec13 and CL17 cells. Lec13 cells are more susceptible to exogenous fucose in culture.
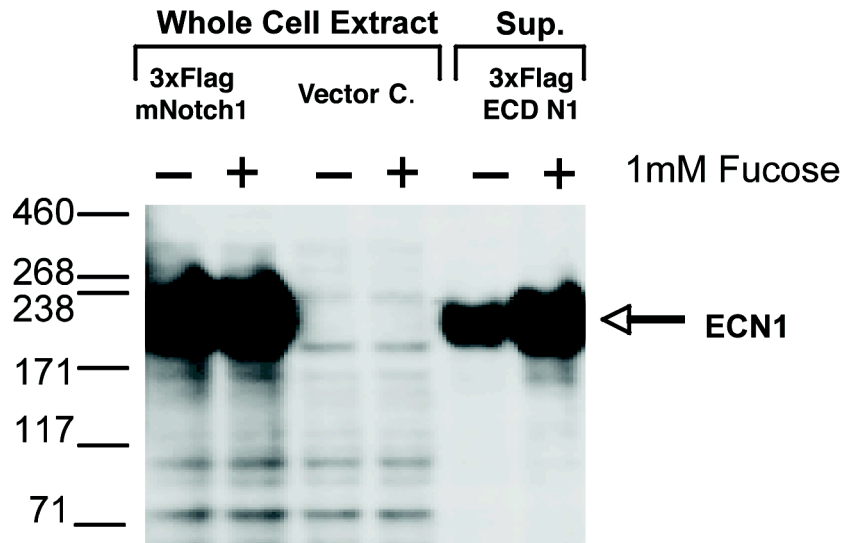
Figure 2-5. Surface expression of 3xFlag-Notch1 in Lec13 cells. 3xFlag-Notch1 was stably expressed in fucosylation-deficient Lec13 cells. Whole cells were lysated to observe the expression of 3xFlag-Notch. Expression of 3xFlag-Notch1 is similar in the presence or absence of fucose. No band was detected in vector control, indicating anti-mouse Notch1(8G10) doesn't have a cross-activity with hamster Notch1. To observe the surface expression of 3xFlag-Notch1 receptors, Notch receptors are dissociated with EDTA.
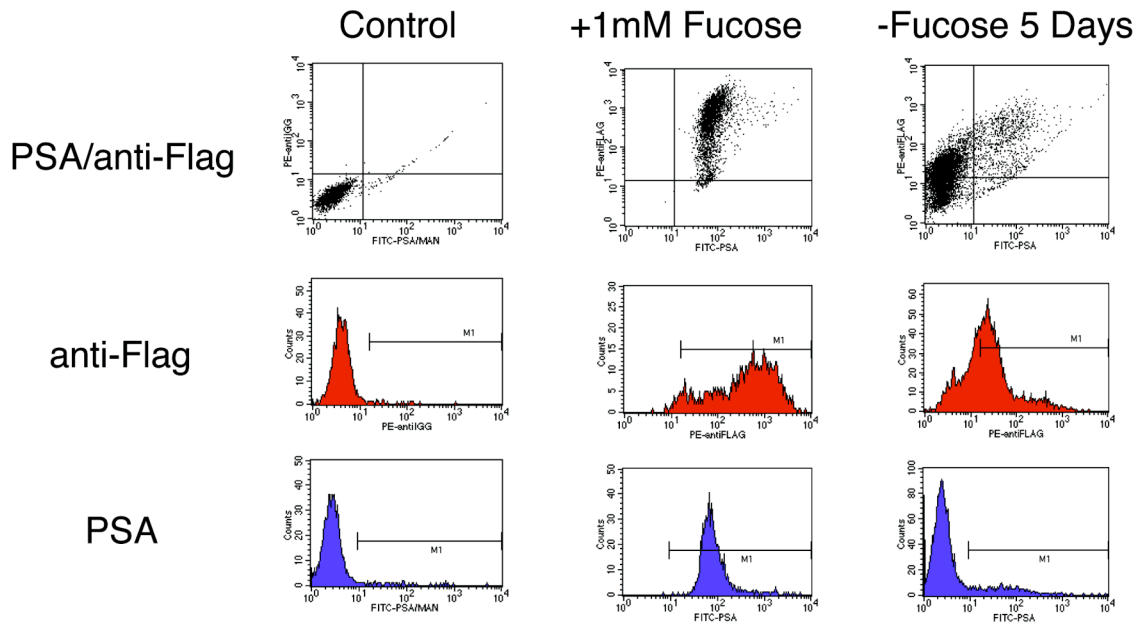
Figure 2-6. FACS analysis for the surface expression of 3xFlag Notch1 in Lec13 cells. 3xFlag-Notch1 was stably expressed in fucosylation-deficient Lec13 cells. To monitor the fucosylated glycan, PSA staining was performed in the presence or absence of fucose. To observe the surface expression of 3xFlag-Notch, 3xFlag-Notch/Lec13 cell was stained with anti-Flag antibody.
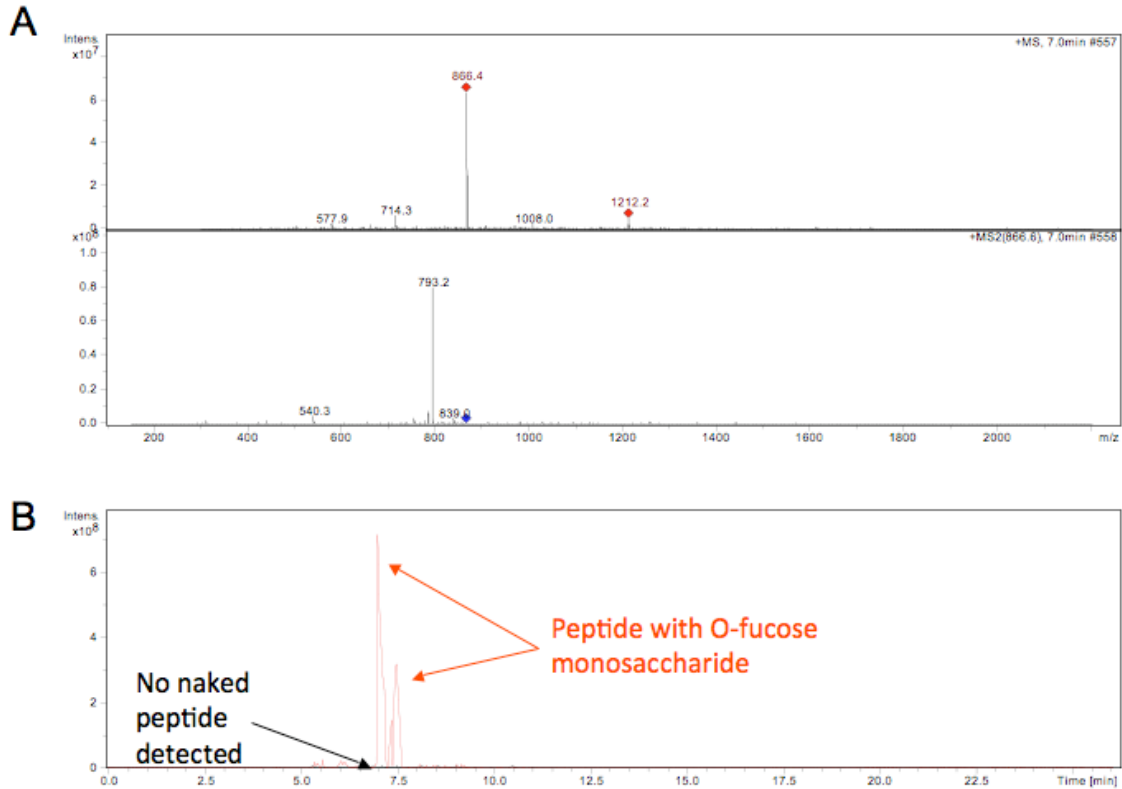
Figure 2-7. Mass spectrometry analysis of Notch1+fucose. Notch1(15)-hIgG produced in CL17 cells with exogenous fucose was subjected to reduction, alkylation, and in gel trypsin digestion as described in the "Methods." The resulting tryptic peptides were analyzed by LC-MS/MS. *A, top panel*, MS spectra showing the major ions eluting at 7.0 min. *M* corresponds to the mass of the peptide (^{113}NGGTCDLLTLTEYK^{126}) plus dHex (fucose). The other ions present in the MS spectrum represent other peptides eluting from the LC at the same time. The *red diamonds* indicated ions selected for CID fragmentation. *Bottom panel*, MS/MS spectra of *m/z* 866.5 ion ([M+2H]$^{2+}$) from the MS spectrum. The *blue diamond* shows the position of the parent ion prior to fragmentation. The major fragments show the sequential loss of a dHex ([M+2H-dHex]$^{2+}$, *m/z* 793.5) from the parent ion. [M+2H-dHex]$^{2+}$ corresponds to the doubly charged mass of a tryptic peptide from EGF domain 3 of Notch that contains an *O*-fucosylation consensus site (^{113}NGGTCDLLTLTEYK^{126}). B. A search of the entire chromatogram for the amount of *m/z* 866.5 ion compared to the same peptide without *O*-fucose (*m/z* 793.5). While the ion corresponding to the *O*-fucosylated peptide (plotted in red) can be seen on the chromatogram, the naked peptide (plotted in black) cannot.

54
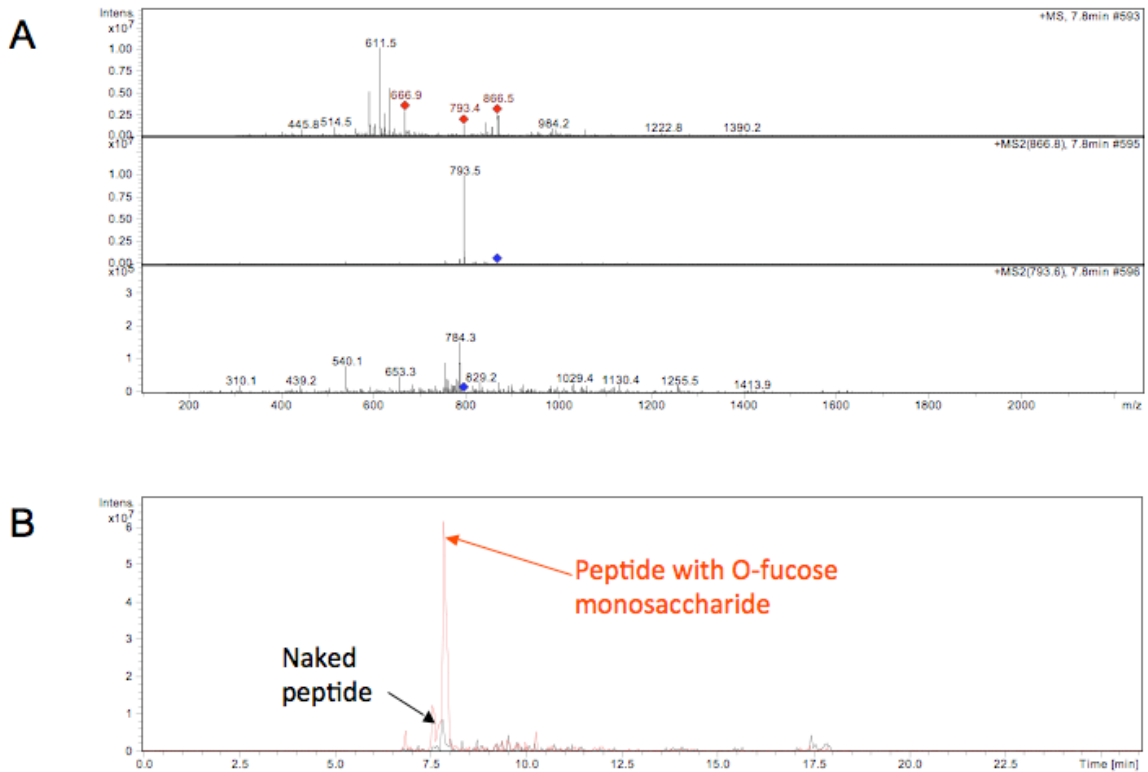
Figure 2-8. Mass spectrometry analysis of Notch1-fucose. Notch1(15)-hIgG produced in CL17 cells without exogenous fucose was subjected to reduction, alkylation, and in gel trypsin digestion as described in the "Methods." The resulting tryptic peptides were analyzed by LC-MS/MS. *A, top panel*, MS spectra showing the major ions eluting at 7.8 min. *M* corresponds to the mass of the peptide (^{113}NGGTCDLLTLTEYK^{126}) plus dHex (fucose). The other ions present in the MS spectrum represent other peptides eluting from the LC at the same time. The *red diamonds* indicated ions selected for CID fragmentation. *Middle panel*, MS/MS spectra of *m/z* 866.5 ion ([M+2H]$^{2+}$) from the MS spectrum. The *blue diamond* shows the position of the parent ion prior to fragmentation. The major fragments show the sequential loss of a dHex ([M+2H-dHex]$^{2+}$, *m/z* 793.5) from the parent ion. [M+2H-dHex]$^{2+}$ corresponds to the doubly charged mass of a tryptic peptide from EGF domain 3 of Notch that contains an *O*-fucosylation consensus site (^{113}NGGTCDLLTLTEYK^{126}). *Bottom panel*, MS/MS spectra of *m/z* 793.5 ion ([M+2H]$^{2+}$) from the MS spectrum. The *blue diamond* shows the position of the parent ion prior to fragmentation. *B*. A search of the entire chromatogram for the amount of m/z 866.5 ion compared to the same peptide without *O*-fucose (*m/z* 793.5). The most abundant species is the *O*-fucosylated peptide (plotted in red), while a small amount of naked peptide (plotted in black) can be seen on the chromatogram.

Chapter 3

The Use of Optical Tweezers to Study Notch-Notch ligand Interactions

Introduction

Single molecule force spectroscopy has emerged as a powerful tool to investigate the binding strength associated with biological molecules. One of the most promising force spectroscopy techniques is optical tweezers (OTs). OTs are a versatile tool for manipulating microscopic objects and making mechanical measurements. OTs use an optical trap that is created by focusing a laser to diffraction-limited spot with a high numerical aperture (NA) microscope objective [133]. OTs can quantify biological forces ranging from hundreds to less than one pN. Compared to other instruments used for micro-mechanical force measurement, such as glass needles or micro-fabricated cantilevers, OTs are generally better suited to detect very small forces (0.1-100pN). OTs are successfully used for many studies: DNA zipping and unzipping, DNA unfolding, DNA-transcription factor interaction, protein unfolding, and protein-protein binding.

Notch signaling is correlated with the adhesion force between the Notch signal sending cell and the Notch signal receiving cell [134]. It has been proposed that the conformational change of Notch1 negative regulatory region (NRR) is critical for the activation of Notch signaling. NRR consists of three Lin12/Notch repeats (LNR) and the juxtamembrane heterodimerization (HD) domain. Three LNR repeats cover around the

HD domain to stabilize it and sterically occlude the S2 sites from proteolytic cleavage [135]. Although it is not known where the mechanical force is generated, endocytosis would be exerted as the pulling force to induce the conformation change of NRR. For the Notch activation, at least the first two LNR need to be taken away from the HD domain, and subsequently the S2 sites exposed to the metalloprotease for further processing. In this biological context, the bond between the Notch-Notch ligand binding complex needs to be resistant to the force of endocytosis and strong enough to induce the unplugging of the HD domain from LNR modules.

Notch receptor and Notch ligand binding is modulated by *O*-fucosylated glycan. In this Chapter, we will use OTs to investigate the glycan-dependent Notch-Notch ligand binding strength and to study the capability and the limitation of OTs for direct force measurement in this context.

Methods

Optical Tweezers System- The optical tweezers system of Dr. Alan Hunt at the University of Michigan was used for the force measurement [136]. Figure 3-1 is the complete optical tweezers schematic, with an inset photograph of the microscope and its significant modifications. All components are mounted to a vibration isolation table (RS 2000, Newport Corp.). The microscope (Axioplan2, Zeiss Inc., Fig 1(H)) is principally outfitted for video-enhanced differential interference contrast [103] and epi-flourescence microscopy, using a 1.3-NA objective (Plan-NEOFLUAR 100X, Zeiss Inc.). An Nd:YVO$_4$ laser beam (T20-BL10-106Q, Spectra-Physics Lasers, Inc.) in continuous TEM-00 mode is expanded and collimated (Figure 3-1A and B) to overfill slightly the

back aperture of the microscope's objective. To create two noninterfering, independent traps, a polarizing beam splitting cube, preceded by a λ/2 wave plate, divides the laser into orthogonally polarized beams (Figure 3-1C). A liquid crystal attenuation system (LCR-IR05m Newport Corp.) controls the laser power for each beam (Figure 3-1D). A two axis acousto-optic deflection system (DTD-406BA6, IntraAction Corp.) steers each beam through 1:1 telescope lenses into microscope (Figure 3-1E and F). To preserve the polarity of the laser beams, before he entry into the microscope a λ/2 wave plate rotates the two beams to meet the orthogonal ordinary and extraordinary axes of the Wollaston prisms (Figure 3-1G). After existing the microscope, the beams are separated by polarity and terminate onto separate QPDs (Spot 9DMI, UDT Instruments) located at a plane made conjugate with the back focal plane of the microscope's condenser (Figure 3-1I). Differential amplifiers amplify the QPD signal and produce an output voltage proportional to position with a bandwidth of at 7kHz. A data acquisition card digitizes this signal at up to 100kHz (PCI-MIO-16XE10, National Insruments), and software analyzes the signal and records it to disk (LabVIEW).

Channel Preparation- As shown in Figure 3-3, double-sided scotch tape (3M) was put on the glass slide. The glass coverslip was put on top of the tape. After the bead solutions were injected, microscope oil was dropped at both ends of the channel to prevent the evaporation of the liquid solution.

Protein Immobilization- Streptavidin coated polystylene beads were purchased from Bangs Lab. Soluble forms of mNotch1 and each of ligands were constructed and coated

on beads. The density of the protein on the bead surface was measured by flow cytometry with anti-c-Myc antibody (data not shown).

Solid-phase Binding Assay- Bead solution with soluble Notch1 was injected into the channel and incubated for 5 min upside down to immobilize the bead on the coverslip. Bead coated with Notch ligands was allowed to flow inside the chamber and grabbed with the laser trap for further manipulation (Figure 3-3). Trap stiffness (k) was measured and the bead position (x) was recorded to calculate the rupture force by Hooke's law, F=kx.

Results and Discussion

To study the binding strength between glycan-dependent Notch-Notch ligands, optical tweezers were used. Soluble mNotch1 was immobilized on the 2μm beads and soluble Dll-11 was on the 5.5μm beads. Dll-1 coated bead was attached on the coverslip and the mNotch1 coated bead was grabbed by the laser trap. The mNotch1 coated bead approached to the Dll-1 coated beads to form a bond and subsequently retracted to break the bond (Figure 3-2). Although the software was not programmed with the continuous pulling, binding and rupture events were observed with optical tweezers. Before developing this system further, we found two issues in this two-bead system: a sample heating problem [137] and optical interference [138].

Sample Heating Problem- Output power of the trapping laser and the throughput of the optical system determine the maximum attainable stiffness and force. Trapping forces

depend on multiple parameters and are difficult to calculate for most conditions of practical interest. Generally speaking, maximum trapping forces on the order of 1 pN per 10 mW of power delivered to the specimen plane can be achieved with micron-scale beads [139].

To generate around 100pN force with optical tweezers, 1W power is needed. That amount of power can easily induce protein sample heating that can give damage to the protein because in the focused trap the temperature is increased by 7.7 ± 1.2 K/W for 500-nm silica beads and 8.1 ± 2.1 K/W for 444-nm silica beads in water [137]. Even though the heating effect in water is rather small it can have non-negligible effects on trap calibration in typical biophysical experimental circumstances and should be taken into consideration when laser powers of more than 100 mW are used.

The high intensity at the focus of the trapping laser that forms the optical trap, typically 10^9–10^{12} W cm^{-1}, results in local heating. Trapping transparent dielectric particles in water at a trapping wavelength of 1,064 nm results in modest heating on the order of 1 °C per 100 mW of power in the specimen plane. Trapping absorbing particles or trapping at laser wavelengths more strongly absorbed by water can result in considerably more heating. Local heating can influence enzymatic activity and change the local viscosity of the medium, whereas steep thermal gradients may produce convection currents that can adversely affect the measurements. Local heating in the vicinity of the optical trap can be calculated, and several techniques have been developed to measure the temperature directly [133, 137].

Optimal operational range of optical tweezers is 0-100pN, while the single binding force of protein-protein interaction is 50-200pN. Practically, multiple bonds may

be formed, which can reach up to several μN. For this reason, we found that optical tweezers are not suitable to study strong protein-protein interaction because of the maximum force limitation and the potential heating problem at the maximum force.

Optical Interference Problem- Vertical manipulation of the bead with the optical trap is not accurate because of current technical limitations. Therefore, the mechanical movement of the beads is on a horizontal plane for the precise measurement of the force. Due to the short binding length of Notch-Notch ligand, the physical contact of two beads is indispensable (Figure 3-3). Optical interference can be caused by a non-trapped object such as a bead or a glass slide. This technical obstacle can be resolved with a micropatterned structure [138]. However, this method is expensive and hard to calibrate the protein density on the micropatterned surface.

In summary, we developed a two-bead system to study protein-protein binding. In this system, the physical contact of two beads is indispensable, but this causes an optical interference that prevents the calibration of the laser trap stiffness and the detection of bead position. A special design was proposed for this optical interference issue [138], but it is very expensive and hard to quantify the protein density on that complicated structure. In addition, due to the limited maximum force, optical tweezers cannot break the bead-bead contact by the nonspecific binding or unwanted multiple bond, which can easily exceed several hundreds of pN.
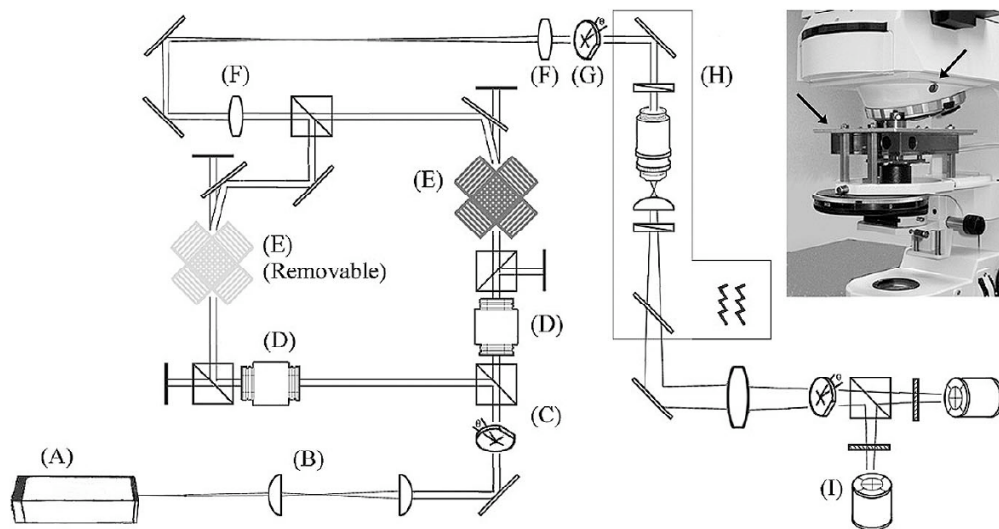
Figure 3-1. Optical tweezers schematic diagram. (A) Nd:YVO$_4$ laser; (B) collimating lenses; (C) $\lambda/2$ wave plate + PBSC for dividing beam; (D) liquid crystal attenuators; (E) AODs; (F) 1:1 telescope lenses; (G) $\lambda/2$ wave plate for alignment to Wollaston prisms; (H) schematic of microscope showing 1.3-NA objective, condenser, two Wollaston prisms, and the illumination source; and (I) quadrant photodiode detectors preceded by neutral density filters; (inset) photograph of microscope with arrows pointing to laser entry port and custom mounted nano-positioning stage (Adapted from reference [136])
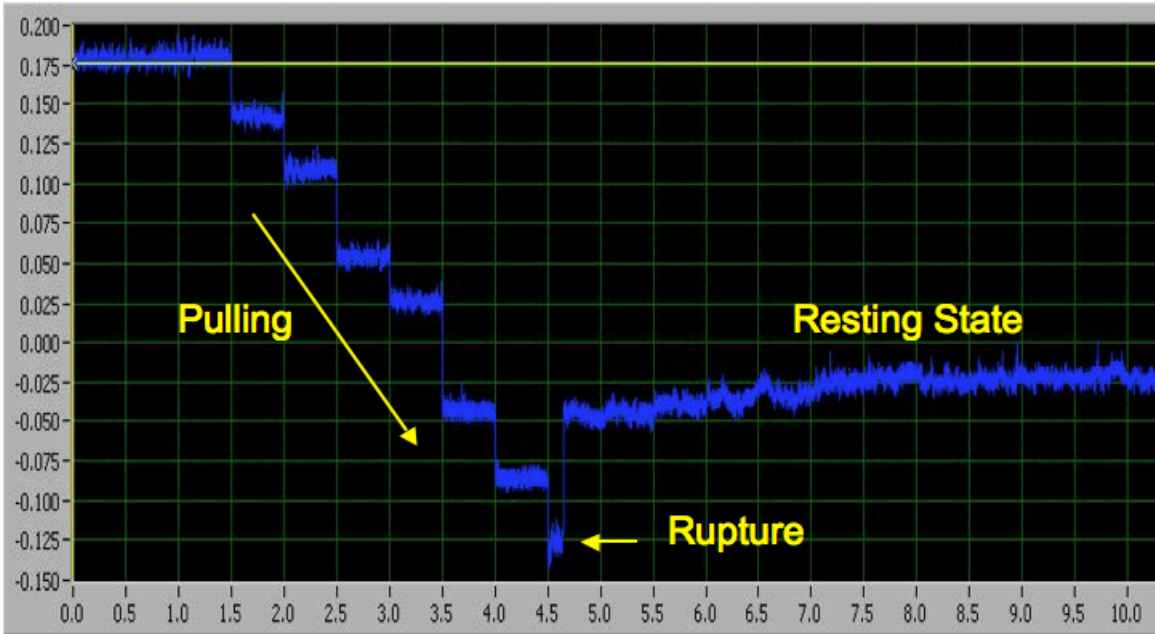
Figure 3-2. Measurement of Notch1 and Dll-1 binding strength. After two beads are attached each other to make the bond between N1 and D1, Notch1 immobilized bead is retracted, followed by the rupture of bond if any binding is formed.
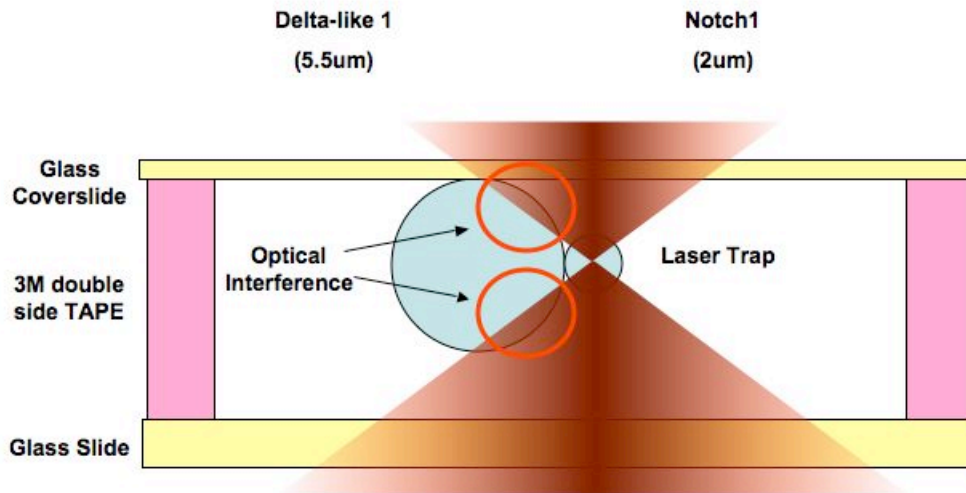
Figure 3-3. Optical Interference in the two bead system. A big bead is stuck on the surface of a glass coverslip, which is attached to a glass slide with 3M double side tape. As the small bead approaches to the big bead, the path of the laser is interfered by the other bead. This optical interference alters the calibration of stiffness of the optical trap.

Chapter 4

Direct Force Measurement of Notch-Notch Ligand Interactions using Atomic Force Microscopy (AFM)

Introduction

The atomic force microscope is a version of the scanning probe microscope in which the properties of the surface are investigated with a micromachined probe [140]. This technique allows mapping of the surface characteristics at sub-nanometer resolution. The possibility of modifying the surface and manipulating individual molecules made AFM an ideal tool for biological applications. One important advantage of the technique is simple and rapid sample preparation. Another important feature of AFM is the ability to conduct measurements of biological samples under near-physiological conditions [141].

Although the atomic force microscope is primarily an imaging tool, it also allows measurement of inter- and intramolecular interaction forces with piconewton resolution. The vertical motion of the cantilever is controlled by piezoelectric actuators with sub-nanometer resolution. The displacement of the cantilever is monitored directly with either a capacitor or a linear voltage differential transformer. As a result, high-resolution force-versus-extension curves of single molecules can be recorded. This force-extension

relationship provides valuable information on the structure, the folding and unfolding processes and even the activity of the molecule. Measurement of the stretching curve is relatively straightforward. The AFM tip is lowered toward the surface or the sample is lifted toward the cantilever tip by piezoelectric actuators. After the initial contact with the surface, the cantilever is pressed into the surface on which the sample is deposited with a predetermined constant force. The tip is then retracted. Attachment of the sample (RNA, DNA or protein) tethers the cantilever tip to the surface, causing the cantilever to bend toward the surface as the tip is retracted. The value of this force is obtained by Hooke's Law, $F=kx$, where F is the rupture force, k the spring constant of the AFM cantilever, and x displacement. In most cases the force-versus-extension curve displays nonlinear behavior indicative of an entropic spring, which is well described by the worm-like chain (WLC) entropic elasticity model. AFM first used to measure the forces between complementary strands of DNA [142]. Later, AFM has been successfully used to probe protein-protein binding [143-147] and glycan-mediated binding [127].

The following technical requirements must be satisfied to immobilize proteins on these surfaces: (a) avoidance of surface-induced denaturation and mechanical force (or indentation)-induced conformational deformation, (b) minimized nonspecific adhesive interactions with the bare probe surface or bare substrate surface, and (c) enhanced motional freedom of proteins after their immobilization on the surface to increase the binding chance [146]. Spacer chemistry has been proposed to meet these requirements, which includes end-functionalized, flexible polymeric spacer such as poly(ethylene glycol) (PEG) [143]. Moreover, the elastic behavior of polystyrene glycol (PEG) has been well-characterized. Therefore, polymer linkages are very useful for isolation

66

reactive sites in single molecule experiments as well as for suppression of rebinding events. However, it is possible that polymer linkages to stiff probes can introduce unexpected deviation in bond strength under steady speed detachment [101, 148].

Autoinhibition of Notch signaling is regulated by Notch1 negative regulatory region (NRR), which consists of three Lin12/Notch repeats (LNR) and the juxtamembrane heterodimerization (HD) domain. Structure of the Notch1 NRR shows that three LNR repeats wrap around the HD domain to stabilize it and sterically occlude the S2 sites [135]. For the Notch activation, at least the first two LNR need to be taken away from the HD domain, and subsequently the S2 sites is exposed to the metalloprotease for further processing. This conformational change to displace the LNR is required for the Notch activation. It has been proposed that the conformational change is induced by mechanical force or allosteric events. However, the source of mechanical force for Notch activation is not known. One potential candidate is the trans-endocytosis, which is essential for Notch signaling in Drosophila and mammals. In this biological context, Notch-Notch ligand binding force needs to be resistant to the force from the endocytosis and strong enough to unplug the HD domain from LNR modules. Also, bond lifetime needs to be long enough to finish all of these processes.

It is believed that bond strength correlates with the Notch signaling [134]. Direct force measurement using AFM was performed to measure the binding force of the glycan-dependent Notch-Notch ligands. Unexpectedly, we found that the rupture forces between Dll-4 and Notch1(15) with different glycosylation status were very similar, indicating the *O*-fucosylated glycans on Notch1(15) do not have a significant effect on the rupture force. These data imply that *O*-fucosylated glycans of EGF1-15 of Notch1

receptor are not the major substrate of the Fringe enzyme and the promising alteration of Notch signaling by Fringe action may be caused by the modification of EGF16-36 of Notch1 receptors. This result will be discussed and confirmed in Chapter 5, where SPR will be used to measure the dissociation rate, which is the determinant of the bond strength. This result increases our understanding of glycan-dependent Notch-Notch ligand binding.

Methods

Reagents- Notch1(15)-cmyc-BT-fucose, Notch1(15)-cmyc-BT+fucose, Notch1(15)-cmyc-BT+fucose+Lfng, and D4-hIgG were prepared as described in Chapter 2.

Functionalization of AFM tips and substrates- Figure 4-1 showes the protein immobilization method. In brief, for cleaning and hydroxylation, glass coverslips (12mm, Fisher Scientific) were boiled in Piranha solution (70% of sulfuric acid and 30% of hydrogen peroxide) for 30 minutes on hot plate. Piranha etched coverslips were rinsed in deionized water, dried with ultrapure nitrogen gas and thoroughly dried for 30 minutes at 90 °C. The coverslips were immersed in 2% (3-Mercaptopropyl)triethoxysilane (Sigma) for 30 minutes at room temperature to construct the thiol group on the surface. The silanized coverslips were rinsed with acetone and subsequently dried with ultrapure nitrogen gas. The silanized coverslips were incubated for 30 minutes at room temperature in 30µl of 10mM NHS-PEG-Maleimide cross-linker (succinimidyl-[(N-malemidopropionamido)-diethyleneglycol]ester, Spacer arm 25 nm, Nektar) in anhydrous DMSO. N-hydroxysuccinimide (NHS) esters react with primary amines of proteins at pH

7-9 to form amide bond, while maleimides react with sulfhydryl groups at pH 6.5-7.5 to form stable thioester bonds. PEG-coupled coverslips were washed with water, dried with ultrapure nitrogen gas and subsequently immersed in PBS containing 1mg/ml streptavidin (Pierce). Coverslips were then washed with PBS and incubated in Tris buffer (Tris=tris(hydroxymethyl)aminomethane, 25mM Tris, 0.15M NaCl, pH 7.4) for 30 minutes to block NHS group on PEG. Coverslips were washed with PBS and incubated with mono-biotinylated proteins for 30 minutes at room temperature, followed by a final incubation in HBSS (Hank's Balanced Salt Solution) supplemented with 2mM $CaCl_2$. Protein coupled coverslips were stored at 4°C for up to 2 days.

Silicon nitride (Si_3N_4) cantilever tip (MLCT, Veeco, Santa Barbara, CA) were washed in cooled piranha solution (90% of sulfuric acid and 10% of hydrogen peroxide) for 30 minutes. Piranha etched coverslips were rinsed in deionized water and gently dried with ultrapure nitrogen gas. After this, other processes are same with the substrate functionalization.

AFM Experimental configuration- AFM experimental configuration was shown in Figure 4-2. Soluble mNotch1 was immobilized on the surface by streptavidin and PEG and Dll-4-hIgG on the AFM tip via anti-hIgG and PEG. An mNotch1 coated glass coverslip is approached toward the Notch ligand coated tip and subsequently is retracted. The rupture force will be assessed as a function of (1) loading rate, and (2) the state of glycosylation of Notch1.

AFM Force Measurements- Force spectroscopy measurements were performed using a DI Multimode connected to the NanoScope IV controller (Veeco, Santa Barbara, CA). The interaction between PEG tethered molecules was initiated by bring the surface to the tip and rupture forces were detected during reverse motion of the probe. Force volume experiments were performed with 2-5nm relative trigger, a 0.2s dwell, and a forward velocity of 1um/s. Force-distance curves collected at each probe position were stored for subsequently analysis. The deflection sensitivity was determined by the curve fitting around the tip-surface contact region.

At fast cantilever retraction speeds (>1 μm/s), the hydrodynamic drag on the cantilever resulted in smaller forces recorded than were actually applied to rupture the complex. To correct the hydrodynamic force exerted on the cantilever, the damping coefficient of the cantilever ξ (~2 pN-s/μm) in the buffer was determined by measuring the deflection of the cantilever at different retraction speeds.

Automation of data analysis- Force curves were exported as ASCII files and processed with a custom program written in Matlab (MathWorks, Inc., Natick, MA). Data processing was automated to remove user bias and speed up the data analysis (Appendix 1). The program converted the force curves from deflection versus displacement into force versus separation.

The force-distance curve was categorized into 3 subsets: no binding, non-specific binding, and specific binding (Figure 4-3). To detect the rupture events, student t-test was used. At each data point, t-value from 10 points on the left side and 10 points on right

side were calculated and compared. If the t-values exceeded the threshold, that point was selected as a rupture point.

After this analysis, a filter was applied to remove transitions that occur at ruptures to close to the surface (<15nm). Double tethering used in this work decreaseed the nonspecific binding by moving the specific interaction away from both the AFM tip surface and the substrate surface. Also, this system can correlate the specific binding and nonspecific binding with the rupture distance [149].

A second set of filters refined parameters prior to the curve fitting of WLC (Worm-like Chain) model to select force events that have a force pattern typical for the rupture events coupled to a polymer stretching. Our tests indicate that this initial processing did not eliminate force curves that could be considered for further analysis by a trained user. The remaining rupture events were fit with the extended WLC model to find the loading rate for each rupture event.

The WLC model was first treated numerically by Fixman and Kovac (1973), after which a preliminary analytical approach was performed by Kovac and Crabb (1982). Its complete treatment was achieved by Marko and Siggia and reported by Bustamante et al. (1994).

Marko and Siggia (Bustaminte et al., 1994) proposed the following interpolation formula as a useful approximation to the WLC model:

$$F = \frac{k_b T}{L_p} \left[\frac{1}{4(1 - z/L_0)} - \frac{1}{4} + \frac{z}{L_0} \right].$$

where F reflects the applied force, z the actual length, k_b the Boltzmann constant, T the temperature, L_p the persistence length, and L_0 the contour length. The contour length L_0 is the overall length scale in the force extension curve.

Using this interpolation in the fitting procedure leads to a small overestimate in the value of L_p: the error is typically on the order of 5%, but actually depends upon the range of extensions spanned by the experiment and by the statistical error for each point. This simple WLC model has been used to investigate the elastic properties of DNA and proteins such as titin. Using this model, the contour length of the polypetide chain increase of an Ig domain unfolds of titin was predicted.

Bouchiat et al. [150] subtracted the Marko-Siggia interpolation formula from the exact numerical solution a seventh-order of the WLC model and expressed the residuals as a seventh-order polynomial, which provides all the correction terms.

$$F = \frac{k_b T}{L_p} \left[\frac{1}{4(1 - z/L_0)} - \frac{1}{4} + \frac{z}{L_0} + \sum_{i=2}^{i \le 7} \alpha_i \left(\frac{z}{L_0} \right)^i \right],$$

with $a_2 = -0.5164228$, $a_3 = -2.737418$, $a_4 = 16.07497$, $a_5 = -38.87607$, $a_6 = 39.49944$, and $a_7 = -14.17718$. The order of the polynomial is arbitrary; lower or higher order could also be used. They chose the seventh order since it leads to an accuracy of better than 0.01% over the useful extension range.

Close fit of the WLC model to the experimental data indicates that the observed traces indeed correspond to the rupture of a single pair of interacting molecules connected to the surfaces of tip and sample by double PEG tethers. Force events that are not well fit by the model are eliminated following this step.

Analysis of energy landscape of glycan-dependent Notch-Notch ligand interaction- The rupture force of Notch1-Notch ligand interaction was analyzed by the Bell-Evans model [151], which has been successfully applied to studies of other ligand-receptor systems. In the context of this model, a pulling force *f* distorts the energy landscape of the ligand-receptor complex, resulting in a lowering of the activation barriers, and consequently increasing the dissociation rate constant *k(f)* as follows:

$$k(f) = k^0 \exp\left(f\gamma / k_B T\right),$$

where k^0 is the dissociation rate constant in the absence of the pulling force, γ is the width of the potential barrier projected along the direction of the applied force, T is absolute temperature, and k_B the Boltzmann constant.

Under conditions of a constant loading rate r_f ($r_f = df/dt$), the probability density function for the unbinding of a complex at force *f* is given by (Evans and Ritchie, 1997):

$$P(f) = k^0 \exp\left\{\frac{\gamma f}{k_B T}\right\} \exp\left\{\frac{k^0 k_B T}{\gamma r_f}\left[1 - \exp\left(\frac{\gamma f}{k_B T}\right)\right]\right\}.$$

From this equation, the most probable force *f** (i.e., the maximum of the distribution $\partial P(f) / \partial f = 0$) is

$$f^* = \frac{k_B T}{\gamma} \ln\left\{\frac{\gamma}{k^0 k_B T}\right\} + \frac{k_B T}{\gamma} \ln\left\{\gamma_f\right\}.$$

Hence, this equation shows that the most probable unbinding force *f** is a linear function of the logarithm of the loading rate. Experimentally, the most probable rupture force *f**was obtained for the mode of the rupture force histogram. The Bell model parameter k^0 and γ was obtained from the plot of *f** versus *ln[r_f]* [111]. Dynamic force spectroscopy

with the Bell-Evans model can identify the molecular determinants that give rise to the dynamic properties of the Notch-ligand interaction.

Results

Evaluation of surface immobilization method with AFM imaging- For the direct force measurement using AFM, a surface with very low roughness is essential to measure the rupture force at single molecule level in order to reduce the noise and non-specific binding. Silanization method is a common approach for the surface functionalization. Silane has three branches to cross-link to another silane by hydrolysis, which is very sensitive to water concentration. Due to the difficulty of controlling the water concentration precisely, this surface provides very high surface roughness. Therefore, we developed the surface functionalization with esterification. Here, glass surface cleaned by Piranha solution was esterified with ethanolamine to create the amine group for the functionalization. PEG was elongated through NHS as a linker between the surface and the protein. Streptravidin or anti-hIgG was attached to PEG via NHS. To assess the surface property, AFM imaging was performed. The piranha cleaned surface is shown in Figure 4-5A. This surface has very low roughness, showing that this surface is suitable for the single molecule study. Streptavidin immobilized surface is imaged in Figure 4-5B. Surface roughness is about 4nm, which is the size of streptavidin and confirms that streptavidin is immobilized. This result demonstrates that the immobilization method by esterification and PEGylation gives very low surface roughness and may reduce noise caused by the nonspecific binding.

Dynamic force spectra of mNotch1 and Dll-4 interaction- To test how the *O*-fucosylated glycans of Notch1 alter the binding strength, AFM was used to measure the rupture force between soluble mNotch1 and Dll-4 binding. Soluble Dll-4-hIgG was immobilized on the AFM tip through anti-hIgG. Soluble mNotch1 was attached on the surface via streptavidin. Streptavidin-biotin and anti-hIgG are a well-established methods for the protein immobilization in AFM.

Four different configurations were used: Dll-4 binding to streptavdin, Notch1(15)-fucose, Notch1(15)+fucose, and Notch1(15)+fucose+Lfng. Specific binding was selected from ~1000 force-distance graphs. Specific binding has special characteristics that the curve has a non-linear stretching shape, which is the characteristic of polymer stretching. Binding frequency at the retraction speed of 7140 nm/s is shown in Figure 4-6. The binding frequency of the specific binding is twice that of the non-specific binding, indicating the Notch-Notch ligand binding is specific.

We observed that force spectra of Notch1(15)-fucose, Notch1(15)+fucose, and Notch1(15)+fucose+Lfng are almost identical (Figure 4-7). This indicates that the *O*-fucosylation and Fringe modification of Notch1(15) has no effect on the rupture force. Together, this result implies that Notch1(15) and Dll-4 binding do not depend on fucose and binding enhancement is likely due to Fringe modifications of fucose moieties within EGF domains 16-36.

We found two different slopes of rupture force versus loading rate. The existence of multiple loading regimes in the force spectrum of the Notch1(15) and Dll-4 interaction can be interpreted as evidence for multiple activation barriers, at least two, in the dissociation potentials of the complexes.

Discussion

The study in this chapter is directed towards using AFM to define the relative and/or absolute strength of binding between single Notch1-Notch ligand couples, as a function of Notch1 fucosylation. This requires the generation of soluble forms of Notch1 and Notch ligands and the development of in vivo site-specific mono-biotinylation to enable the immobilization of these soluble recombinant proteins to the AFM surface and cantilever tip via a single biotin molecule site at the COOH-terminus of the proteins.

We observed that the rupture forces of Dll-4 to Notch1(15)-fucose, Notch1(15)+fucose and Notch1(15)+fucose+Lfng are very close. We cannot exclude the technical limitation of AFM force measurement. Firstly, because of the force resolution limit (~10pN) of AFM, it may not be possible to distinguish the rupture force differences as a function of fucosylated status if the resulting force differences are less than 10 pN. Secondly, it is hard to rule out the possibility that the force spectra are contaminated from nonspecific binding because the frequency of the specific binding is twice that of non-specific binding. However, as discussed in Chapter 5, we found that the dissociation rates of Dll-4 binding to Notch1(15)-fucose, Notch1(15)+fucose, and Notch1(15)+fucose+Lfng are very similar from the SPR data in Figure 5-10, where it is believed that the dissociation rate determines the binding strength. Taken together, *O*-fucosylated glycans in EGF1-15 of Notch1 receptors have no significant effect on the binding strength to Dll-4. This observation gives new insight to study the role of EGF16-36 of Notch1, which are the major active sites of Fringe modification that regulate the Notch binding and signaling.
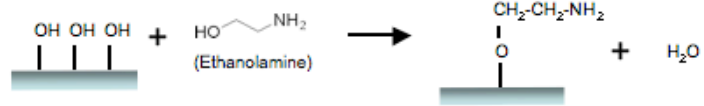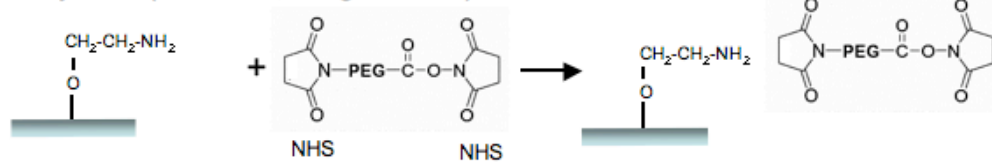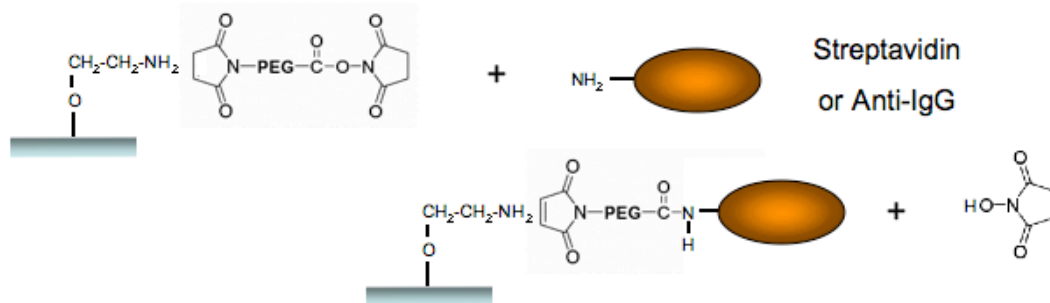
Figure 4-1. Protein immobilization method by esterification. Mica is esterified with ethanolamine (1) and PEGylated with PEG of MW3400 (2). Streptavdin or Anti-IgG is attached to PEG by NHS.
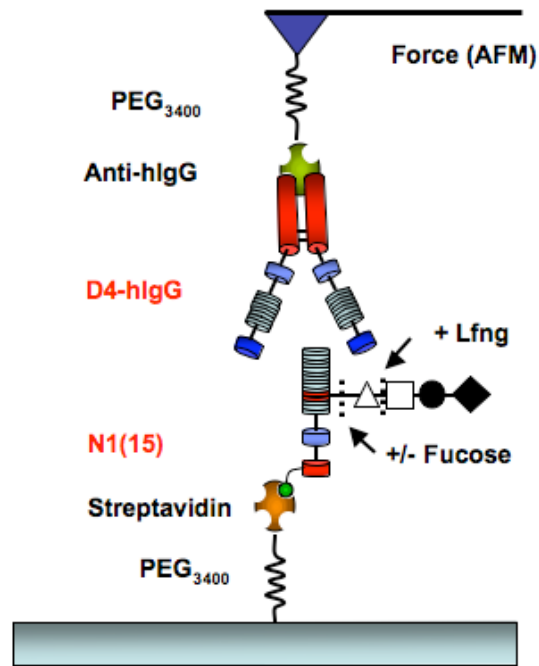
Figure 4-2. AFM experimental setup to measure the Notch1 and Dll-4 binding strength. Notch1 is attached to the glass surface through neutroavidin and PEG. D4-IgG is immobilized to the AFM tip through anti-IgG and PEG.
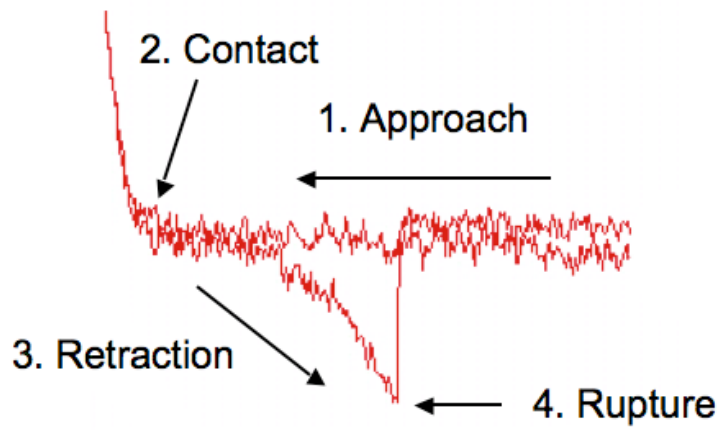
Figure 4-3. Force-distance curve from AFM force measurement. AFM tip approaches to the protein immobilized surface (1) and contacts to form the bond (2). Subsequently, AFM tip is retracted (3), followed by the rupture if it has a specific bond (4).
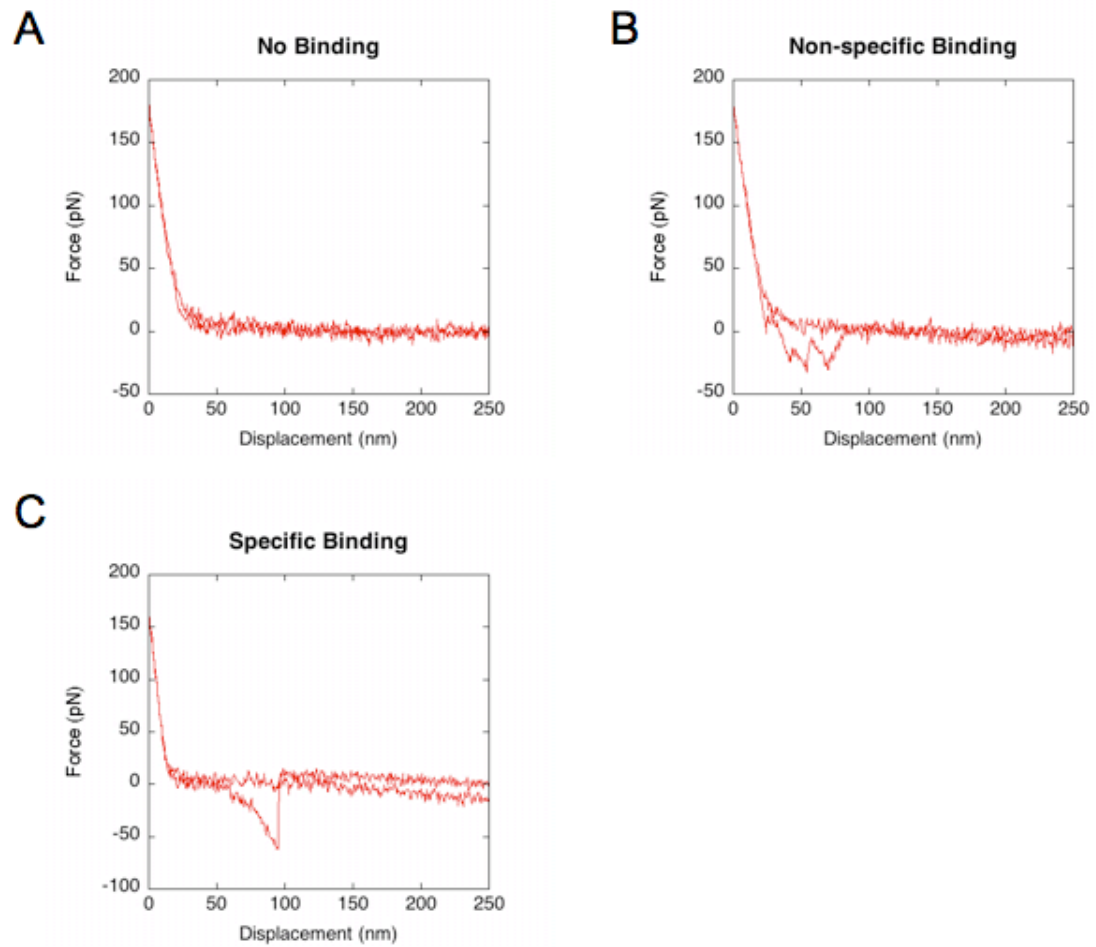
Figure 4-4. Representative force-distance graph of Notch1 and Dll-4 binding. A. No binding, B. Non-specific binding, C. Specific binding.
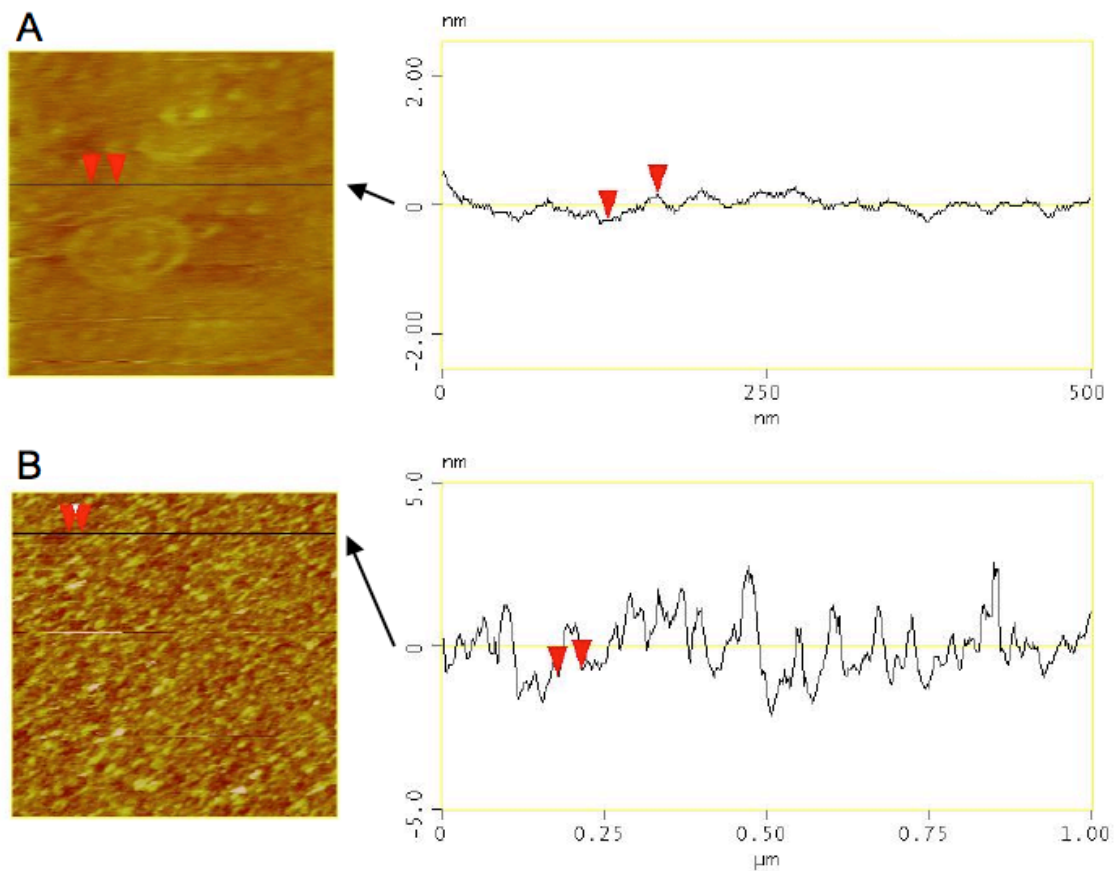
Figure 4-5. AFM image of esterified surface and SA immobilized surface. (A) AFM image of esterfied surface, (B) AFM image of SA immobilized surface on the esterified surface.
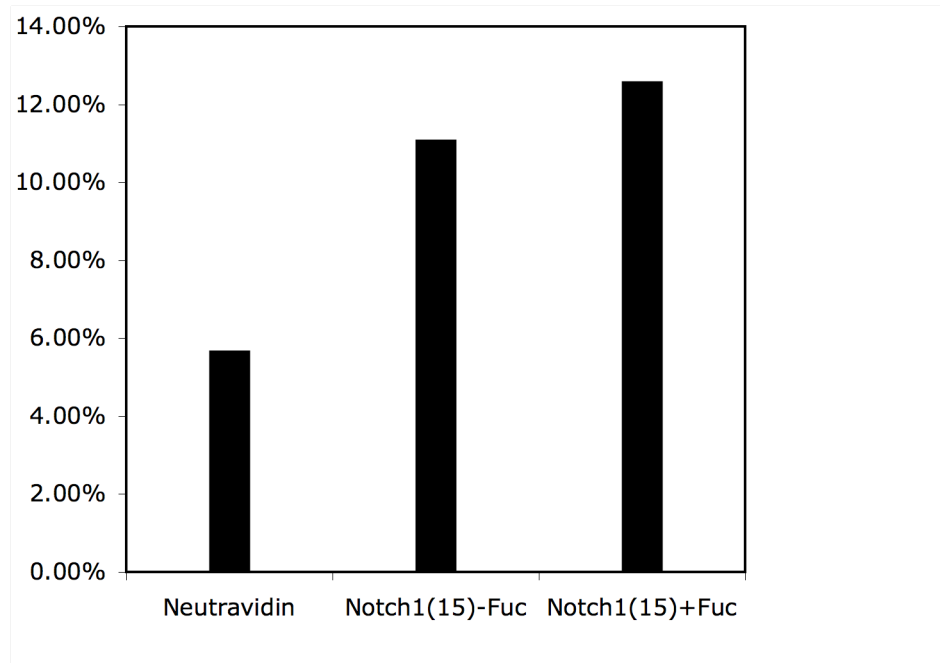
Figure 4-6. Binding frequency at the retraction speed of 7140 nm/s. The binding frequency of the specific binding is twice than that of the non-specific binding.
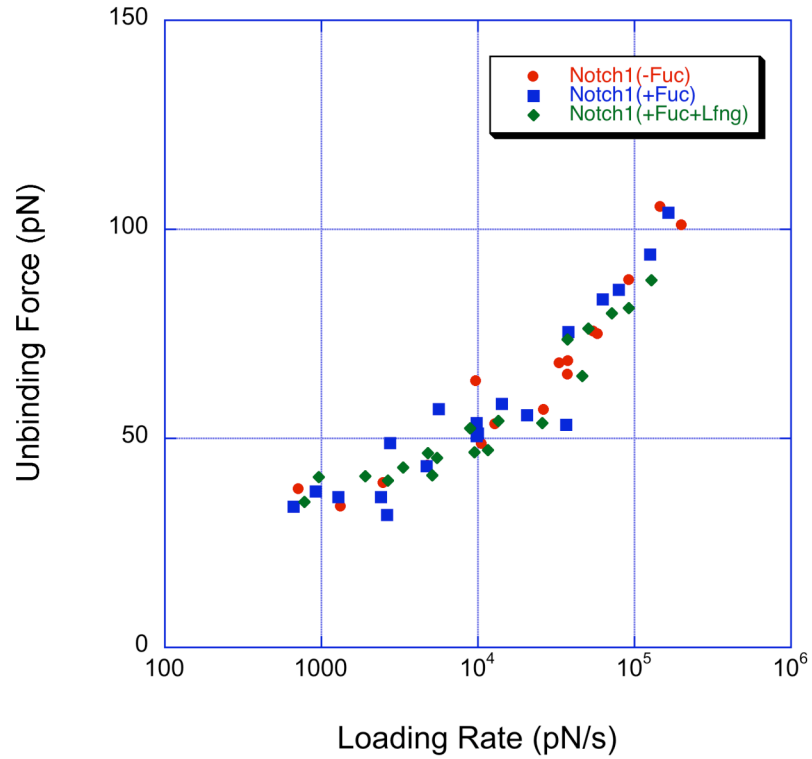
Figure 4-7. Force spectrum of Notch1 and Dll-4 binding. Rupture forces of Notch1(15)-fuc (red) , Notch1(15)+fuc (blue), and Notch1(15)+fuc+Lfng (green) to Dll-4-hIgG were plotted as a function of loading rate.

Chapter 5

Kinetic Analysis of Glycan-dependent Notch-Notch Ligand Interactions using Surface Plasmon Resonance (SPR)

Introduction

Notch receptors play a critical role in many developmental and pathophysiological processes [45, 46, 56]. Because of the importance of Notch function in health and disease, the Notch signaling pathway has emerged as a potential therapeutic target [152, 153].

A Notch receptor expressed by a receiving cell is activated when the receptor's extracellular domain (ECD) interacts with a ligand on an adjacent (sending) cell, and is apparently pulled away from the membrane of the receiving cell by endocytosis-dependent processes on the sending cells [91, 154]. Activation of a Notch receptor leads to the protease-dependent release of a specific intracellular fragment of the Notch receptor. This intracellular fragment then translocates to the nucleus of the receiving cell and modulates transcriptional events that in turn dictate changes in the phenotype of the receiving cell.

Notch ligands were first identified in *Drosophila* and are called Delta and Serrate. Five Notch ligands have now been identified in humans, in mice and in other mammals. These are termed Jagged1, Jagged2, Delta-like1, Delta-like3, and Delta-like4. Each of

these ligands is a single-pass transmembrane protein with a conserved N-terminal Delta, Serrate, LAG-2 (DSL) motif, which is essential for binding to Notch receptors [112].

Mammalian Notch receptors contain 29-36 EGF like repeats, which are modified with one or more *N*-glycans, and are heavily modified by *O*-glycans initiating with protein-linked, *O*-fucose [21, 42, 44, 68], *O*-glucose, and possibly *O*-GlcNAc [72]. The fucosyltransferase termed Pofut1 transfers fucose to the serine or threonine residue of the *O*-fucosylation consensus sequence $C^2X_{4-5}(S/T)C^3$ on some EGF domains of Notch receptors. In mammals, glycosyltransferases termed Lunatic Fringe (Lfng), Radical Fringe (Rfng), and Manic Fringe (Mfng) can elongate *O*-fucose moieties by adding GlcNAc, which may be subsequently modified by galactose and sialic acid moieties, respectively, to form elongated structures of the form Sia-α2,3-Gal-β1,4-GlcNAc-β1,3-α1-*O*-Ser/Thr [21]. Pofut1-mediated *O*-fucosylation of Notch receptor EGF repeats occurs in the endoplasmic reticulum [23]. By contrast, subsequent modification of the fucose moiety, leading to the elongated, sialic acid-terminated structures noted above, takes place in the Golgi lumen [42]. These *O*-linked glycans play key roles in modulating Notch-mediated signal transduction events, since, for example, *O*-fucosylated glycans, which modify some EGF-like repeats within the ECD of Notch family members, have been observed to regulate signaling from Notch receptors, in correspondence with their ability to modulate the interaction between Notch receptors and their ligands [82]. *O*-linked fucose is required for Notch binding to Notch ligands and the Notch activation [73, 155]. Extension of *O*-fucose by Fringe enhances the Dll-1 signaling, while reduces the Jag-1 signaling [82].

While these studies begin to provide insight into how specific *O*-fucosylated

glycans control Notch receptor-ligand interactions, they do not provide a precise understanding about how different *O*-fucosylated glycans dictate the kinetics with which Notch receptors and their ligands associate, or dissociate, nor do they provide corresponding precision about the affinities that characterize each receptor-ligand couple, as a function of their fucosylated glycan phenotype. An understanding of these issues will help to provide a molecular understanding of the biological variation that is characteristic of each different Notch-Notch ligand couple, and each distinct fucosylated glycoform.

Likewise, while it is apparent that the information on individual *O*-fucosylated glycans will be required to dissect the mechanism by which these sugars affect Notch function. Although multiple EGF domains on Notch receptors are thought to be involved in Notch receptor binding to Notch ligands [112], published evidence indicates that the ligand binding region (EGF 11-12; [112]) and the *Abruptex* region (EGF 24-29; [156, 157]) of Notch receptors are critical to Notch binding and signaling. Specifically, mutation in distinct *O*-fucosylation site in EGF12 within the binding region inhibits Notch activation [85] and the mutation of *O*-fucosylation sites in EGF 26 and 27 inside the *Abruptex* region results in enhancement and decrease of Notch signaling, respectively [87]. Moreover, these three *O*-fucosylation sites in EGF repeats 12, 26, and 27 are highly conserved in all known Notch homologues of Notch1 receptors. This observation has implied that these *O*-fucosylation sites are biologically relevant for Notch signaling.

Indeed, mutation of the *O*-fucosylation site in EGF repeat 12 of mNotch1 results in reduced signaling in Drosophila and mammals [51, 85, 86]. This suggests that the effects of the mutation at EGF repeat 12 are mediated largely by loss of the *O*-fucose

monosaccharide. Mutation of the *O*-fucosylation site in EGF repeat 27 of mNotch1 results in faulty trafficking of this Notch receptor to the cell surface and a decreased S1 processing of the receptor. In mammals, mutation of the *O*-fucosylation site in EGF repeat 26 of Notch1 results in hyperactive signaling in response to Delta1 and Jagged1 interaction due to unknown mechanism. These observations begin to provide insight into regions of the Notch1 molecule that play important roles in receptor-ligand interactions. Nonetheless, they do not yet allow a detailed understanding of how individual domains, or glycans on those domains modulate the rates of association and dissociation between Notch1 and its ligands, nor do they provide deeper insight into how domains or specific glycans dictate receptor-ligand affinities.

In experiments we report here, we have sought to advance the understanding of how Fringe-mediated glycan modifications modulate the kinetics and affinities of the interactions between mouse Notch1 and its ligands, how distinct *O*-fucosylation sites on mouse Notch1 contribute to these binding interactions, and how Fringe-dependent glycan modification of Notch ligands themselves may modulate Notch receptor-ligand interactions, using surface plasmon resonance techniques. Efficient binding was observed between mNotch1 and the Notch ligands Dll-1, Dll-4, Jag-1, and Jag-2, but not between mNotch1 and Dll-3. A biphasic binding and dissociation pattern was observed with the four binding-competent Notch1-Notch ligand pairs, suggesting a two-state receptor-ligand interaction model characterized by initial formation of a transient receptor-ligand complex followed by a conformational change that leads to a more stable receptor-ligand complex. Primary and secondary on and off-rates for the four binding-competent mNotch1-Notch ligand pairs were observed to be distinct and characteristic for each

Notch ligand. The magnitudes of the overall association constants (K) generated by the mNotch1-Dll-1 couple or the mNotch1-Dll-4 couple were similar, and much greater than the overall association constants generated in couples involving mNotch1 and either Jag-1 or Jag-2. The overall association constants observed when Dll-1 or Dll-4 interacted with Fringe-modified mNotch1 were significantly greater than when these ligands interacted with unmodified mNotch1, with enhancement likely due to Fringe modifications of fucose moieties within EGF domains 16-36. By contrast, Fringe modification of mNotch1 did not significantly modulate interactions with Jag-1 or Jag-2. Mutational analyses confirm prior observations that the *O*-fucosylation site within EGF repeat number 12 dictates much, if not all of the binding between Notch1 and its ligands. Finally, we observe that Fringe modification of Dll-4 enhances its ability to bind to mNotch1.

Methods

Protein Reagents- Construction and characterization of soluble mNotch1 and Notch ligands were discussed in Chapter 2. The protein configuration used in this Chapter is summarized in Figure 5-1.

Surface Plasmon Resonance (SPR)- Mono-biotin tagged soluble mNotch1 proteins with various glycosylation status were immobilized on the Biacore Sensor Chip SA at the level of 600-1200RU using Biacore 3000 and Notch ligands were injected at the speed of 50μl/mL (Figure 5-2). Dll-1, Jag-1, and Jag-2 were injected for 1 min and Dll-4 for 3 min because of the slow association. The dissociation phase was held for 5 minutes. The surface was regenerated with 10mM Hepes, 0.5M NaCl, 0.01% Triton-X 100, 3mM

EDTA in hepes buffer (Figure 5-3). All experiments were performed at least 3 times at 25°C.

Mass Transfer Limitation (MTL) was tested followed by the Biacore manual. Checking for MTL was performed by injecting Notch ligands at different flow rates. The association and dissociation rate constants were the same between different flow rates. This indicates that no mass transfer limitation is present.

The obtained sensorgrams were modified by double subtraction method shown in Figure 5-4. Binding curves were analyzed with a two interconverting receptor binding model or conformational change model ($A + B \underset{kd1}{\overset{ka1}{\leftrightarrow}} AB \underset{kd2}{\overset{ka2}{\leftrightarrow}} AB*$) using BiaEvaluation software.

Results

Patterns of the association and dissociation phases of mNotch1 and Notch ligand binding are biphasic - To examine how the glycans alter the Notch binding to Notch ligands, kinetic study was performed using SPR to determine the association and dissociation rate of the interaction. Various glycosylation forms of mNotch1 were immobilized on Biacore sensor chip SA and then Notch ligand binding to various mNotch1 were observed.

Because the multiple EGF repeats in Notch1 contribute to ligand binding, directional immobilization is important. Site-specific mono-biotinylation was used to express the Notch1 proteins. In this system, the extracellular domain of mNotch1 was fused to c-Myc tag and a biotinylation tag in the C-terminal. Through biotin in the biotinylation tag, soluble mNotch1 was immobilized on the Biacore sensor chip SA.

We observed the biphasic binding and dissociation patterns (Figure 5-5A and B), which suggests that the Notch-Notch ligand binding complexes may have at least two-state compartments. However, to rule out the possibility that simple 1:1 binding model dictates Notch-Notch ligand binding, the binding curves were first fitted with a 1:1 Langmuir binding model. The binding curves were not fitted well by 1:1 Langmuir binding model with high χ^2 number (χ^2=39.1) as shown in Figure 5-5C.

We tested several models which are proposed for the biphasic dissociation pattern.

$$A + B \underset{kd1}{\overset{ka1}{\leftrightarrow}} AB \underset{kd2}{\overset{ka2}{\leftrightarrow}} AB* \qquad \text{(Two interconverting receptor state binding) (1)}$$

$$A + B \underset{kd1}{\overset{ka1}{\leftrightarrow}} AB, A + C \underset{kd2}{\overset{ka2}{\leftrightarrow}} AC \quad \text{(Two non-interconverting receptor state binding) (2)}$$

$$A + B \underset{kd1}{\overset{ka1}{\leftrightarrow}} AB + B \underset{kd2}{\overset{ka2}{\leftrightarrow}} ABB \qquad \text{(Bivalent ligand binding) (3)}$$

$$A + B \underset{kd1}{\overset{ka1}{\leftrightarrow}} AB \overset{kx}{\rightarrow} AB* \underset{kd2}{\overset{ka2}{\leftrightarrow}} A + B* \quad \text{(Two-site interconverting receptor binding) (4)}$$
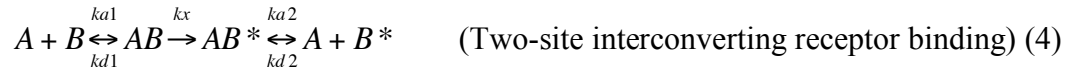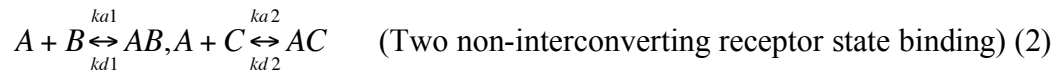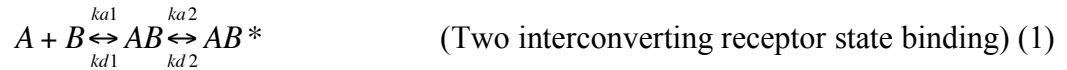
where A is Notch ligand and B and C are different forms of Notch receptors at surface.

To test which binding model dictates Notch-Notch ligand binding, the binding curves of Notch1+fucose and Dll-4 binding were fitted with a two interconverting receptor state model (equation 1), a two non-interconverting receptor state model (equation 2), and a bivalent ligand binding model (equation 3). The binding data were not fitted well by a two non-interconverting receptor state model (χ^2=23.5), and a bivalent ligand binding model (χ^2=35.1) as shown in Figure 5-5E and F, respectively, while a two interconverting receptor state model significantly enhanced the fit with low χ^2 number (χ^2 =2.4) as shown in Figure 5-5D, indicating that a two interconverting receptor state binding model may dictate Notch1-Dll-4 binding.

In a two interconverting receptor state model, ligand (A) binds to surface receptors (B) with rate constant ka1 to form low-affinity receptor-ligand complexes (AB), which convert to high-affinity complexes (AB*) with the rate constant ka2. To test whether a two interconverting receptor state model dictates Notch-Notch ligand binding, linked reaction test was performed according to the Biacore manual. Dll-4 (250nM) was injected to Notch1+fuc and Notch1+fuc+Lfng immobilized surface and compared the dissociation rate constant after injection times of 1, 3, and 20 minutes. This interconverting receptor state model assumes that the conversion rate of low-affinity complexes to high-affinity complexes is proportional to the incubation time. The identical dissociation profiles may indicate that the reactions are not linked. In Figure 5-6A and B, the dissociation rate constant was gradually decreased after longer injection time and the biphasic patterns in association and dissociation phases are also observed from all of the injection time, indicating that the formation of high-affinity complexes was increased over time in both Notch1+fuc and Notch1+fuc+Lfng binding to Dll-4. This result supports that a two interconverting receptor state model dictates Notch-Notch ligand binding.

A two non-interconverting receptor state model can be caused by heterogeneity of immobilized Notch1 receptors. Immobilized Notch1 may be pure because Notch1 receptors were captured by streptavidin and biotin bond which is equivalent with the purification step. Another potential source of heterogeneity may be induced from different glycosylation status. However, all the glycosylated forms of Notch1 have biphasic patterns in the association and dissociation stage (Figure 5-7). Therefore, the biphasic pattern is not from the heterogeneity of immobilized Notch1 receptors.

If one Notch ligand contains two binding sites, a bivalent ligand binding model may dictate Notch-Notch ligand binding. It is known that DSL domain has one binding surface to Notch receptor from the structural study [158]. Therefore, it is not likely that bivalent ligand binding model dictates Notch-Notch ligand binding.

A two-site interconverting receptor state model also supports the biphasic patterns in association and dissociation phase of Notch-Notch ligand binding. Ligand (A) binds to surface receptors (B) with rate constant ka1 to form low-affinity receptor-ligand complexes (AB), which convert to high-affinity complexes with rate constant kx. High-affinity complexes are also formed by ligand binding to high-affinity state receptors (B*) with the rate constant ka2. Ligand can dissociate from low- or high-affinity receptor-ligand complexes with rate constants, kd1 and kd2. In this model, the conversion of low-affinity complexes to high-affinity complexes is irreversible. If the dissociation curve can be described with a single exponential, it indicates the absence of a low affinity site and the complete conversion of receptors to a high affinity state. However, as shown in Figure 5-6A and B, the biphasic pattern is still seen on long injection (20 minute), suggesting that the dissociation is occurred with two rate constants and the conversion of high-affinity receptor-ligand complexes directly to receptor and ligand is minimal.

To exclude the possibility that the biphasic pattern is due to the mass transfer limitation. Mass transfer limitation was tested according to the Biacore manual. No difference was observed in kinetics with different injection speed (data not shown) and with different immobilized level of soluble mNotch1 receptors on the surface (data not shown).

Taken together, a two interconverting receptor state model dictates Notch1 and Notch ligand binding. A two interconverting receptor state model is also known as a conformational change model because the conversion of the low-affinity complexes to high-affinity complexes is induced by the conformational change of the receptor-ligand binding complexes. In this model, Notch binding to Notch ligand is the binding step to form a low-affinity receptor-ligand binding complex and conversion from a low-affinity complex to a high-affinity complex is a conformation change step. This indicates that conformational change is involved in Notch-Notch ligand binding. All the binding data in this chapter will be analyzed with a two interconverting receptor state model or the conformational change model.

Effect of fucosylation and Fringe modification of mNotch1 receptor in ligand binding kinetics- To test how fucosylation and Fringe modification of Notch1 alter the binding to Notch ligands, mNotch1 and Notch ligand binding kinetics were measured by SPR. Soluble mNotch1 was expressed from CL17 cells and CL17/Lfng cells with exogenous fucose. All of the Notch ligands except Dll-3 were expressed from HEK 293T cells. We were unable to express Dll-3 consistently and found that Dll-3 is very unstable after secretion. Recent literature proposed that Dll-3 is not a transmembrane protein, while it is resident in Golgi [159]. However, the mechanism of Dll-3 is still controversial although Dll-3 mutation may induce severe axial skeletal defects [160, 161].

Conditional fucosylation-deficient CL17 cells were used to express non-fucosylated mNotch1. His-tagged mNotch1(EGF1-15) was expressed from CL17 without exogenous fucose. With MS analysis, we found that *O*-fucose existed in some of EGF

repeats of soluble mNotch1, indicating Notch1 receptor expressed in the absence of fucose contains fucose to some extent. The potential source of fucose may be from serum. For simplicity, Notch1 cultured in the absence of fucose (*i.e.* Notch1-fucose) is correspondent to Notch1 cultured in the presence of very low concentration of fucose.

Sensorgram and kinetic information on mNotch1 binding to Notch ligands is summarized in Figure 5-7 and Figure 5-8, respectively. A negative control ligand wherein the DLS domain of DLL-4 was mutationally inactivated (Dll-4 (*DSL)) did not bind to any mNotch1 surfaces (data not shown).

Most of the kinetic information on Notch ligand binding to Notch1-fucose and Notch1+fucose analyzed a two interconverting receptor state model are almost identical (Figure 5-8) because Notch1-fucose and Notch1+fucose may have the similar level of *O*-fucosylated glycans as suggested in mass spectrometry analysis in Chapter 2. As shown in Figure 5-8E, in overall association constant, Dll-1 and Dll-4 have high affinity to Notch1+fucose compared to Jag-1 and Jag-2 which have low affinity to Notch1+fucose.

To observe how lunatic Fringe modification of mNotch1 changes the binding to each ligand, soluble mNotch1 was expressed from lunatic Fringe stably transfected CL17 cells. Lunatic Fringe was chosen because lunatic Fringe has been known as a potent modifier in many T cell development studies [162, 163]. CHO cells have an endogenous lunatic and radical Fringe activity, but no manic Fringe activity was detected (Data not shown). As a consequence, a low level of Fringe modification of Notch is expected.

With Fringe modification, overall association constants of Dll-1 and Dll-4 binding were increased, while those of Jag-1 and Jag-2 binding were the same or decreased. The first association rate constant (ka1) of Dll-1 and Dll-4 were increased with Fringe

modification, while those of Jag-1 and Jag-2 were about the same. The first dissociation rate constant (kd1) of Dll-4 was significantly reduced with Fringe modification, while Dll-1, Jag-1, and Jag-2 were about the same or a bit increased. The second association rate constant (ka2) of all Notch ligands were decreased or about the same, indicating that Fringe action hinders advancing from low-affinity complexes to high-affinity complexes of Notch-Notch ligand binding. Specially, in Dll-4 binding, lunatic Fringe modification significantly reduces the second association rate constant (ka2), indicating low-affinity state is favorable when Dll-4 binds to lunatic Fringe modified mNotch1. The second dissociation rate constant (kd2) of Dll-1 was reduced. Dll-4 was increased, while Jag-1 and Jag-2 were about the same. Maximum binding capacity (Rmax) was estimated from the curve fitting procedure with the two interconverting receptor state model of BiaEvaluation software. Normalized Rmax was calculated by dividing the estimated Rmax with the immobilized Notch1 on the surface and the molecular weight of each Notch ligand. The value obtained from Dll-1 binding to Notch1-fucose was set as 1. The normalized Rmax indicates the relative amount of bound Notch ligand per Notch1 molecule on the surface (RU). Normalized Rmax of Dll-1 was significantly increased about 8 fold with Fringe modification of mNotch1. These data are consistent with results showing that Dll-1 binding to Notch2 is detectable after Notch2 is processed by Lunatic Fringe [164]. Also, Dll-4 has similar maximum binding level (normalized Rmax) in this work, reflecting the apparent reduced dependence of the interaction on Lunatic Fringe by flow cytometry [164]. Jag-1 and Jag-2 increased with around 2 fold with *O*-fucosylation and Fringe modification, respectively.

Once Notch1 is modified by Fringe, Dll-1 and Dll-4 have the same affinity and same maximum binding capacity. However, in Figure 5-8B, Dll-4 has a smaller overall dissociation rate compared to Dll-1, implying that Notch1-Dll-4 binding complex triggers the stronger signal. This result demonstrates that Dll-4 is the most potent ligand for Notch signaling, which is known as the essential, non-redundant ligand in thymus for T cell development [162, 163].

Taken together, Fringe modification of Notch1 significantly alters Notch1-Dll-4 binding kinetics. In Notch1-Dll-1 binding, binding kinetics including overall association constant and the maximum binding level (Rmax) are dramatically changed with Fringe modification. Jag-1 and Jag-2 binding to Notch1 are almost the same or a bit decreased by the Fringe action. We propose that lunatic Fringe modification makes the Delta ligands (Dll-1 and Dll-4) more competent for Notch signaling.

Role of individual O-fucosylation sites of mNotch1 in ligand binding kinetics- To evaluate how the individual *O*-fucosylation sites alter the kinetics of Notch-Notch ligand binding, mNotch1 mutants with mutations in *O*-fucosylation sites in EGF12, 24, 26, and 27 were constructed (Figure 5-9A) and the binding kinetics was measured by SPR. In many studies, mutation in the *O*-fucosylation site of EGF12 reduced the binding and signaling. Also, *O*-fucosylation sites in EGF24, 26, and 27 are of interest because they are in the *Abruptex* domain reported as the negative regulatory region. Specially, *O*-fucosylation sites in EGF12, 26, and 27 are highly conserved in many species. These mutations are unlikely to disrupt the structure of the EGF domain of Notch.

As shown in Figure 5-9E, mNotch1 mutant in the *O*-fucosylation site in EGF 12 inhibits the binding to Notch ligand, Dll-4. Both the binding step and the conformational step were significantly altered.

Still, Dll-4 can bind to mNotch1 at a detectable level, which is rescued by Fringe action to some extent. However, Dll-1, Jag-1, and Jag-2 binding were significantly reduced, so the binding level from the sensorgram was too low to fit with the model, even though the same Notch mutant immobilized surface and the same range of Notch ligand concentration were used (data not shown). Our result suggests that *O*-fucose of EGF12 is important for both the binding and the conformational step in binding kinetics and may influence the intensity of Notch signaling.

We observed no difference in the kinetic information from the point mutation study of *O*-fucosylation sites in EGF 24, 26, and 27 (Figure 5-9A, B, C, and D). However, in terms of normalized Rmax, maximum binding capacity of Dll-4 and Notch1(EGF26f)-fucose and Notch1(EGF26f)+fucose was increased 1.5 fold compared to the wild type mNotch1 binding to Dll-4, while Rmax of this binding was back to the same level to other mutant with Fringe modification. Haltiwanger's group reported that mutation in *O*-fucosylation site of EGF26 of mNotch1 has increased Notch signaling, while mutation in *O*-fucosylation site of EGF 24 of mNotch1 has the same signaling compared with wild type [87]. Our data suggest that the Notch signaling increase in the EGF 26 mutant is induced by the increased maximum binding level of Notch ligand, not by a change of the binding kinetics. Also, this result implies that the *O*-fucose in EGF26 is an inhibitory molecule for Notch binding to the ligand.

Role of EGF16-36 of mNotch1 in ligand binding kinetics- To further study the role of EGF16-36 of mNotch1 in binding kinetics, a deletion mutation of mNotch1 was constructed by removing EGF domains 16-36 of the Notch1 receptor, and binding of the resulting Notch1(EGF1-15) to Dll-4 was examined with SPR. The kinetic binding data we observed when Notch1(EGF1-15) and Dll-4 interacted were not altered with the Lfng modification of Notch1(EGF1-15) (Figure 5-10). These data are consistent with the result of Haltiwanger's group, showing that because the *O*-fucosylation site in EGF12 is a poor substrate for Fringe, other *O*-fucosylation sites are susceptible to Fringe modification and can alter Notch binding and signaling. Our data indicate that EGF repeats 16-36 of Notch1 are involved in both the binding step and conformational change steps. We propose that a dramatic increase in Notch-Notch ligand binding by Fringe is induced by the modification of EGF16-36, which includes the *abruptex* domain. This result suggests the importance of the *abruptex* region, which is the one of the major substrate of lunatic Fringe [87].

Effect of fucosylation and Fringe modification of Dll-4 in mNotch1 binding kinetics- Notch ligands are also substrates of protein *O*-fucosylatransferase-1 as well as Fringe. To test how Fringe modification on Dll-4 alters Notch binding to Notch ligands, soluble Dll-4 was expressed from CHO/CL17 cells and CHO/CL17/Lfng with fucose. Kinetic binding information was obtained from a Biacore experiment. Kinetic studies on mNotch1 binding to various glycosylated forms of Dll-4 are summarized in Figure 5-11. In these experiments, we observed that Fringe modification of Dll-4 enhanced its binding to mNotch1. This result indicates that Lfng modification of Dll-4 enhances mNotch1

binding. This demonstrates that Fringe modification influences the binding characteristics of both Notch and Notch ligand.

Discussion

In this chapter, we investigated how the *O*-fucosylated glycans on Notch1 receptors alter the ligand binding kinetics and affinities using SPR. We observed the biphasic patterns in the association and dissociation phases, indicating that Notch-Notch ligand binding has two-state complexes which is caused by the conformational change of low-affinity receptor-ligand binding complexes to high-affinity receptor-ligand binding complexes, where the binding is dictated by a two interconverting receptor state model. Fringe modification on Notch1 significantly enhances the overall association constants of Dll-1 and Dll-4, while has no significant effect on Notch1 binding to Jag-1 and Jag-2 in the overall association constants. The *O*-fucosylation site in EGF repeat 12 of Notch1 is critical in formation of low- and high-affinity complexes of Notch and Notch ligand. EGF16-36 is the critical substrate of lunatic Fringe, which influences the formation of both a low- and high-affinity receptor-ligand binding complex.

Models for Notch-Notch ligand binding compartments- In this study, we observed the biphasic patterns in the association and dissociation phases of Notch-Notch ligand binding curves in SPR experiments. We considered a binding model that has two dissociation rate constants and proposed that a two interconverting receptor state model dictates Notch-Notch ligand binding. However, we cannot exclude the possibility that

other binding models can dictate Notch-Notch ligand binding, which have three or more association and dissociation rate constants. One such three rate constant model may be represented by the equation $A + B \underset{kd1}{\overset{ka1}{\leftrightarrow}} AB \underset{kd2}{\overset{ka2}{\leftrightarrow}} AB^* \underset{kd3}{\overset{ka3}{\leftrightarrow}} A + B^*$. The only difference between this model and a two-site interconverting receptor state model is that the conversion from the low-affinity complexes to the high-affinity complexes is reversible. This model is difficult to test because the conversion from the low-affinity complexes to the high-affinity complexes and the dissociation of the high-affinity complexes are slow and may be overlapped in the slow dissociation region of SPR binding curves. Consequently, in the SPR analysis, the binding curves may not have the triple-phasic patterns in association and dissociation phases. Further studies would be required to determine the physical nature of the distinct Notch-Notch ligand binding compartments.

Dissociation rate correlates with Notch signaling- Many studies have suggested that Notch binding correlates with the Notch signaling [73, 165, 166]. Free ligands in solution do not have the ability to activate Notch signaling [92, 167]. Furthermore, Notch signaling is not activated when Notch receptor binds to its ligand in the same cell surface (*i.e. cis*-inhibition) [125, 158]. These considerations and othes make it evident that ligand binding itself is not the sole determinant of Notch signaling. Some biophysical microevironment, in addition to ligand binding, seems to be required for proper Notch signaling. Endocytosis of the Notch ligand expressing cells is critical in Notch signaling in Drosophila and mammals [88, 89]. Endocytosis serves as a pulling force that may induce a conformational change in Notch, preceding, if not actually causing exposure of the S2 proteolytic cleavage site of Notch required for the Notch signaling activation [135,

168, 169]. The strength of the Notch-Notch ligand bond apparently needs to be stronger than the external pulling force by endocytosis. Indeed, the binding strength is determined by the dissociation rate of the binding. This implies that the dissociation rate might be the critical kinetic information in Notch signaling. As shown in Figure 5-8, the binding affinity of Jag-2 is very weak compared to other Notch ligands. However, Jag-2 is capable of triggering Notch signal better than Dll-1 and Jag-1 in some cell lines [170].

To test this hypothesis, we analyzed the kinetic variables obtained from the SPR experiment. Because the overall association rate constant and the overall dissociation rate constant were not directly obtained from the two interconverting receptor binding model, the overall association rate constant was calculated from $A + B \underset{kd1}{\overset{ka1}{\leftrightarrow}} AB \overset{ka2}{\to} AB^*$ with assumption *kd2*=0 and the overall dissociation rate constant from $A + B \underset{kd1}{\leftarrow} AB \underset{kd2}{\overset{ka2}{\leftrightarrow}} AB^*$ with the assumption *ka1*=0 as shown Appendix 3. As shown in Figure 5-12, the overall association rate constant and overall dissociation rate constant were calculated from the general solution of the rate equations is shown in Appendix 3 [171].

A correlation between Notch signaling and the dissociation rate constant is evident in the context of Notch downstream signaling that has been observed when bone marrow progenitor cells are co-cultured with OP-9 stromal cells expressing Notch ligands [172]. In these experiments, the level of mRNA transcribed from the Notch downstream target Deltex was observed to be increased by co-culture with OP-9 cells bearing Dll-1, Dll-4, and Jag-2, not in co-culture with OP-9 cells expressing Jag-1 [172].

In here, the first dissociation rate constant (kd1) or the overall dissociation rate constant (kd) may correlate with Notch signaling, however, no correlation was found from other rate constants or the affinities. If the first or overall dissociation rate constant

(kd1 or kd, respectively) is larger than that of Dll-1, there is no signal from Jag-1, but if smaller, it will signal from Dll-1, Dll-4 and Jag-2 (Figure 5-12).

Together, I propose that the first dissociation rate constant (kd1) must be below a certain threshold before activation of Notch signaling can occur. This is relevant because all of the Notch ligands except Dll-3 have the ability to signal in vitro. If the first or overall dissociation rate constant (kd1 or kd, respectively) is smaller the threshold (*i.e.* stronger bond), the Notch signaling would be activated.

Binding Model- We found that a two interconverting receptor state model best correlates with our SPR-derived Notch-Notch ligand binding data, where the binding complex forms a low-affinity complexe and then a high-affinity complexe. Although the overall conformation of all EGF domains of Notch receptor is not known, a structural model has been proposed by others [115, 158, 173]. In this model, one EGF domain containing 6 cysteines adopts a fold with three disulfide bonds (C1-C3, C2-C4, C5-C6). A calcium binding EGF domain is arranged in a linear form with a neighboring EGF domain. NMR and X-ray analysis of Notch binding domain (EGF 11 and 12) showed that Ca^{2+} participates in a stiff, extended arrangement on calcium binding domain of Notch receptors. Regions containing non-calcium binding EGF domains are flexible and bent, having a U-shaped fold. Together, calcium binding plays a role in holding the structure of ligand binding domain of Notch receptors [174]. However, *O*-fucose on the EGF domain has no significant effect on the structure of the EGF domain itself [175].

Based on the implication from these structural studies, the Irvine group proposed a triple-stranded structure for Notch receptor [112]. In this model, EGF10-21 of the

Notch receptor forms a rod-like shape and both EGF6-9 and EGF22-27 are folded back against EGF10-21, forming the binding pocket. In this model, EGF1-5 and EGF28-36 may mask some of the EGF repeats around the central region prior to the ligand binding. We propose that ligand binding may induce the strand displacement of EGF1-5 and EGF28-36 to facilitate the docking of a Notch ligand within the binding pocket of a Notch receptor revealed by strand displacement.

Although speculative, we propose a two interconverting receptor states model with the triple stranded structure as shown in Figure 5-13B. Binding is initiated by the interaction of the DSL domain of Notch ligand and EGF11-12 of the Notch1 receptor. Subsequently EGF domains of Notch ligand reside in the binding pocket. After this initial binding step, low-affinity complexes convert to high-affinity complexes by conformational change. Although the nature of this conformational change is not known EGF6-9 and EGF22-27 of Notch1 receptor may "clip" the ligand against the EGF 10-21 backbone of Notch receptor to help form stable complexes.

Trans-activation and cis-inhibition- In the biological contexts, Notch receptors are expressed on signal receiving cells, while Notch ligands are expressed on signal sending cells to achieve activation of proper Notch signaling (*i.e. trans*-activation). However, if Notch receptors and Notch ligands are expressed in the same cell, as has observed to be true in many instances, there is no Notch signaling event, and in some instances, prevents activation by Notch ligands presented in *trans* (*i.e.* cis-inhibition). An anti-parallel complex between Notch and its ligand has been proposed for achieving *trans*-activation and a parallel complex between the two has been proposed for achieving *cis*-inhibition

[158]. In the proposed parallel complex model, most of the EGF domains of Notch ligands reside inside the binding pocket of Notch receptor. In this model, EGF10-21 of the Notch1 receptor and the EGF domains of the Notch ligand are parallel to each other. In the proposed anti-parallel complex model, the DSL domain of a Notch ligand binds to the ligand binding domain (*i.e.* EGF11-12) of Notch receptor, but the binding direction is anti-parallel. In this model, most of the EGF domains of Notch receptor and Notch ligand do not interact and exist in an unbound state. This anti-parallel complex model seems unlikely to exist, however, because there is evidence that most of the EGF repeats of Notch receptors contribute to ligand binding [112], and this is likely to require interactions between the Notch EGF repeats and some aspects of the Notch ligand.

We propose that a parallel complex may be consistently applied to both *trans*-activation and *cis*-inhibition, by using a two interconverting complex state model with the triple stranded arrangement as shown in Figure 5-13C. In this proposed model, parallel complexes are formed to achieve *cis*-inhibition, as in the previous proposed model. However, in contrast to the previous model, trans-activation is achieved when the Notch ligand binds to a triple stranded Notch receptor to form parallel complexes. In *trans*-activation, stabilization of the lower part (EGF16-36) of the binding complex is important. If the bond strength of this region is not strong enough, the whole structure would be unclipped when endocytosis pulls out the binding complex. The region around *Abruptex* domain may play a role in stabilizing the docking of a Notch ligand to Notch binding pocket.

Role of O-fucosylated glycans on Notch-Notch ligand binding- In our model, EGF11-12 domains of Notch receptor as the site for the initial recognition of Notch by a Notch ligand. Although mutation of the *O*-fucosylation site in EGF12 of Notch receptors alters ligand binding and signaling [85, 87, 112], the exact mechanism by which this occurs is not known. It has been proposed that the *O*-fucosylated glycan does not directly contact the ligand, since protein structure studies show that the *O*-fucose of EGF12 is on the opposite site of the proposed binding surface of Notch receptor [158]. Since the *O*-fucose on EGF12 is a poor substrate for Fringe [87], and since Lfng modification of Notch1 containing EGF 1-15 does not affect the ligand binding in our experiments, we propose that the Fringe action on the binding domain of Notch1 receptor (i.e EGF12) has no significant effect on ligand binding. However, the mechanism by which this *O*-fucose in the binding domain of Notch receptor alters ligand binding is unknown. Though speculative, it is possible that *O*-fucose on EGF12 interacts with EGF6-9, but not directly Notch ligand [112], and in doing so, disturbs the upper part (EGF1-15) of triple stranded structure, and the binding pocket of the Notch binding region, and thereby reduce ligand binding.

We found that Notch1 EGF domains 16-36 modulate both the binding (step 1) and conformational change (step 2) in our 2 stage model. EGF domains 16-36 are of interest because they encompass an *Abruptex* domain, which plays a prominent role in regulating Notch signaling events. The literature concerning the role of the *Abruptex* domain and of the *O*-fucosylated glycans on *Abruptex* is inconsistent, because both decreased and increased Notch activation have been observed in studies where the *Abruptex* domain has been mutated [85, 156, 157, 176-178].

Elimination of the *O*-fucosylation site in EGF26 of mouse Notch1 receptor via point mutation of the *O*-fucosylated serine increased Notch signaling elicited by Dll-1 and Jag-1 binding [87]. In our studies of the same EGF26 mutation, we observed increased Dll-4 binding in the absence of *O*-fucosylation, relative to binding to wild type Notch1. These observations indicate that *O*-fucose in the *Abruptex* domain conveys as an inhibitory influence on Notch1 ligand binding, and thus inhibits Notch1 signaling.

In this work, we observed that Fringe modification of Notch1 alters the binding of Delta significantly. By contrast, Fringe modification of Notch1 does not alter binding by Jagged 1 or 2. These observations imply that Fringe modification of Notch EGF domains 16-36 can strongly modulate the biological consequences of Dll-1 and Dll-4 interactions, but not of Jag-1 or Jag-2 interactions. Fringe-modified Notch receptor is characterized by enhanced formation of low-affinity complexes, and slow conversion from low-affinity complexes to high-affinity complexes. Since Fringe modified Dll-4 also has the increased binding ability to Notch1 receptors, indicating Fringe extension is involved in binding, not maintaining the overall structure of Dll-4. Fringe modification may mainly alter the binding, but not maintain the overall structure of Notch receptor or Notch ligands although we cannot exclude the possibility that the *Abruptex* domain is structurally correlated with NLR.

Taken together, *O*-fucosylation of the *Abruptex* region may inhibit the ligand binding, while Fringe modification on *O*-fucose may increase the ligand binding, but still serve as an inhibitory domain to reduce the formation of high-affinity Notch-Notch ligand complexes.

Our model can be interpreted to be consistent with our mutational study and mutational studies of others. We propose that the effect of mutations in the *Abruptex* domain depends on the type of mutation. Point mutation of the *O*-fucosylation site would increase the binding and signaling by removing the inhibitory molecule (i,e, fucose), while point mutation of the cysteine residue, or missense mutation would reduce binding by inducing a distortion of triple stranded structure. Deletion mutation of some of the *Abruptex* domain would hyperactivate Notch signaling by removing the inhibitory domain.

Delta and Jagged- Delta and Jagged hierarchically modulate the Notch binding with the combination of Fringe modification [124]. Mammalian Delta ligands (Dll-1 and Dll-4) have 8 EGF repeats and Jagged ligands (Jag-1 and Jag-2) 16 EGF repeats. In Jagged, 9th EGF domain and 10th EGF domain are separate by short linker peptides. Notch ligands have also calcium binding EGF and interestingly the first and second EGF domain of all of Notch ligands except Dll-3 are non-calcium binding domain, suggesting that this region is flexible and the relative orientation of DSL domain is free. These first and second EGF repeats are called DOS (Delta and OSM-11-like proteins) domain, which is involved in receptor binding along with DSL domain [179, 180]. The mutation study indicated that the integrity of DSL and DOS domain is required for the Notch binding, indicating DOS domains play a role in facilitating DSL binding to Notch receptor [65].

The EGF11-12 domains of Notch receptor would bind to the DSL domain of Notch ligand, suggesting that the DSL domain would dock in-between two EGF domains of Notch receptor. In here, two EGF domains of Notch receptor may form one binding

site for the DSL domain or one EGF domain. Consistent with this implication, the maximum number of DSL and/or EGF domain to fit within the binding pocket of Notch1 receptor might be 10 DSL and/or EGF domains because EGF11-21 domains of Notch1 receptors would form 10 binding sites (Figure 5-13A).

Previous studies and this study found that the whole domain of Notch is involved in the binding [112], indicating that the whole EGF domain of Delta and at least the first 9 EGF domains of Jagged would contribute to the binding. Due to this structural difference, Delta and Jagged might have a distinct binding capability in physiological contexts. Fitting of the first 9 EGF repeats of Jagged to the Notch binding pocket may be tight compared to the fitting of 8 EGF repeats of Delta. In consequence, the interaction between Notch and Jagged may be weaker than that of Notch and Delta.

It has been proposed that Dll-4 expression is essential in thymus epithelial cells (TECs) for T cell development in vivo, but not Dll-1 expression, indicating that the function of Dll-1 and Dll-4 are different in vivo [122, 162, 163]. However, it remains to be determined why these two ligands are not functionally equivalent in vivo.

Both Dll-1 and Dll-4 have *O*-fucosylation sites in EGF repeat 8 and 9, which may contact with the EGF repeat 24 of Notch1 receptors as shown in Figure 5-13B. Dll-4 has one more potential *O*-fucosylation site compared to Dll-1, which may contact with EGF26 and/or 27 of the *Abruptex* domain in Notch1 receptors. This raises the possibility that the *O*-fucosylation site in EGF 5 of Dll-4 is a distinct site compared to Dll-1 *and* may play a role in Notch binding.
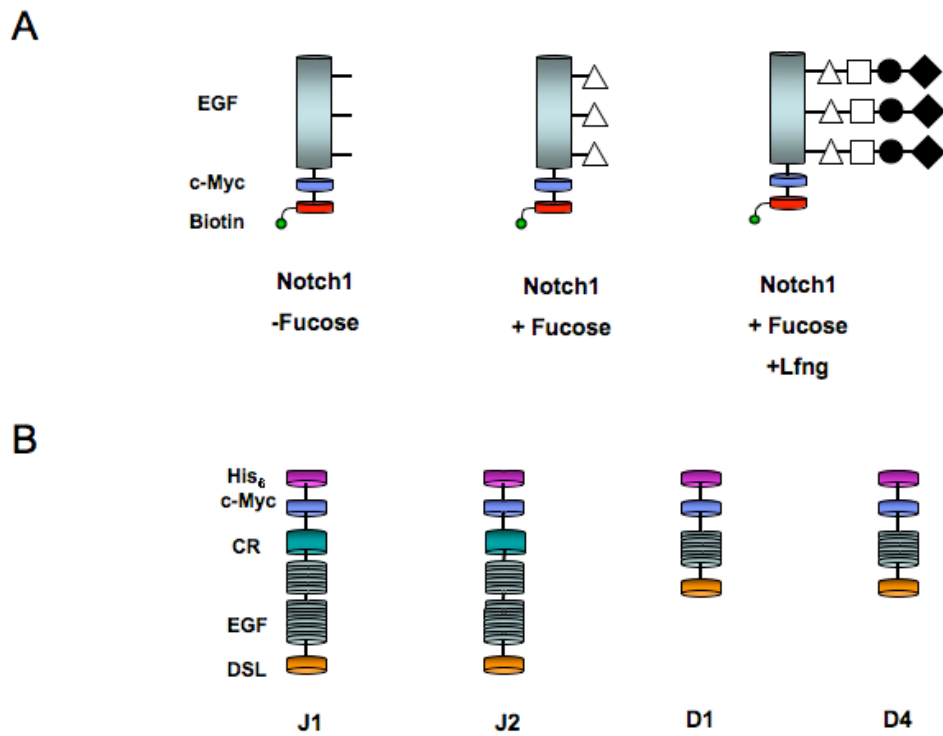
Figure 5-1. Reagent configuration. A. EGF1-36 of Notch1 was fused to c-Myc tag and biotinylation tag. Soluble Notch1 was expressed from CL17 cells with or without fucose and in CL17/Lfng with fucose. B. Extracellular domain of Notch ligands (J1, J2, D1, and D4) was fused into c-Myc tag and His tag. Soluble Notch ligands was expressed from HEK 293T cells.
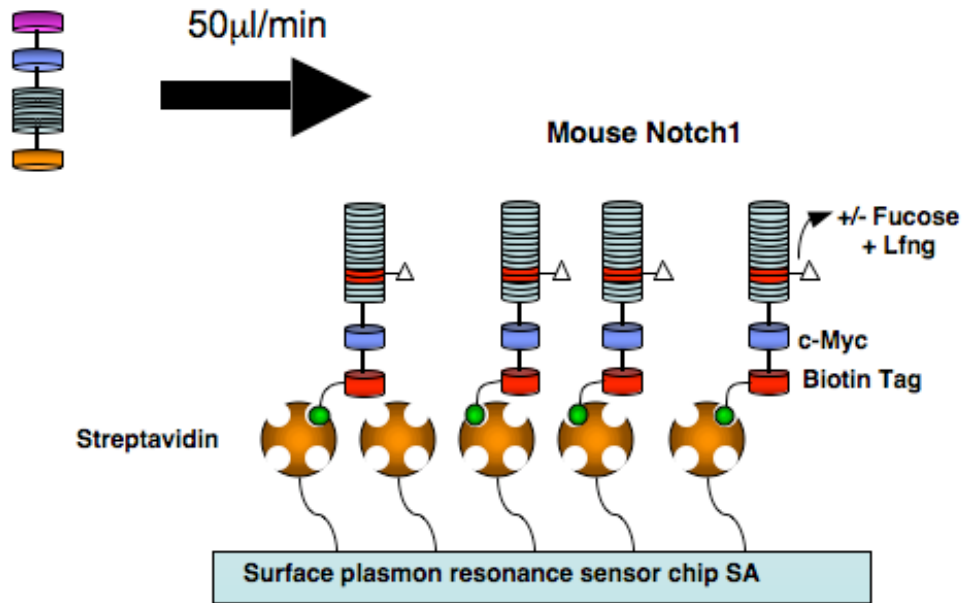
Figure 5-2. SPR experimental setup. Soluble mouse Notch1 receptors were immobilized through streptavidin and biotin bond on the Biacore sensor chip SA. Monomeric Notch ligands were injected at the speed of 50μl/min over the Notch1 immobilized surface to analyze the binding kinetics of Notch1-Notch ligands.
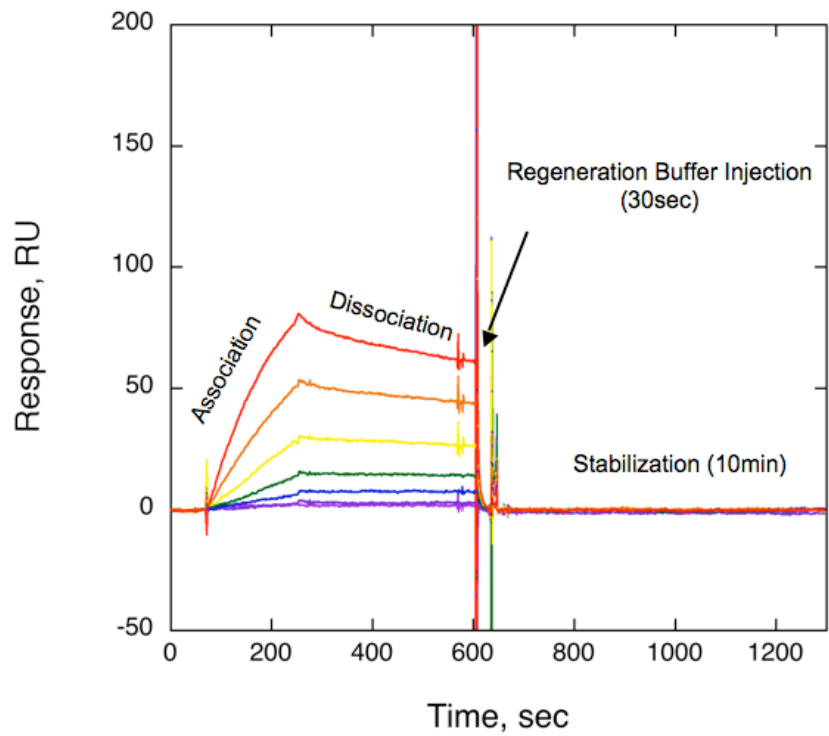
Figure 5-3. Evaluation of regeneration condition. Regeneration buffer (0.5M NaCl, 0.01% Triton X-100, 10mM Hepes, and 3% EDTA) is injected for 30 seconds after the dissociation phase. After the injection, the response level was back to the background level.
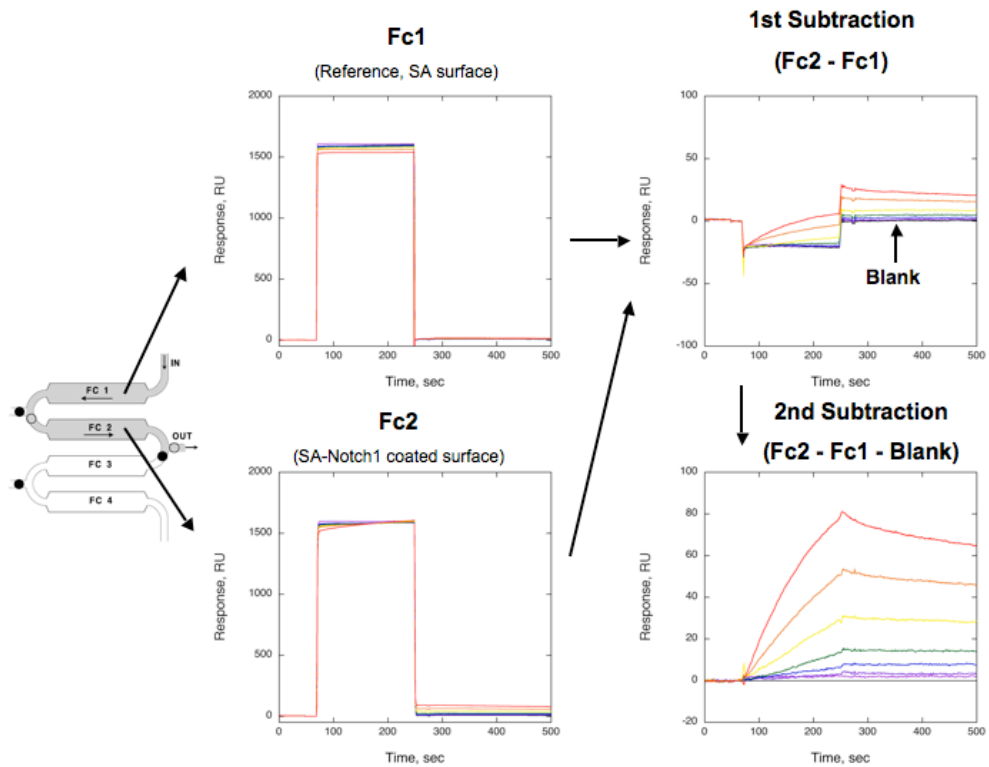
Figure 5-4. SPR data analysis with double subtraction. Signals are recorded from reference channel (Fc1) and soluble Notch1 immobilized channel (Fc2) when the Notch ligand is injected. The first subtraction is carried out by calculating the difference of Fc1 and Fc2 to remove the background. Subsequently, the second subtraction is performed by subtracting the signal from blank injection to set the blank reaction to zero.

Figure 5-5. Binding model determination. A. Biphasic pattern in association and dissociation phase of Notch1+fucose and Dll-1 binding. Dll-1 was injected over Notch1+fucose immobilized surface with different concentration. In the arrowed region, biphasic pattern was observed. In association phase, binding is initially fast and then slowed down. In dissociation phase, dissociation is fast and then slow. B. Biphasic pattern in association and dissociation phase of Notch1+fucose and Dll-4 binding. Dll-4 was injected over Notch1+fucose immobilized surface with different concentration. In the arrowed region, biphasic pattern was observed. In association phase, binding is initially fast and then slowed down. In dissociation phase, dissociation is fast and then slow. C. a 1:1 Langmuir binding model. For Notch+fucose and Dll-4 binding, 1:1 Langmuir binding model was applied. χ^2 is 39.1. D. a two interconverting receptor binding model. For Notch+fucose and Dll-4 binding, two-state binding model was applied. χ^2 is 2.4. E. a two non-interconverting receptor binding model. For Notch+fucose and Dll-4 binding, a two non-interconverting receptor binding model was applied. χ^2 is 23.5. F. a bivalent ligand binding model. For Notch+fucose and Dll-4 binding, a bivalent ligand binding model was applied. χ^2 is 35.1.
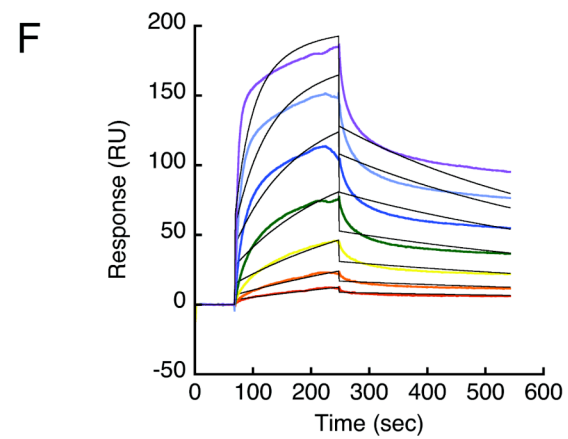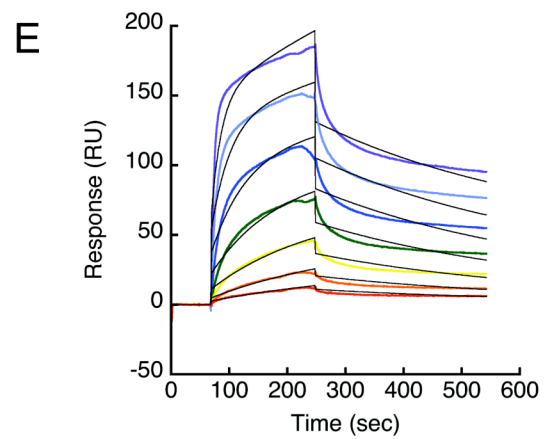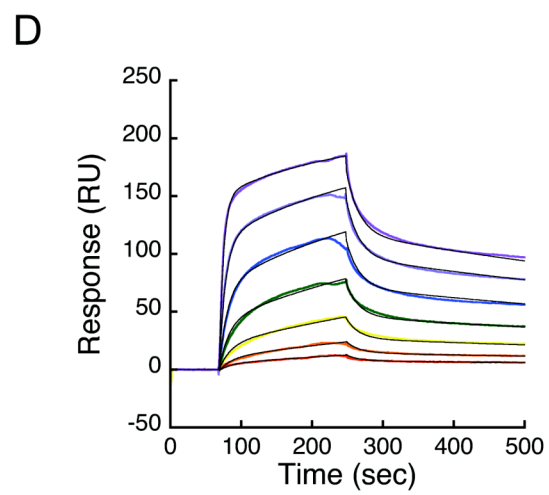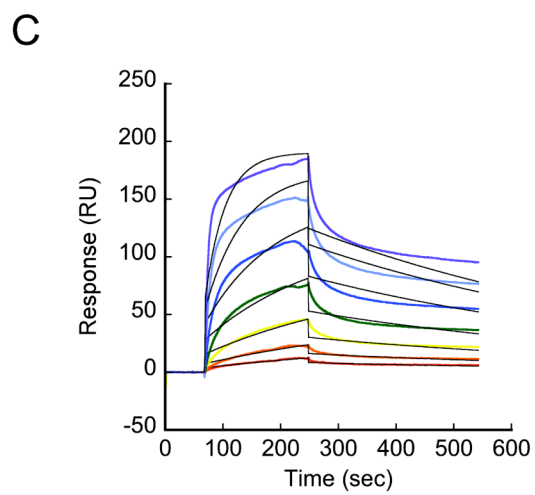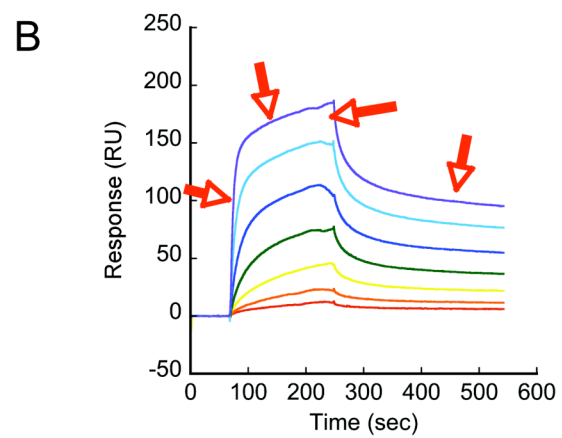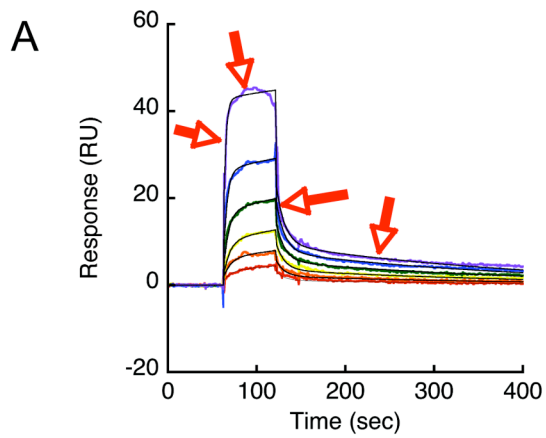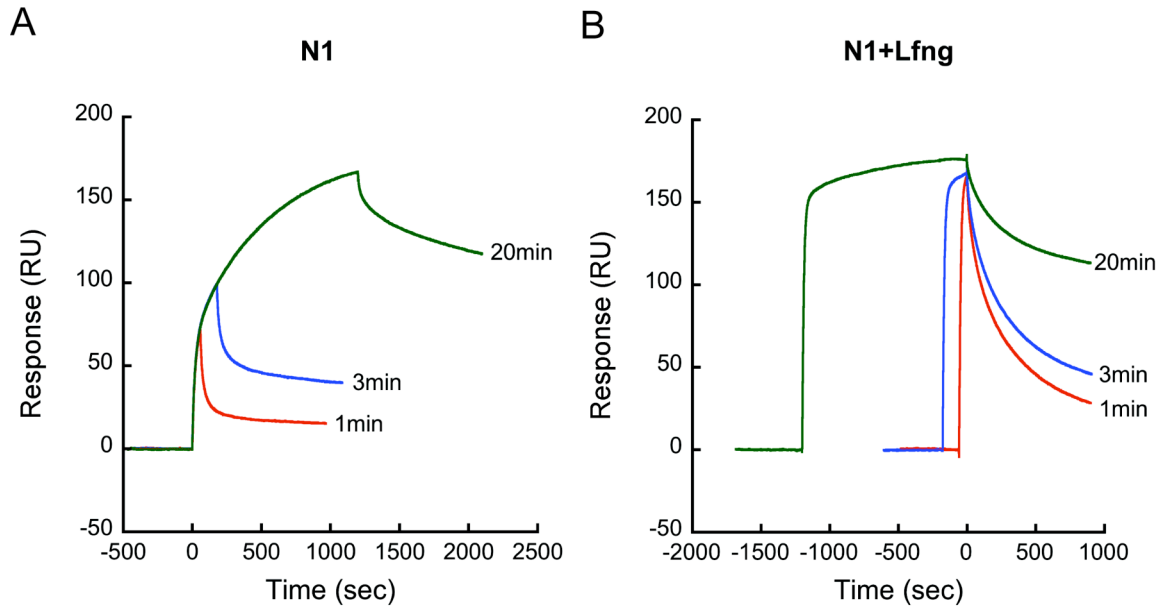
Figure 5-6. Conformational change in Notch1 and Dll-4 binding. A. Sensorgram of Dll-4 binding to wild type Notch1. Dll-4 was injected to wild type Notch1 with three different injection times (1, 3, and 20 minutes). The binding complex is more stable with the long injection time. B. Sensorgram of Dll-4 binding to Notch1+Lfng. Dissociation phase is different with the different injection time, although Dll-4 binding in the association step reaches the similar binding level.
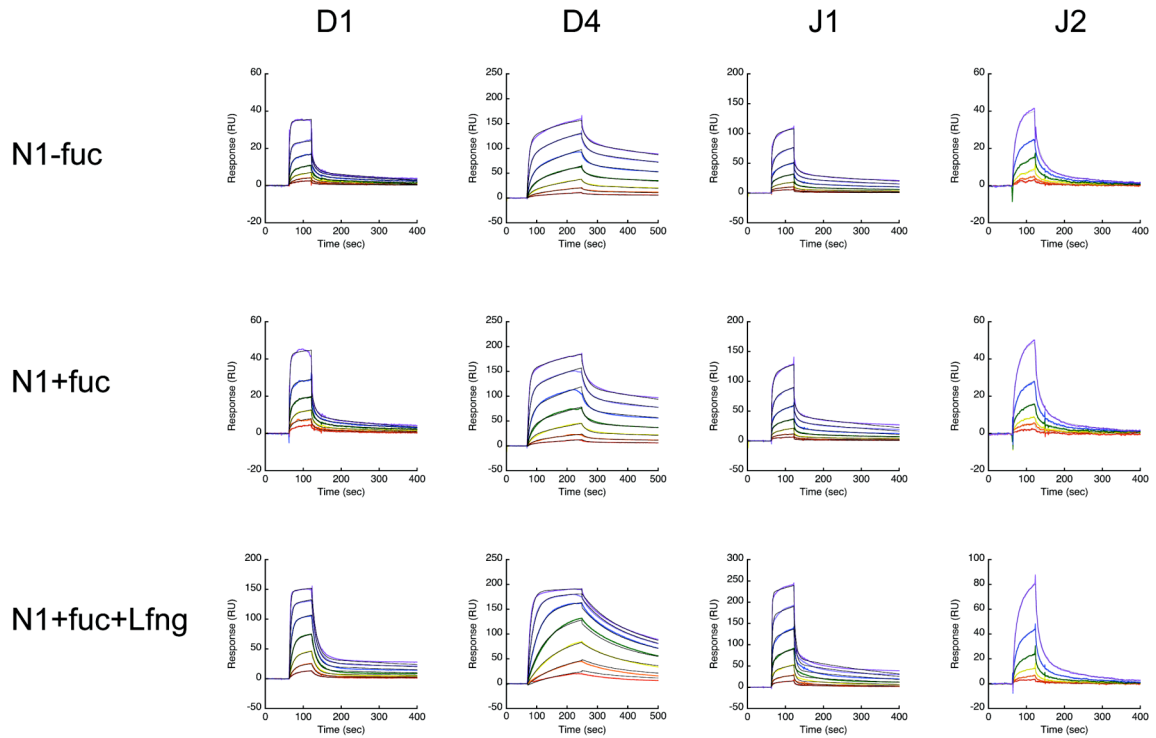
Figure 5-7. Representative sensorgram of Notch1-Notch ligand binding. Notch ligands, Dll-1, Dll-4, Jag-1, and Jag-2 were injected to the Notch1 immobilized surface. Dll-1, Jag-1, and Jag-2 were injected for 1 minute, while Dll-4 for 3 minutes because of the relatively slow association. Dissociation phase was held for 5 minutes. Purple line is the highest concentration (Dll-1:1μM, Dll-4:1.3μM, Jag-1:2.3μM, and Jag-2:1μM) and subsequent lines are diluted by factor 2.
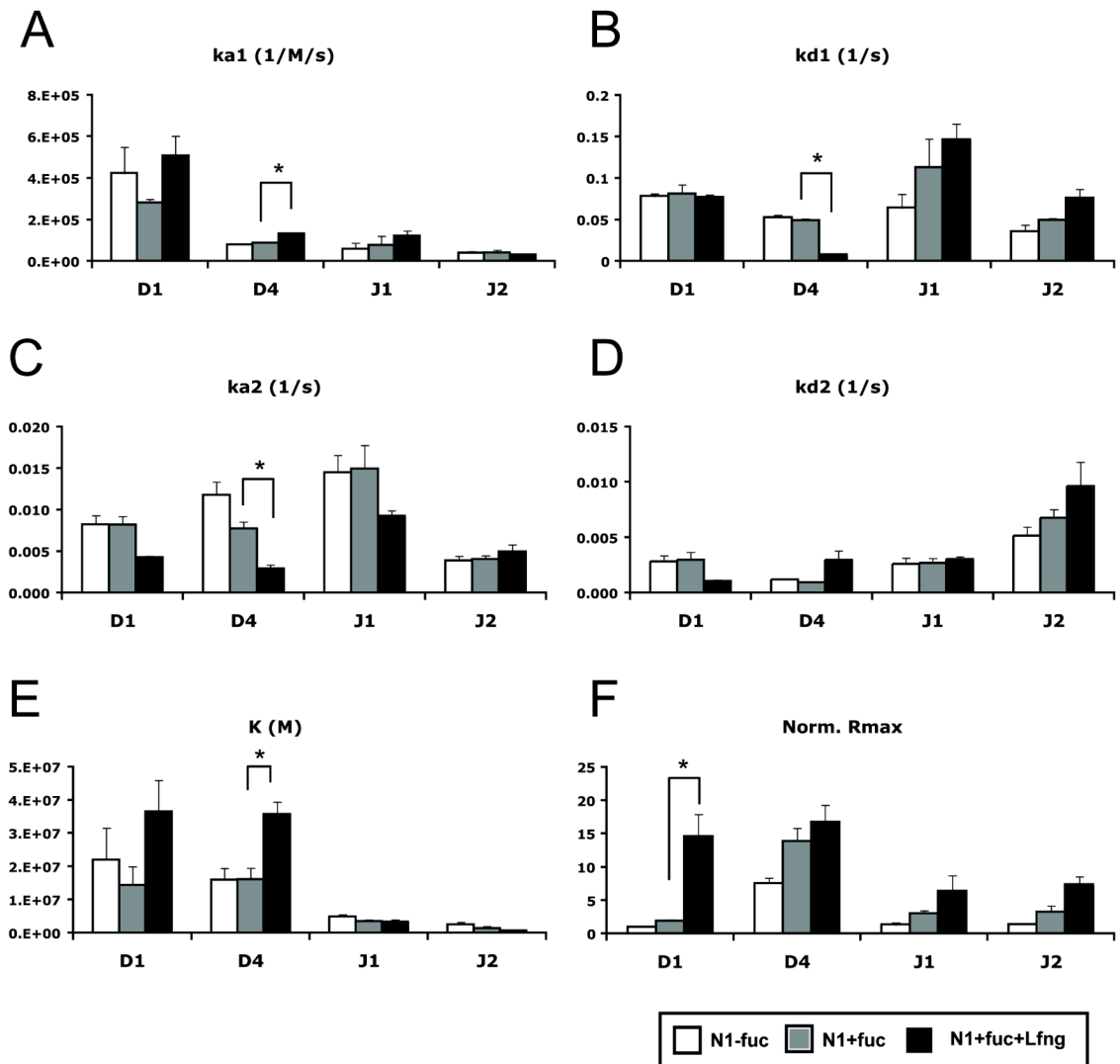
Figure 5-8. Kinetic analysis of Notch1-Notch ligand binding. A. ka1 (first association rate). B. kd1 (first dissociation rate). C. ka2 (second association rate). D. kd2 (second dissociation rate). E. K (overall association constant). F. Normalized Rmax (i.e. relative number of Notch ligand per immobilized Notch1). Rmax (maximum binding capacity) was estimated from the curve fitting procedure with the two state model of BiaEvaluation software. Normalized Rmax was calculated by dividing the estimated Rmax with the immobilized Notch1 on the surface and the molecular weight of each Notch ligand. The kinetic information was calculated with two-state binding model $A + B \underset{kd1}{\overset{ka1}{\longleftrightarrow}} AB \underset{kd2}{\overset{ka2}{\longleftrightarrow}} AB^*$. The value obtained from Dll-1-fucose was set as 1. All experiments were performed at least 3 times. Data are shown as the mean±SE. *, statistical significance ($P<0.05$).
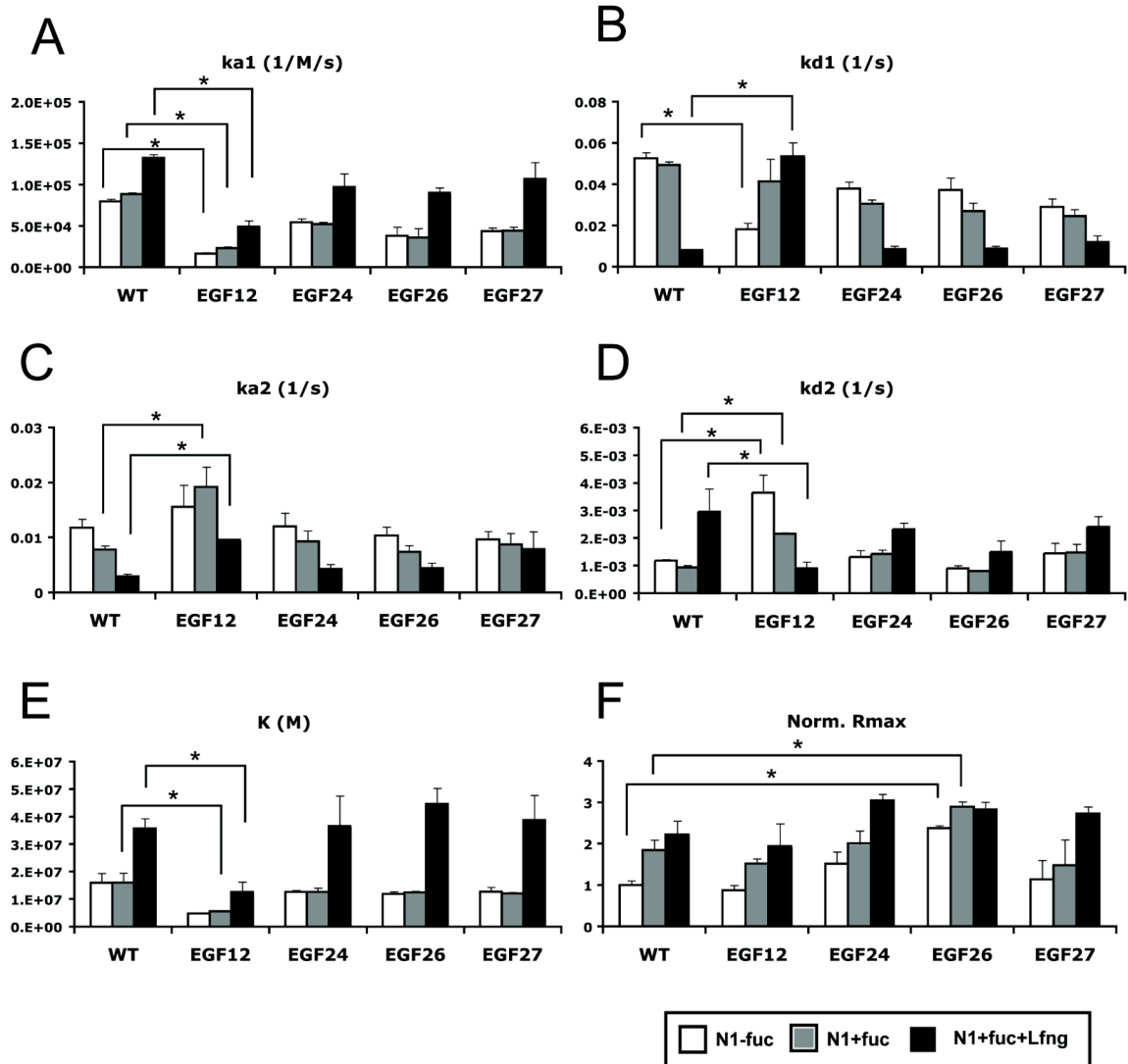
Figure 5-9. Kinetic analysis of Notch1 mutants and Dll-4 binding. A. Notch mutants. B. First association rate. C. First dissociation rate. D. Second association rate. E. Second dissociation rate. F. Association constant. G. Normalized Rmax. Rmax was estimated from the curve fitting procedure with the two state model of BiaEvaluation software. Normalized Rmax was calculated by dividing the estimated Rmax with the immobilized Notch1 on the surface and the molecular weight of D4. The value obtained from Dll-4-fucose was set as 1. All experiments were performed at least 3 times. Data are shown as the mean±SE. *, statistical significance ($P<0.05$).
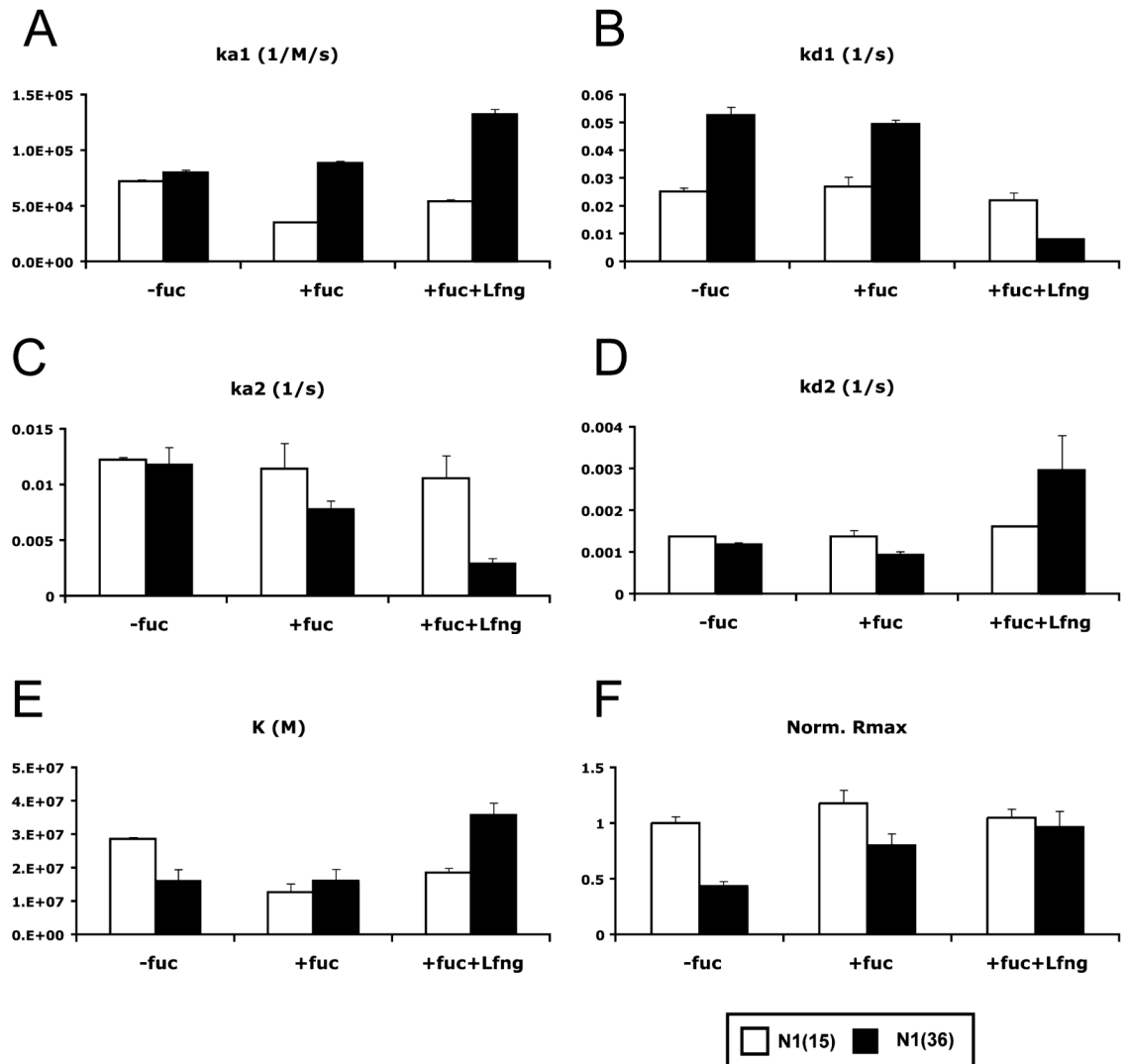
Figure 5-10. Kinetic analysis of Dll-4 to Notch(15) and Notch1(36) binding. A. First association rate. B. First dissociation rate. C. Second association rate. D. Second dissociation rate. E. Association constant. F. Normalized Rmax. Rmax was estimated from the curve fitting procedure with the two state model of BiaEvaluation software. Normalized Rmax was calculated by dividing the estimated Rmax with the immobilized Notch1 on the surface and the molecular weight of D4. The value obtained from Notch1(15)-fuc was set as 1. All experiments were performed at least 3 times. Data are shown as the mean±SE. *, statistical significance ($P<0.05$).
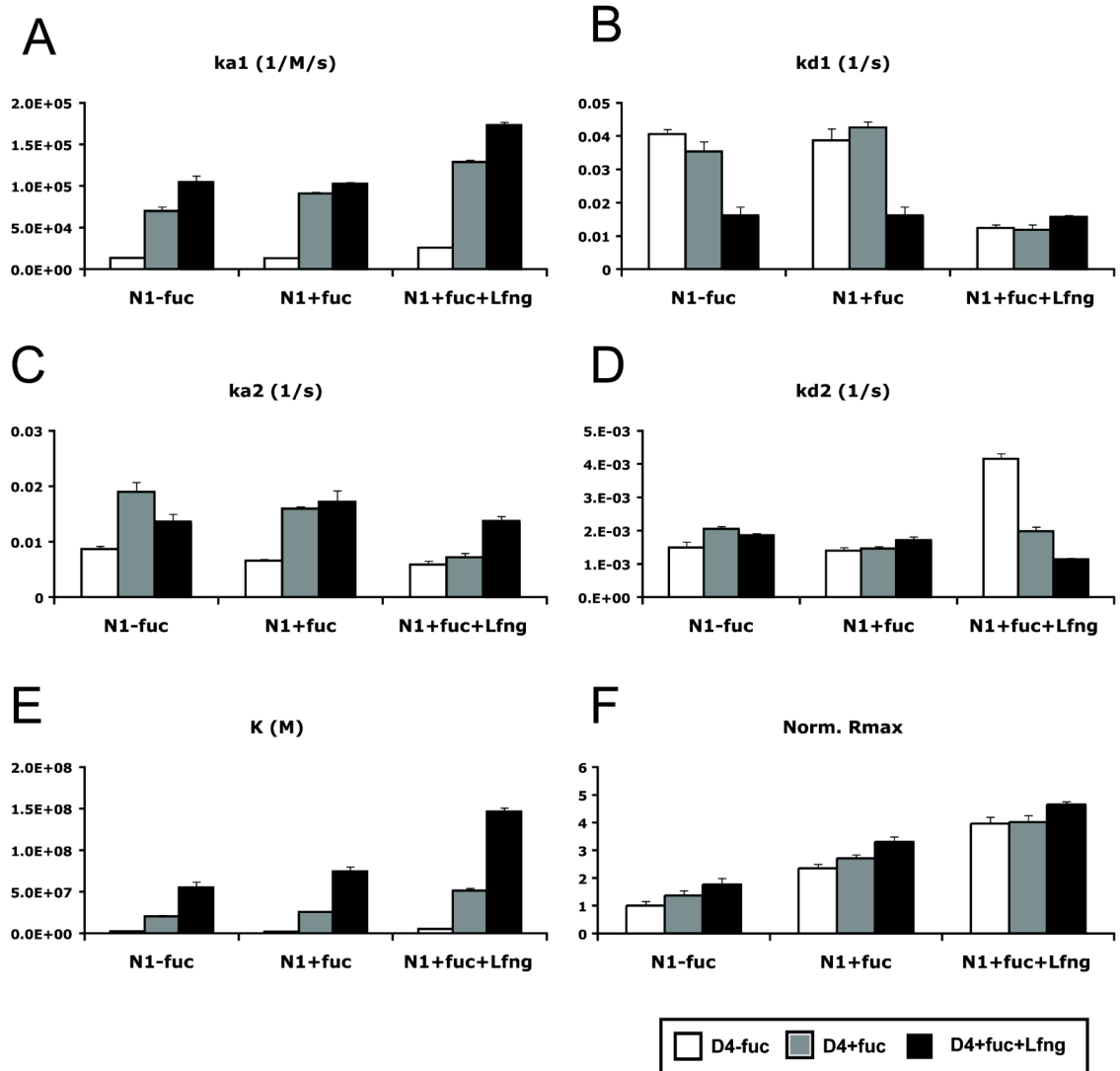
Figure 5-11. Kinetic analysis of Notch1-Dll-4 binding with different glycosylation status. A. First association rate. B. First dissociation rate. C. Second association rate. D. Second dissociation rate. E. Association constant. F. Normalized Rmax. Rmax was estimated from the curve fitting procedure with the two state model of BiaEvaluation software. Normalized Rmax was calculated by dividing the estimated Rmax with the immobilized Notch1 on the surface and the molecular weight of Dll-4. The value obtained from the binding of Notch1-fuc and Dll-4-fuc was set as 1. All experiments were performed at least 3 times. Data are shown as the mean±SE.
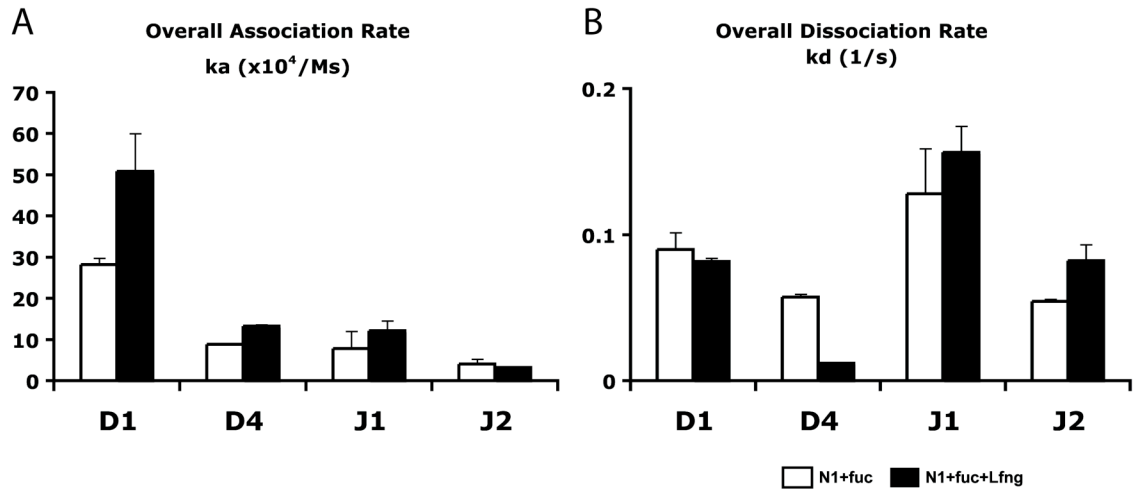
Figure 5-12. Overall association and dissociation rate of Notch-Notch ligand binding. A. Overall association rate of Notch ligands binding to Notch1+fucose or Notch1+fucose+Lfng. B. Overall dissociation rate of Notch ligand binding to Notch1+fucose or Notch1+fucose+Lfng.

Figure 5-13. Model for Notch-Notch ligand binding. A. Schematic of *O*-fucosylation sites and calcium binding sites of mouse Notch ligands and mouse Notch1 receptors. *O*-fucosylation sites are predicted with broader consensus sequence ($C^2X_{4-5}S/TC^3$). Calcium binding EGF domains were adopted from SMART software. Red triangle denotes *O*-fucosylation sites. Hexagon is DSL domain of Notch Notch ligand, which is the binding site to Notch receptors. B. Two-state binding model with triple stranded structure. First, Notch ligand bind to Notch receptor via the binding region of Notch1 receptor and DSL domain of Notch ligand and subsequently EGF repeats of Notch ligand dock with lower part of the triple stranded structure of Notch receptor. Secondly, the Notch-Notch ligand binding complex adopts a conformational change to form the stable complex. C. Parallel model for both *trans*-activation and *cis*-inhibition. Solid circle in Notch1 receptor is the calcium binding EGF domain and white circle the non-calcium binding EGF domain.
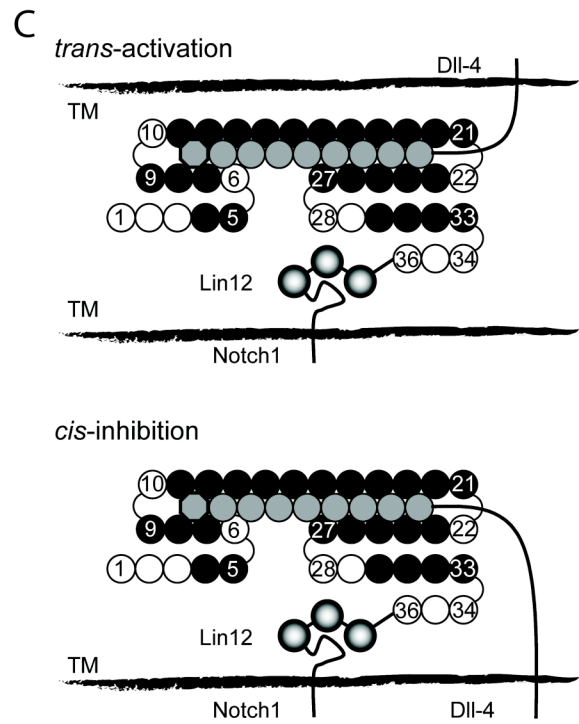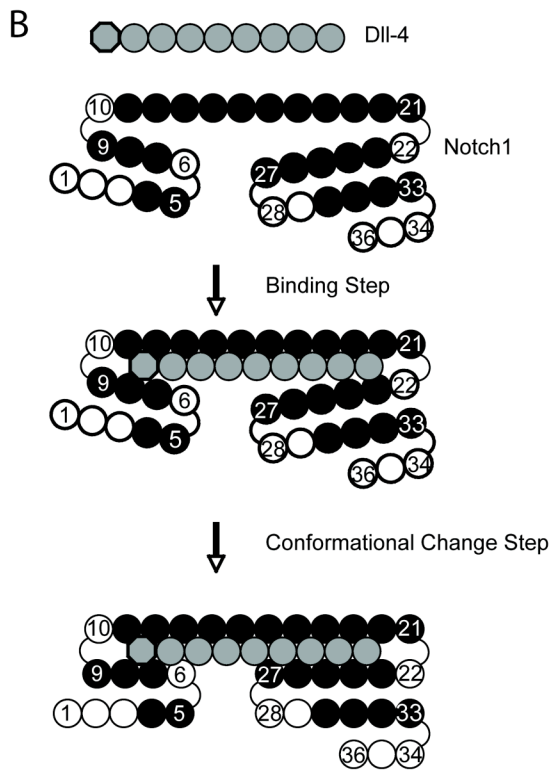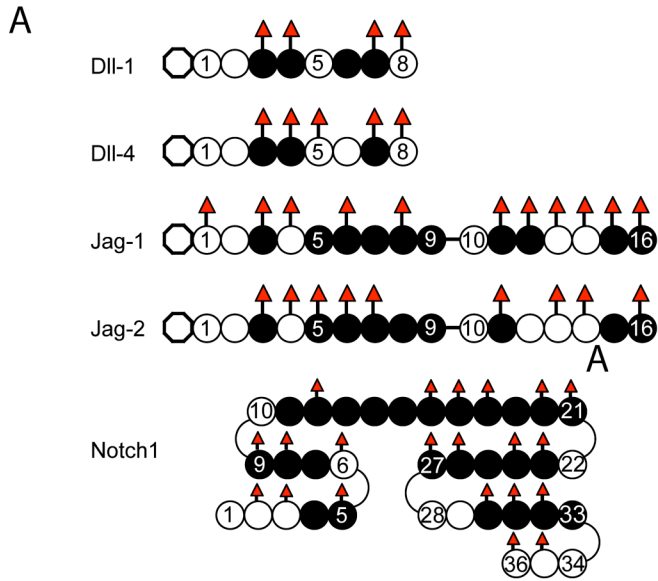
Chapter 6

Conclusions

Notch signaling is a very complicated cellular event because of the variety of Notch receptor and Notch ligand combinations, the involvement of complex glycosylation state such as unusual O-fucosylation, proteolytic events, endocytosis, and cross-talk with other signaling transduction pathway [181]. Notch signaling is involved in many biological contexts such as cancer, stem cell development [84, 182], and neural development. However, the molecular basis of Notch signaling mechanisms remains to be elucidated. In this work, OTs, AFM, and SPR experiment were performed to elucidate the characteristics of Notch-Notch ligand binding.

Direct Force Measurement by Force Spectroscopy

In Chapter 3 and 4, OTs and AFM systems were used to study the glycan-related Notch binding. These apparatuses have the capability to measure the single bond strength of the binding complex with pN resolution and successfully used in many biological systems such as DNA zipping and unzipping, DNA-protein interaction, protein-protein interaction, and cell adhesion.

Notch signaling is a force-induced event, where the force is generated by *trans*-endocytosis. Force causes the retraction of ECN, and subsequently induces a

conformational change of NLR to expose the S2 cleavage site for signal activation. The binding strength should be strong enough to endure this retraction and conformational process. As suggested in previous studies, *O*-fucosylated glycans play a role in modulating the binding and signaling of Notch transduction events. We hypothesize that *O*-fucosylated glycans regulate the strength of Notch-Notch ligand binding and finally signaling. We tested the applicability of OTs and AFM for the direct force measurement of Notch-Notch ligand bond. We found several issues from OT-based force measurement. The first issue was the optical interference. To generate the optical trap, the laser path should not be blocked. To probe the protein-protein bond, two objects immobilized with two proteins need to be in contact each other, causing the optical interference by objects such as beads. To prevent this interference, a special design would be required, but it would be expensive and difficult to characterize the coating of the proteins on the surface. Secondly, OTs are hard to generate forces exceeding 200pN because of the power limitation and heating. Therefore, the use of OTs is restricted when the binding strength is over 200pN, which frequently occurs when the multiple bonds of protein-protein binding or non-specific bonds are formed. However, AFM does not have these pitfalls and was successfully adopted to measure the single binding strength of Notch-Notch ligand binding complex. We found that *O*-fucosylated glycans of Notch1(EGF1-15) have no significant effect on binding to Dll-4, demonstrating that EGF1-15 repeats are not strongly modulated by Fringe modification and implying that EGF domains 16-36 are the major target for Lfng modification. This conclusion is consistent with the results from Chapter 5.

Kinetic Analysis of Notch-Notch Ligand Binding

Notch signaling mainly correlates with ligand binding [73]. In experiments we report here, we have sought to advance the understanding of how Fringe-mediated glycan modifications modulate the kinetics and affinities of the interactions between mouse Notch1 and its ligands, how distinct O-fucosylation sites on mouse Notch1 contribute to these binding interactions, and how Fringe-dependent glycan modification of Notch ligands themselves may modulate Notch receptor-ligand interactions, using surface plasmon resonance techniques. Efficient binding was observed between mouse Notch1 and the Notch ligands Dll-1, Dll-4, Jag-1, and Jag-2, but not between Notch1 and Dll-3. We observed a biphasic pattern of association and dissociation phases. If the conformational change is involved in the binding, the binding complex is more stable with time. To test this hypothesis, we carried out the linked reaction test with three different injection times. We found that the binding complex was more stable as the injection time was increased. A biphasic binding and dissociation pattern was observed with the four binding-competent Notch1-Notch ligand pairs, suggesting a two-state receptor-ligand interaction model characterized by initial formation of a transient receptor-ligand complex followed by a conformational change that leads to a more stable receptor-ligand complex. Here, the initial complex is rapidly formed and the intermediate binding state is then followed by the slow production of the tight complex.

We observed that the ratio of maximum binding capacity of Dll-1 to wild type Notch1 and Notch1+Lfng is about 1:8. Although we don't know the stoichiometry of the Notch-Notch ligand binding, we believe that this value doesn't reflect the altered

stoichiometry from the Fringe modification. However, this is typical in two state binding model [183].

Primary and secondary on and off-rates for the four binding-competent mNotch1-Notch ligand pairs were observed to be distinct and characteristic for each Notch ligand. The magnitudes of the overall association constants (K) generated by the Notch1-Dll-1 couple or the Notch1-Dll-4 couple were similar, and much greater than the overall association constants generated in couples involving mNotch1 and either Jag-1 or Jag-2. The overall association constants observed when Dll-1 or Dll-4 interacted with Fringe-modified Notch1 were significantly greater than when these ligands interacted with unmodified Notch1, with enhancement likely due to Fringe modifications of fucose moieties within EGF repeats 16-36 by altering both the binding and conformational step. By contrast, Fringe modification of Notch1 did not significantly modulate interactions with Jag-1 or Jag-2. Mutational analyses confirm prior observations that the *O*-fucosylation site within EGF repeat 12 dictates much, if not all of the binding between Notch1 and its ligands. Mutation in the *O*-fucosylation site in EGF repeat 26 of Notch1 receptor enhances the binding level of Dll-4, indicating *O*-fucosylation in EGF 26 is the inhibitory molecule to the ligand binding. Finally, we observe that Fringe modification of Dll-4 enhances its ability to bind to Notch1, demonstrating that Lfng is mainly the binding modulator.

We propose a two interconverting complex state model with a triple stranded structure. In this model, EGF repeats 10-21 form a rod-like shape and both EGF domains 6-9 and 22-27 are folded back against EGF repeats 10-21, forming a binding pocket when Notch1 binds to a Notch ligand.

This model can explain the *trans*-activation and *cis*-inhibition as shown in Figure 5-13C. In this proposed model, parallel complexes are formed to achieve *cis*-inhibition. *Trans*-activation is also achieved when the Notch ligand binds to a triple stranded Notch receptor to form parallel complexes.

O-fucosylated glycans may have two functions in Notch binding in this model. Firstly, *O*-fucosylated glycans in EGF12 of Notch1 receptor may stabilize the triple stranded structure because *O*-fucosylated glycans on EGF12 may interact with EGF6-9, but not directly Notch ligand, and in doing so, disturbs the upper part (EGF1-15) of triple stranded structure, and the binding pocket of the Notch binding region, and thereby reduce ligand binding. Secondly, *O*-fucose in the *Abruptex* domain is inhibitory, while Fringe extended *O*-fucose is a positive regulator for binding. Fringe modified *O*-fucose in the *Abruptex* domain appears to be critical in the binding by enhancing the formation of low-affinity complexes, and slow conversion from low-affinity complexes to high-affinity complexes. Since Fringe modified Dll-4 also has the increased binding ability to Notch1 receptors, indicating Fringe extension is involved in binding, not maintaining the overall structure of Notch receptors and Notch ligands, although we cannot exclude the possibility that the *Abruptex* domain is structurally correlated with other domains such as NLR.

In conclusion, the kinetics of glycan-dependent Notch-Notch ligand binding has been explored in Chapter 5. Our study of the kinetics of Notch-Notch ligand binding suggests a molecular basis for Notch-Notch ligand binding, and the role of glycans in binding. This work opens a new avenue to elucidate canonical Notch signaling.

Future Direction

There are still several key questions left to be investigated: force-induced Notch signaling, Notch or Notch ligand clustering, and the structure of Notch-Notch ligand binding complexes.

(1) Force-induced Notch signaling

Many studies have suggested that mechanical force may trigger the Notch signaling by inducing the decomposition of the NRR domain. There is evidence that conformational change induced by mechanical force is critical.

(i) Effect of immobilization and pre-clustering

Free ligands in solution are not capable of activating Notch signaling. This indicates that Notch signaling is not activated merely by binding to its ligand, suggesting that other factors are involved in the signaling process. It has been reported that immobilization or pre-clustering of Notch ligand is required for induction of Notch signaling [92]. In this experimental system, the other end of the immobilized or pre-clustered ligands is stationary and can support the pulling force if any force is produced. From the mechanical point of view, this is the only difference between free ligand and immobilized (or pre-clustered) Notch ligand systems. In other words, free ligand cannot retain the tension, but the supported ligand can. Although further studies are needed to elucidate the source of the mechanical force in immobilized (or pre-clustered) Notch

ligand systems (this will be discussed more in the next page), these *in vitro* data suggest that the mechanical force may contribute to the activation of Notch signaling.

(ii) Role of NRR domain

Calcium depletion dissociates the ECD and activates Notch signaling [184]. This suggests that conformational change of the extracellular domain of Notch can trigger ligand-independent activation by unfolding some calcium binding domains. Recently, the x-ray crystal structure of Notch1 NRR was reported. A key feature is a conserved hydrophobic plug that occludes the metalloprotease cleavage sites (S2 sites) by a steric mechanism [135]. A novel mutation (H1545P), which alters a residue at the LNR-HD interface, results in ligand-independent increases in signaling. Also, mutations in the calcium binding sites in the LNR domain gave the same result. Together, these mutations release the autoinhibitory clamp on the HD domain imposed by Lin12/Notch repeats.

In summary, S2 cleavage sites need to be exposed by the displacement of LNR modules away from the HD domain by the mechanical force for the Notch signaling.

This conclusion leads to the next question. What is the source of the mechanical force that activates the Notch signaling? Two external sources (*trans*-endocytosis and cell movement) and one internal force (conformational change) can be postulated.

(i) Trans-endocytosis

Endocytosis is required for Notch signaling. Notch1 receptors are physically dissociated by endocytosis before activating proteolysis can occur [89]. Endocytosis

produces the pulling force after the protein-protein complexes are formed. Endocytosis can provide the mechanical force to induce the conformational change of NRR domain.

An understanding of the magnitude of forces generated by endocytosis will help to increase our understanding of whether Notch-Notch ligand interactions are "stronger" than the force of endocytosis and thus allow endocytosis to "pull" a Notch-Notch ligand pair "away" from the cell surface to enable an S2 cleavage event by unclamping the NRR domain.

(ii) Membrane tension

Exposure of cultured cells to the mechanical stimuli and matrix stiffness or elasticity is sufficient to induce endocytosis by altering the membrane tension [185-187]. In *in vitro* cell culture systems, cells are in direct contact with the immobilized proteins on the surface of the culture dish, which has a specific stiffness. This environment causes the alteration of the membrane tension and induces endocytosis or exocytosis which may generates the mechanical force to activate the Notch signaling.

(iii) Cell movement

To our knowledge, there is no report that cell movement can generate the force, which can induce the conformational change in protein-protein complexes. However, during cell movement, forward and rearward traction forces are distributed on the cell surface, which are measured by the micromachined devices [188, 189] and traction force microscopy [190-192]. Moreover, the mechanical environment induced by matrix elasticity [185] and tensile force [193] plays a critical role in cell function. This suggests

the possibility that traction force or protrusion force generated by cell movement between the cells or on the ligand immobilized surface can induce the conformational change of Notch1 NRR domain to expose the S2 cleavage site for the metalloprotease enzyme.

(iv) Conformational change of Notch-Notch ligand binding complexes

It has been reported that the conformational change of protein structure can generate mechanical force. For example, in G-protein, the force is transduced by changes in the configurational space of the protein produced by substrate hydrolysis [194]. Also, ligand binding induced conformational change can generate mechanical force. For example, a two-step binding mechanism was proposed for T cell receptor recognition of peptide-MHC [195-199]. The mechanical force caused by binding pulls the TCR-CD3 complexes towards the APC in a piston-like movement [196, 199]. The resulting change in the positions of transmembrane and/or cytoplasmic portions of TCR-CD3 relative to the membrane could result in conformational changes in the TCR-CD3 cytoplasmic tails such as exposure of the Nck-binding site on CD3ε [196, 199].

In this study, we propose that the mechanism of Notch-Notch ligand binding can be explained by the two-step binding mechanism, which consists of a binding step and a conformational change step. Although, there is no direct evidence of force-induced Notch signaling, it is possible that conformational change of Notch-Notch ligand components can produce the mechanical force to unplug the HD domain from the LNR domain.

In summary, mechanical force appears to contribute to the Notch activation. The mechanical force might be generated from trans-endocytosis, membrane tension, cell

movement, and/or conformational change of protein complexes. The binding force of Notch-Notch ligand needs to be stronger than ligand binding induced mechanical force to unclamp of the NRR domain. This bond strength is hierarchically modulated by the combination of Notch ligand and Fringe action. Recent progress in force spectroscopy technology opens the door to study the very small mechanical force generated by the single biomolecule. Using the force spectroscopy such as AFM and OTs, the force-induced Notch signaling can be probed.

(2) Notch receptor and Notch ligand clustering

In many signaling transduction systems, protein clustering is critical to magnify the signal. One well-established clustering system is the immunological synapse formation. T-cell activation requires clustering of a threshold number of T-cell receptors (TCRs) at the site of antigen presentation, a number that is reduced by CD28 co-receptor recruitment of signalling proteins to TCRs. It was demonstrated that deficiency in beta1,6 N-acetylglucosaminyltransferase V (Mgat5), an enzyme in the N-glycosylation pathway, lowers T-cell activation thresholds by directly enhancing TCR clustering. *Galectin-3* was associated with the TCR complex at the cell surface, an interaction dependent on Mgat5. A galectin-glycoprotein lattice strengthened by Mgat5-modified glycans restricts TCR recruitment to the site of antigen presentation, *i.e.* Mgat5 enhances the TCR clustering [95]. These data suggest that the glycan may modulate receptor clustering.

Several studies reported that Notch signaling is density- or dose-dependent [93, 200], suggesting that there is a threshold level of Notch signaling [124]. These data imply that the Notch receptor and/or Notch ligand clustering facilitate Notch signaling, but not

simply the dimerization of Notch receptors on the cell surface [201]. However, It is not reported yet whether Notch clustering is facilitated by a glycan and/or lectin.

Two mechanisms were proposed for the role of endocytosis in ligand expressing cells. The first mechanism is that the endocytosis pulls the Notch ligand after it binds to Notch receptor as discussed above. Secondly, ligands are endocytosed and then re-trafficked to the cell surface as an activated and mostly clustered form. However, there is no direct evidence for an effect of ligand clustering on Notch signaling.

In summary, Notch and Notch ligand clustering might be modulated by glycans. Using the single biomolecule detection system, glycan-dependent Notch and Notch ligand clustering can be investigated. This will give new insight about the role of glycans in receptor clustering for signal activation.

(3) Structure of the Notch-Notch ligand binding complex

To understand Notch signaling, it is important to know the molecular basis of Notch-Notch ligand binding. Because of the difficulty associated with obtaining a crystal of the transmembrane protein, the structure of the binding region of Notch and Notch ligand have been explored. The crystal structure of the human Notch1 ligand binding region (EGF11-13) shows a rod-like shape rigidified by calcium, which is very similar to well-studied calcium binding EGF domains, but the angle of tilt is significantly different [173]. EGF repeats of Notch also include non-calcium binding EGF domains. The combination of calcium binding domain and non-calcium binding domain give the unique structure to the EGF bearing proteins. Several studies suggested the importance of calcium binding domains for the protein structure containing EGF repeats [158, 174,

202]. In NMR studies of a pair of tandem EGF domains from *Plasmodium falciparum* merozoite surface protein-1, the linker between two non-Ca^{2+} biding EGF domains bends, and the EGF domains pack against each other along their length. Finally, this gives the protein a U-shaped overall structure [202]. Following this result, "triple-stranded" structure was proposed for the Notch structure [112]. In this model, EGF10-21 will form a long rigid chain, with EGF6-9 and EGF22-26 folded back against them and EGF1-5 and EGF 27-33 involved in a strand displacement process after ligand binding [112]. This creates the possibility that strand displacement of the EGF22-33 domain would effect a conformational change as proposed in this work. The location of *Abruptex* domain suggests that they could play a role in conformational change with Fringe modification on this region. To understand the exact molecular mechanism of Notch-Notch ligand binding, the structure of the Notch-Notch ligand binding complex needs to be explored. Also, the stoichiometry of Notch-Notch ligand binding remains to be investigated.

Appendices

1. Automated AFM data analysis program

```
% AFM
clc;
clear;
filenameo= ['040706004'];
springcons=20;        %Spring Constant pN/nm
m=-57.5; % use when mon=0
%----------
sepcutoff=30;        %Separation cut-off
forcecutoff=10;        %Force cut-off
samplenumber=512;                %Sampling number
totalsample=2*samplenumber;
scansize=256;                %Force volume size 256=16x16
rampsize=256;                 %Ramp size nanometer
itvr=10;      %t-test points
tvrcf=8;      %t-value cut-off for rupture
sepwlccutoff=10;      %Separation cut-off for WLC model curve fitting
tvrcfs=1.9;      %t-value to determine the starting point for WLC model curve fitting
iunclerupture=-8;
ifitexp=10;                % index for loading rate curve fitting
nomaxrup=3;                 % tolerance for the maximum rupture force
wdforcediff=15;            % force difference after rupture
contourlow=30;                % cutoff of contour length for the WLC model
contourhigh=130;
stddiffrupstancutoff=1.5; % stadard error cutoff for matching with the WLC model
wlcintercutoff=-10;
%----------
convfactor=17.219;        %converting from bit to nanometer
convfactor2=0.1156531;      %converting from volt to nanometer
filename=cellstr(filenameo);
filenamesize=size(filename);
nfile=filenamesize(1,1);
clc;
clear origdata originaldata data1;
filenameinput=char(filename(1,1))
origdata = textread(filenameinput,'%s');
xn=length(origdata);
nonb=0;
nonsb=0;
nowd=0;
for ii=1:50000
    forw='\Forward';
    vel='vel.:';
    forwcom=strcmp(forw,origdata(ii,1));
    velcom=strcmp(vel,origdata(ii+1,1));
    if (forwcom==1)&(velcom)==1
```

```matlab
            forwardvelvolt=str2double(origdata(ii+2,1));
            forwardvel=forwardvelvolt/convfactor2;
            break
        end
    end
end
for ii=1:50000
    rev='\Reverse';
    vel='vel.:';
    revcom=strcmp(rev,origdata(ii,1));
    velcom=strcmp(vel,origdata(ii+1,1));
    if (revcom==1)&(velcom)==1
            reversevelvolt=str2double(origdata(ii+2,1));
            reversevel=reversevelvolt/convfactor2;
            break
    end
end
for ii=1:100000
    list='list';
    endofdeader='end';
    listcom=strcmp(list,origdata(ii,1));
    endcom=strcmp(endofdeader,origdata(ii+1,1));
    if (listcom==1)&(endcom==1)
            indexofdata=ii+1;
            break
    end
end
startindex=indexofdata+1;
data1(:,1)=str2double(origdata(startindex:xn,1));
total_data_number=xn-indexofdata;
ndata1=numel(data1);
dt=ndata1/samplenumber;
for ii=1:dt
        originaldata(ii,:)=data1((ii-1)*samplenumber+1:ii*samplenumber);
end
if total_data_number~=ndata1
    disp('total_data_number and ndata1 are not same!')
%       break
end
inipoint=2*scansize+1;
iquit=0;
for i=1:scansize;
if iquit==1,break,end
%Loading data
dtpos=2*(i-1)+inipoint;
rawdata1=originaldata(dtpos,:);
rawdata2=originaldata(dtpos+1,:);
rdata=[rawdata2';rawdata1'];
incr=rampsize/samplenumber;
displace1=(0:incr:samplenumber*incr-incr);
displace=[displace1';displace1'];
totaltime=rampsize/reversevel;
```

138

```
timeincr=totaltime/samplenumber;
timecourse1=(0:timeincr:samplenumber*timeincr-timeincr);
%Calculate the Force
def=(rdata./-m);
defavg=mean(def((samplenumber-20):(samplenumber-2)));
relsep=displace+def;
avgsep=mean(relsep(1:10));
sep=relsep-avgsep;
force=springcons*(def-defavg);
%Split the data to approch and retraction
force1=force(1:samplenumber);
force2=force(samplenumber+1:totalsample);
sep1=sep(1:samplenumber);
sep2=sep(samplenumber+1:totalsample);
indentforce=force(1);
%determine the separation point and the rupture force
tvrupture=zeros(size(force1));
samplingpt=(1:size(force1));
tvcutoff=tvrcf*ones(size(force1));
sepcutoffm=sepcutoff*ones(size(force1));
sepcutoffy=(-300:1:300);
sepcutoffx=sepcutoff*ones(size(sepcutoffy));
forcecutoffm=-forcecutoff*ones(size(force1));
for j=itvr:samplenumber-itvr
    xtl=force1(j-itvr+1:j);
    xtr=force1(j+1:j+itvr);
    meanxtl=mean(xtl);
    meanxtr=mean(xtr);
    covxtl=cov(xtl);
    covxtr=cov(xtr);
    tvrupture(j)=-(meanxtl-meanxtr)/sqrt((covxtl+covxtr)/itvr); % calculate t-value
end
tcount=0;
unclerupture=0;
isepdiff=0;
for j=itvr:samplenumber-itvr
    tvl=tvrupture(j)-tvrupture(j-1);
    tvr=tvrupture(j+1)-tvrupture(j);
    if tvl>0&tvr<0
    if tvrupture(j)>=tvrcf
        tcount=tcount+1;
%          for k=j:-1:j-10
%              tvml=force1(k)-force1(k-1);
%              tvmr=force1(k+1)-force1(k);
%              if tvml<0&tvmr>0
                for k=j-1:-1:j-5
                    forcediffp(k)=abs(force1(k)-force1(k-1));
                end
                forcediffpavg=0.5*mean(forcediffp);
                forcediff=force1(j)-force1(j-1);
                if forcediff>forcediffpavg
```

```
                    indexrupture(tcount)=j-1;
                else
                    indexrupture(tcount)=j;
                end
                septcount=sep(indexrupture(tcount));
%                 break
%             end
%         end
        for l=j-2:-1:50
                if tvrupture(l)>tvrcfs&tvrupture(l+1)<tvrcfs
                        indexzerorup(tcount)=l+5;
                        sepdiffs=sep(indexrupture(tcount))-
sep(indexzerorup(tcount));
                        if sepdiffs<sepwlccutoff
                            isepdiff=1;
                        end
                    for ll=j-2:-1:l
                        if tvrupture(ll)<=iunclerupture
                            unclerupture=1;
                            break
                        end
                    end
                    minforce1=min(force1(l:indexrupture(tcount)))
                    minforce1dif=force1(indexrupture(tcount))-minforce1;
                    if minforce1dif>forcecutoff
                        unclerupture=1;
                    end
                    for ll=j-2:-1:l
                        if tvrupture(ll)<0&tvrupture(ll+1)>0
                            tvzero=ll;
                            break
                        end
                    end
                    for ll=j-2:-1:tvzero
                            tvl=tvrupture(ll)-tvrupture(ll-1);
                            tvr=tvrupture(ll+1)-tvrupture(ll);
                            if tvl>0&tvr<0
                            if tvrupture(ll)>=0
                                unclerupture=1;
                                break
                            end
                            end
                    end
                    break
                else
                        indexzerorup(tcount)=50;
                minforce1=min(force1(indexzerorup(tcount):indexrupture(tcount)))
                        minforce1dif=force1(indexrupture(tcount))-minforce1;
                        if minforce1dif>forcecutoff
                            unclerupture=1;
                        end

                                    140
```

```matlab
                    end
                end
                indexfitexp(tcount)=j-ifitexp;
        end
        end
end
%Print the data to the file
subplot(2,2,1);
plot(displace1,force1,'r-',displace1,force2,'b-');
grid on;
axis([0 250 -300 50]);
xlabel('Displacement[nm]');
ylabel('Force[pN]');
title({['File name=',num2str(filenameinput)];['Dataset=',num2str(i)];['Indent
Force=',num2str(indentforce)]});
subplot(2,2,3);
plot(displace1,tvrupture,'r-',displace1,tvcutoff,'g--');
grid on;
axis([0 250 -20 20]);
xlabel('Displacement[nm]');
ylabel('t-value');
title({['Dataset=',num2str(i)];['t-test to find the rupture force']});
% Plot the force and separation
subplot(2,2,4);
plot(sep1,force1,'r-',sep1,force2,'b-',sepcutoffx,sepcutoffy,'g--',sep1,forcecutoffm,'g-.');
grid on;
axis([-10 250 -300 50]);
xlabel('Separation[nm]');
ylabel('Force[pN]');
if tcount==0
    nonb=nonb+1;
    title({['Dataset=',num2str(i)];['No Binding']});
    pause(1)
elseif tcount>=1
    count=tcount;
    for jjj=count:1
    irt=indexrupture(jjj);
    if tcount>=2
        irtp=indexrupture(tcount-1);
    end
        irtz=indexfitexp(jjj);
        irtc=indexzerorup(jjj);
        finalrup=force(irt);
        finalsep=sep(irt);
        finalrupture=abs(finalrup);
clear   tvx diffrup tvn noise;
    % data quality test
if septcount<sepcutoff
    nonsb=nonsb+1;
    title({['Dataset=',num2str(i)];['Non-Specific Binding (Separation is less than cut-
off)']});
```

```
        pause(1)
        break
    end
    mfavgsta=indexrupture(count)+10;
    mfavgend=indexrupture(count)+30;
    if mfavgsta>samplenumber
        mfavgsta=samplenumber;
    end
    if mfavgend>samplenumber
        mfavgend=samplenumber;
    end
    forceavg=abs(mean(force1(mfavgsta:mfavgend)));
    if forceavg>wdforcediff
        nowd=nowd+1;
        title({['Dataset=',num2str(i)];['Wrong dataset (Irregular data points)']});
        pause(1)
        break
    end
    if finalrupture<forcecutoff
        nonsb=nonsb+1;
        title({['Dataset=',num2str(i)];['Non-Specific Binding (Rupture force is less than cut-
off)']});
        pause(1)
        break
    end
    sepdiff=sep(irt)-sep(irtc);
    if sepdiff<sepwlccutoff
        isepdiff=1;
    end
    if isepdiff==1
        nonsb=nonsb+1;
        title({['Dataset=',num2str(i)];['Non-Specific Binding (Short distance for WLC model
curve fitting)']});
        replyrup=menu('Dataset Quality','Next','Quit');
        if replyrup==2
            iquit=1;
        end
        break
    end
    if tcount>nomaxrup
        nonsb=nonsb+1;
        title({['Dataset=',num2str(i)];['Non-Specific Binding (Too many rupture event)']});
        pause(1)
        break
    end
    if count>=2
    sepdiffbr=sep(irt)-sep(irtp);
    if sepdiffbr<sepwlccutoff
        nonsb=nonsb+1;
        title({['Dataset=',num2str(i)];['Non-Specific Binding (Two peaks are too close)']});
        pause(1)
```

```matlab
            break
    end
end
if unclerupture==1
    nonsb=nonsb+1;
    title({['Dataset=',num2str(i)];['Non-Specific Binding (Unclear Rupture Point)']});
    replyrup=menu('Dataset Quality','Next','Quit');
    if replyrup==2
        iquit=1;
    end
    break
end
%----------
                            lrx=[displace1(irtz:irt)]';
                            lry=force1(irtz:irt);
                            [coef model]= fitexp(lrx,lry);
                            sepint=1/coef(2)*log(1-finalrup/coef(1));
                            slpexp=-coef(2)*coef(1).*exp(coef(2)*sepint);
                            intercept=finalrup-slpexp*sepint;
                            lrxi=[displace1(irt-10:irt+10)]';
                            lryi=slpexp*lrxi+intercept;
                            lrxci=[displace1(irtz:irt+10)]';
                            lryci=coef(1).*(1- exp(coef(2).* lrxci));
    sysspringcon=-slpexp;
    loadrate=sysspringcon*reversevel;
    finalloadrate=loadrate;
subplot(2,2,1);
plot(displace1,force1,'r-',displace1,force2,'b-',lrxci,lryci,'b-',lrxi,lryi,'g-');
grid on;
axis([0 250 -300 50]);
xlabel('Displacement[nm]');
ylabel('Force[pN]');
title({['File name=',num2str(filenameinput)];['Dataset=',num2str(i)];['Indent
Force=',num2str(indentforce)];['System Spring
Constant=',num2str(sysspringcon)];['Loading rate=',num2str(loadrate)]});
%--------
    boltzmann=1.3806503*10^(-23);
    temp=295;     %K
    persistence=0.38*10^(-9);     %m
    wlcx=displace1;
    a2=-0.5164228;
    a3=-2.737418;
    a4=16.07497;
    a5=-38.87607;
    a6=39.49944;
    a7=-14.17718;
%Fixed contour in WLC model
    contourfix=30;
    sepmov=0;
    indexsepmov=0;
    for ij=1:samplenumber
```

```matlab
            nondimenxi=wlcx(ij)/contourfix;
            if nondimenxi<1
                wlcfxfix(ij)=-(boltzmann*temp/persistence)*(0.25/(1-nondimenxi)^2-
0.25+nondimenxi+a2*nondimenxi^2+a3*nondimenxi^3+a4*nondimenxi^4+a5*nondimen
xi^5+a6*nondimenxi^6+a7*nondimenxi^7)*10^12;    %pN
                %wlcfxfix(ij)=-(boltzmann*temp/persistence)*(0.25/(1-nondimenxi)^2-
0.25+nondimenxi)*10^12;    %pN
                if ij>2
                    if wlcfxfix(ij)<finalrup&wlcfxfix(ij-1)>finalrup
                        sepmov=nondimenxi*contourfix-finalsep;
                        indexsepmov=ij;
                    end
                end
            else
                wlcfxfix(ij)=0;
            end
      end
    wlcxifix=wlcx-sepmov;
    wlcxifixmod=wlcxifix(1:indexsepmov+10);
    wlcfxfixmod=wlcfxfix(1:indexsepmov+10);
    contourfix2=250;
    sepmov2=0;
    indexsepmov2=0;
    for ij=1:samplenumber
        nondimenxi=wlcx(ij)/contourfix2;
        if nondimenxi<1
            wlcfxfix2(ij)=-(boltzmann*temp/persistence)*(0.25/(1-nondimenxi)^2-
0.25+nondimenxi+a2*nondimenxi^2+a3*nondimenxi^3+a4*nondimenxi^4+a5*nondimen
xi^5+a6*nondimenxi^6+a7*nondimenxi^7)*10^12;    %pN
            %wlcfxfix2(ij)=-(boltzmann*temp/persistence)*(0.25/(1-nondimenxi)^2-
0.25+nondimenxi)*10^12;    %pN
            if ij>2
                if wlcfxfix2(ij)<finalrup&wlcfxfix2(ij-1)>finalrup
                    sepmov2=nondimenxi*contourfix2-finalsep;
                    indexsepmov2=ij;
                end
            end
        else
            wlcfxfix2(ij)=0;
        end
      end
    wlcxifix2=wlcx-sepmov2;
    wlcxifixmod2=wlcxifix2(1:indexsepmov2+10);
    wlcfxfixmod2=wlcfxfix2(1:indexsepmov2+10);
%     meanirtc=mean(force1(irtc-20:irtc);
%     if meanirtc>-5
    xwlcfit=sep(irtc:irt);
    ywlcfit=force(irtc:irt);
    [wlcfit wlcfitmodel]=wlcmodelcurvefit(xwlcfit,ywlcfit);
    contour=wlcfit(1);
    wlcinterc=wlcfit(2);
```

```
        mwlc=0.25*ones(size(xwlcfit));
        ywlcfitpost=wlcinterc-(boltzmann*temp/persistence)*(mwlc./((1-(xwlcfit/contour)).^2)-
0.25+(xwlcfit/contour))*10^12;
        irtn=irt-irtc+1;
        for ij=1:irtn
            irti=ij+irtc-1;
            nondimenxi=xwlcfit(ij)/contour;
            tvwlcfit(ij)=wlcinterc-(boltzmann*temp/persistence)*(0.25/(1-nondimenxi)^2-
0.25+nondimenxi+a2*nondimenxi^2+a3*nondimenxi^3+a4*nondimenxi^4+a5*nondimen
xi^5+a6*nondimenxi^6+a7*nondimenxi^7)*10^12;    %pN
            %tvwlcfxfix(irti)=-(boltzmann*temp/persistence)*(0.25/(1-nondimenxi)^2-
0.25+nondimenxi)*10^12;    %pN
            diffrup(ij)=force1(irti)-tvwlcfit(ij);
            tvx(ij)=xwlcfit(ij);
            tvn(ij)=sep1(samplenumber-irtn+ij);
            noise(ij)=force1(samplenumber-irtn+ij);
        end
subplot(2,2,2);
plot(tvx,diffrup,'r-',tvn,noise,'b-');
grid on;
axis([-10 250 -50 50]);
xlabel('Separation[nm]');
ylabel('Force Difference[pN]');
        stddiffrup=0;
        for ij=1:irtn
            stddiffrup=stddiffrup+diffrup(ij)*diffrup(ij);
        end
        stddiffrup=sqrt(stddiffrup/irtn);
        nowlc=irt-irtc+1;
        if nowlc<2
            nowlc=1;
        end
        stderror=stddiffrup/sqrt(nowlc);
%      [h,significance,ci,stats] =ttest2(noise,diffrup,0.01);
%title({['t-test to verify the PEG stretching'];['Estimated
Contour=',num2str(contour)];['Interception=',num2str(wlcinterc)];['Standard Error of
Contour=',num2str(stderror)];['h=',num2str(h)];['p-value=',num2str(significance)];['99%
Confidence Level=',num2str(ci)]});
title({['Dataset=',num2str(i)];['t-test to verify the PEG stretching'];['Estimated
Contour=',num2str(contour)];['Interception=',num2str(wlcinterc)];['Standard Error of
Contour=',num2str(stderror)]});
%----------
subplot(2,2,4);
plot(sep1,force1,'r-',sep1,force2,'b-',wlcxifixmod,wlcfxfixmod,'b-
',wlcxifixmod2,wlcfxfixmod2,'m-',xwlcfit,ywlcfitpost,'k--',sepcutoffx,sepcutoffy,'g--
',sep1,forcecutoffm,'g-.');
grid on;
axis([-10 250 -300 50]);
xlabel('Separation[nm]');
ylabel('Force[pN]');
if stderror>stddiffrupstancutoff
```

```
            nonsb=nonsb+1;
        title({['Dataset=',num2str(i)];['Non-Specific Binding (Not match with WLC model:
large Standard Error)']});
        replyrup=menu('Dataset Quality','Next','Quit');
        if replyrup==2
            iquit=1;
        end
        break
end
if wlcinterc<wlcintercutoff
        nonsb=nonsb+1;
        title({['Dataset=',num2str(i)];['Non-Specific Binding (Interception is minus for WLC
model fitting)']});
            replyrup=menu('Dataset Quality','Next','Quit');
        if replyrup==2
            iquit=1;
        end
        break
end
        text(finalsep,finalrup,'\uparrow');
        if or(contour>contourhigh,contour<contourlow)
        title({['Dataset=',num2str(i)];['Non-Specific Binding(Too low or high contour
length)'];['Separation=',num2str(finalsep)];['Rupture=',num2str(finalrupture)]});
        replyrup=menu('Dataset Quality', 'Choose','No Binding','Non-Specfific','Wrong
dataset','Quit');
        if replyrup==1
            frup = fopen('rupture.doc','a');
            fprintf(frup,'%10s %5i %8.1f %8.1f %8.1f
%8.1f\n',filenameinput,i,finalsep,finalrupture,sysspringcon,finalloadrate);
            fclose(frup);
        end
     if replyrup==2
            nonb=nonb+1;
        end
        if replyrup==3
            nonsb=nonsb+1;
        end
        if replyrup==4
            nowd=nowd+1;
        end
        if replyrup==5
            iquit=1;
        end
        break
        else
        title({['Dataset=',num2str(i)];['Specific
Binding'];['Separation=',num2str(finalsep)];['Rupture=',num2str(finalrupture)]});
        frup = fopen('rupture.doc','a');
        fprintf(frup,'%10s %5i %8.1f %8.1f %8.1f
%8.1f\n',filenameinput,i,finalsep,finalrupture,sysspringcon,finalloadrate);
        fclose(frup);
```

```
        replyrup=menu('Dataset Quality','Next','Quit');
        if replyrup==2
            iquit=1;
        end
        break
        end %contour
        end    %for jjj=count:1
end      %if tcount
end
nospec=scansize-(nonb+nonsb+nowd);
total=nospec+nonb+nonsb+nowd
nonbp=100*nonb/scansize;
nonsbp=100*nonsb/scansize;
nowdp=100*nowd/scansize;
nospecp=100*nospec/scansize;
frup = fopen('number.doc','a');
fprintf(frup,'%10s %8.1f %8.1f %8.1f %8.1f %8.1f
%8.1f\n',filenameinput,nonb,nonsb,nowd,nospec,total,scansize);
fprintf(frup,'%10s %8.1f %8.1f %8.1f
%8.1f\n',filenameinput,nonbp,nonsbp,nowdp,nospecp);
fclose(frup);
```

2. Kinetic information of Notch-Notch ligand binding

A. Kinetics of Notch-Notch ligand binding

Notch ligand	mNotch1	ka1 (x10⁴/M/s)	kd1 (x0.01/s)	ka2 (x0.001/s)	kd2 (x0.001/s)	K (x10⁶M)	Norm. Rmax
Dll-1	N1-fuc	42.3±12.53	7.84±0.27	8.2±1.09	2.8±0.56	21.97±9.62	1±0.08
	N1+fuc	28.17±1.71	8.12±1.11	8.18±1.05	2.98±0.70	14.33±5.59	1.90±0.22
	N1+fuc+Lfng	50.8±9.32	7.72±0.27	4.27±0.16	1.04±0.13	36.52±9.41	14.61±3.28
Dll-4	N1-fuc	7.99±0.27	5.26±0.29	11.78±1.58	1.18±0.05	15.97±3.53	7.54±0.81
	N1+fuc	8.85±0.19	4.94±0.16	7.76±0.78	0.93±0.09	16.03±3.54	13.89±1.93
	N1+fuc+Lfng	13.23±0.46	0.80±0.04	2.90±0.49	2.96±0.84	35.7±3.72	16.78±2.51
Jag-1	N1-fuc	5.87±2.90	6.44±1.63	14.5±2.06	2.61±0.52	4.90±0.60	1.36±0.25
	N1+fuc	7.83±4.26	11.3±3.42	14.93±2.83	2.70±0.41	3.5±0.37	3.01±0.45
	N1+fuc+Lfng	12.16±2.54	14.67±1.87	9.26±0.66	3.01±0.25	3.26±0.63	6.39±2.34
Jag-2	N1-fuc	3.93±0.76	3.62±0.72	3.86±0.54	5.15±0.79	2.40±0.80	1.39±0.12
	N1+fuc	4.02±1.32	4.97±0.16	4.04±0.44	6.78±0.74	1.39±0.54	3.24±0.93
	N1+fuc+Lfng	3.16±0.10	7.63±1.05	4.96±0.82	9.62±2.19	0.65±0.08	7.35±1.21

B. Kinetic of Dll-4 binding to Notch mutants

Mutation	mNotch1	ka1 (x10⁴/M/s)	kd1 (x0.01/s)	ka2 (x0.001/s)	kd2 (x0.001/s)	K (x10⁶M)	Norm. Rmax
WT	N1-fuc	7.99±0.27	5.26±0.29	11.78±1.58	1.18±0.05	15.97±3.53	1±0.11
	N1+fuc	8.85±0.19	4.94±0.16	7.76±0.78	0.93±0.09	16.03±3.54	1.84±0.26
	N1+fuc+Lfng	13.23±0.46	0.80±0.04	2.90±0.49	2.96±0.84	35.7±3.72	2.23±0.33
EGF12	N1-fuc	1.64±0.18	1.82±0.30	15.56±3.96	3.65±0.65	4.73±0.08	0.87±0.13
	N1+fuc	2.31±0.19	4.14±1.09	19.13±3.78	2.16±0.05	5.66±0.17	1.53±0.12
	N1+fuc+Lfng	4.89±0.79	5.36±0.67	9.57±0.05	0.90±0.25	12.61±3.75	1.94±0.54
EGF24	N1-fuc	5.44±0.47	3.79±0.34	12.02±2.48	1.31±0.25	12.67±0.69	1.52±0.29
	N1+fuc	5.23±0.25	3.04±0.21	9.31±1.95	1.43±0.15	12.67±1.44	2.01±0.31
	N1+fuc+Lfng	9.68±1.67	0.84±0.18	4.28±0.88	2.31±0.25	36.53±11.14	3.05±0.15
EGF26	N1-fuc	3.78±1.10	3.72±0.60	10.36±1.60	0.91±0.11	11.9±0.96	2.38±0.07
	N1+fuc	3.60±1.11	2.70±0.40	7.40±1.22	0.81±0.02	12.4±0.62	2.90±0.12
	N1+fuc+Lfng	9.01±0.62	0.87±0.14	4.44±0.94	1.50±0.41	44.63±5.79	2.83±0.19
EGF27	N1-fuc	4.38±0.41	2.89±0.42	9.64±1.51	1.45±0.38	12.73±1.64	1.13±0.47
	N1+fuc	4.44±0.44	2.45±0.34	8.74±2.11	1.48±0.31	12.07±0.45	1.48±0.62
	N1+fuc+Lfng	10.68±2.04	1.20±0.31	7.89±3.22	2.4±0.39	38.67±9.18	2.73±0.17

C. Kinetics of Dll-4 binding to Notch1(EGF1-15)

Notch ligand	mNotch1	ka1 (x10⁴/M/s)	kd1 (x0.01/s)	ka2 (x0.001/s)	kd2 (x0.001/s)	K (x10⁶M)	Norm. Rmax
Dll-4	N1(15)-fuc	7.22±0.16	2.51±0.14	12.23±0.23	1.37±0.02	28.6±0.53	1±0.06
	N1(15)+fuc	3.51±0.06	2.69±0.36	11.42±2.29	1.37±0.15	12.64±2.61	1.18±0.12
	N1(15)+fuc+Lfng	5.41±0.16	2.20±0.28	10.57±2.05	1.61±0.02	18.47±1.41	1.05±0.08

D. Kinetics of Dll-4 binding to Notch1 with various glycosylation conditions

mNotch1	Notch ligand	ka1 (x10⁴/M/s)	kd1 (x0.01/s)	ka2 (x0.001/s)	kd2 (x0.001/s)	K (x10⁶M)	Norm. Rmax
N1-fuc	D4-fuc	1.37±0.02	4.06±0.16	8.65±0.58	1.49±0.17	2.35±0.19	1±0.17
	D4+fuc	7.02±0.53	3.54±0.30	19.00±1.75	2.05±0.08	20.4±1.61	1.37±0.17
	D4+fuc+Lfng	10.48±0.76	1.62±0.27	13.60±1.45	1.87±0.05	55.17±6.85	1.76±0.24
N1+fuc	D4-fuc	1.32±0.08	3.87±0.36	6.58±0.31	1.39±0.11	2.00±0.18	2.35±0.19
	D4+fuc	9.08±0.21	4.26±0.19	15.95±0.40	1.46±0.08	25.6±0.80	2.71±0.15
	D4+fuc+Lfng	10.25±0.20	1.62±0.26	17.18±2.07	1.72±0.11	74.23±6.06	3.31±0.25
N1+fuc+Lfng	D4-fuc	2.60±0.09	1.24±0.10	5.92±0.60	4.16±0.16	5.11±0.28	3.96±0.24
	D4+fuc	12.88±0.28	1.19±0.16	7.19±0.78	1.98±0.13	51.45±3.07	4.02±0.19
	D4+fuc+Lfng	17.33±0.37	1.57±0.06	13.73±0.88	1.13±0.04	146.33±4.84	4.65±0.11

3. Relaxation rates of two-state binding model

This calculation for relaxation rates of two-state binding model was adopted from Weikl and Deuster [171]. The association and dissociation of two-state model (N+L⇔NL⇔NL*) have general reaction process of the following form

$$A \Leftrightarrow B \rightarrow C \tag{1}$$

For association process, state A corresponds to N, state B to NL, and state C to NL^*. For dissociation process, state A corresponds to NL^*, state B to NL, and state C to N. We are interested in the dominant, slowest relaxation rate into state C. therefore, the state C is an "absorbing" state, i.e. the rate from C back to B is 0. The probability evolution $P_A(t)$, $P_B(t)$, and $P_C(t)$ of the three states is then governed by the set of differential equations

$$\frac{dP_A(t)}{dt} = k_{AB}P_B(t) - k_{BA}P_A(t) \tag{2}$$

$$\frac{dP_B(t)}{dt} = k_{BA}P_A(t) - (k_{AB} + k_{CB})P_B(t) \tag{3}$$

$$\frac{dP_C(t)}{dt} = k_{CB}P_B(t) \tag{4}$$

where k_{ij} denotes the rate from state j to state i. The three equations can be written in the matrix form

$$\frac{d\mathbf{P}(t)}{dt} = -\mathbf{W}\mathbf{P}(t) \tag{5}$$

with $P(t)=(P_A(t), P_B(t), and P_C(t))$ and

$$\mathbf{W} = \begin{pmatrix} k_{BA} & -k_{AB} & 0 \\ -k_{BA} & k_{AB} + k_{CB} & 0 \\ 0 & -k_{CB} & 0 \end{pmatrix} \tag{6}$$

The general solution of (5) has the form

$$\boldsymbol{P}(t) = c_0\boldsymbol{Y}_0 + c_1\boldsymbol{Y}_1 e^{-\lambda_1 t} + c_2\boldsymbol{Y}_1 e^{-\lambda_2 t} \tag{7}$$

where $\boldsymbol{Y}_0$, $\boldsymbol{Y}_1$, and $\boldsymbol{Y}_2$ are the three eigenvectors of the matrix $\boldsymbol{W}$, and λ_1 and λ_2 are the two positive eigenvalues of the eigenvectors $\boldsymbol{Y}_1$, and $\boldsymbol{Y}_2$. The coefficients c_0, c_1, and c_2 depend on the initial conditions at time $t=0$. The eigenvalue of the eigenvector $\boldsymbol{Y}_0$ is 0, which ensures that $\boldsymbol{P}(t)$ relaxes towards a finite equilibrium probability distribution $\boldsymbol{P}(t\to\infty)=c_0\boldsymbol{Y}_0$ for $t\to\infty$. The two nonzero eigenvalues are

$$\lambda_{1/2} = \frac{1}{2}\left(k_{AB} + K_{BA} + k_{CB} \pm \sqrt{k_{AB}^2 + \left(k_{BA} - k_{CB}\right)^2 + 2k_{AB}\left(k_{BA} + k_{CB}\right)}\right) \tag{8}$$

These eigenvalues, and their eigenvectors $\boldsymbol{Y}_1$ and $\boldsymbol{Y}_2$, capture the time-dependent relaxation process into equilibrium.

Bibliography

1.   Varki, A., et al., *Essentials of glycobiology*. 2nd ed. 2008: Cold Spring Harbor Laboratory Press.

2.   Alberts, B., et al., *Molecular biology of the cell*. Fitth edition ed. 2008: Garland Sciences.

3.   Lowe, J.B. and J.D. Marth, *A genetic approach to Mammalian glycan function.* Annu Rev Biochem, 2003. **72**: p. 643-91.

4.   Becker, D.J. and J.B. Lowe, *Leukocyte adhesion deficiency type II.* Biochim Biophys Acta, 1999. **1455**(2-3): p. 193-204.

5.   Korner, C., et al., *Carbohydrate deficient glycoprotein syndrome type IV: deficiency of dolichyl-P-Man:Man(5)GlcNAc(2)-PP-dolichyl mannosyltransferase.* Embo J, 1999. **18**(23): p. 6816-22.

6.   Wraith, J.E., et al., *Mucopolysaccharidosis type II (Hunter syndrome): a clinical review and recommendations for treatment in the era of enzyme replacement therapy.* Eur J Pediatr, 2008. **167**(3): p. 267-77.

7.   Denecke, J., et al., *Characterization of the N-glycosylation phenotype of erythrocyte membrane proteins in congenital dyserythropoietic anemia type II (CDA II/HEMPAS).* Glycoconj J, 2008. **25**(4): p. 375-82.

8.   Denecke, J. and T. Marquardt, *Congenital dyserythropoietic anemia type II (CDAII/HEMPAS): Where are we now?* Biochim Biophys Acta, 2008.

9.   Fridovich-Keil, J.L., *Galactosemia: the good, the bad, and the unknown.* J Cell Physiol, 2006. **209**(3): p. 701-5.

10.   Fuster, M.M. and J.D. Esko, *The sweet and sour of cancer: glycans as novel therapeutic targets.* Nat Rev Cancer, 2005. **5**(7): p. 526-42.

11.   Zaia, J., *Mass spectrometry and the emerging field of glycomics.* Chem Biol, 2008. **15**(9): p. 881-92.

12.   Park, S., M.R. Lee, and I. Shin, *Chemical tools for functional studies of glycans.* Chem Soc Rev, 2008. **37**(8): p. 1579-91.

13.   Liang, P.H., et al., *Glycan arrays: biological and medical applications.* Curr Opin Chem Biol, 2008. **12**(1): p. 86-92.

14.   von Itzstein, M., *The war against influenza: discovery and development of sialidase inhibitors.* Nat Rev Drug Discov, 2007. **6**(12): p. 967-74.

15.   Galonic, D.P. and D.Y. Gin, *Chemical glycosylation in the synthesis of glycoconjugate antitumour vaccines.* Nature, 2007. **446**(7139): p. 1000-7.

16.   Larsen, R.D., et al., *Molecular cloning, sequence, and expression of a human GDP-L-fucose:beta-D-galactoside 2-alpha-L-fucosyltransferase cDNA that can form the H blood group antigen.* Proc Natl Acad Sci U S A, 1990. **87**(17): p. 6674-8.

17.   Kelly, R.J., et al., *Sequence and expression of a candidate for the human Secretor blood group alpha(1,2)fucosyltransferase gene (FUT2). Homozygosity for an enzyme-inactivating nonsense mutation commonly correlates with the non-secretor phenotype.* J Biol Chem, 1995. **270**(9): p. 4640-9.

18.   Kaneko, M., et al., *Alpha1,3-fucosyltransferase IX (Fuc-TIX) is very highly conserved between human and mouse; molecular cloning, characterization and tissue distribution of human Fuc-TIX.* FEBS Lett, 1999. **452**(3): p. 237-42.

19.   Miyoshi, E., et al., *The alpha1-6-fucosyltransferase gene and its biological significance.* Biochim Biophys Acta, 1999. **1473**(1): p. 9-20.

20.   Panin, V.M., et al., *Notch ligands are substrates for protein O-fucosyltransferase-1 and Fringe.* J Biol Chem, 2002. **277**(33): p. 29945-52.

21.   Moloney, D.J., et al., *Fringe is a glycosyltransferase that modifies Notch.* Nature, 2000. **406**(6794): p. 369-75.

22.   Shao, L. and R.S. Haltiwanger, *O-fucose modifications of epidermal growth factor-like repeats and thrombospondin type 1 repeats: unusual modifications in unusual places.* Cell Mol Life Sci, 2003. **60**(2): p. 241-50.

23.   Luo, Y. and R.S. Haltiwanger, *O-fucosylation of notch occurs in the endoplasmic reticulum.* J Biol Chem, 2005. **280**(12): p. 11289-94.

24.   Roos, C., et al., *Composition of Drosophila melanogaster proteome involved in fucosylated glycan metabolism.* J Biol Chem, 2002. **277**(5): p. 3168-75.

25.   Becker, D.J. and J.B. Lowe, *Fucose: biosynthesis and biological function in mammals.* Glycobiology, 2003. **13**(7): p. 41R-53R.

26.   Tonetti, M., et al., *The metabolism of 6-deoxyhexoses in bacterial and animal cells.* Biochimie, 1998. **80**(11): p. 923-31.

27.   Somoza, J.R., et al., *Structural and kinetic analysis of Escherichia coli GDP-mannose 4,6 dehydratase provides insights into the enzyme's catalytic mechanism and regulation by GDP-fucose.* Structure, 2000. **8**(2): p. 123-35.

28.   Ohyama, C., et al., *Molecular cloning and expression of GDP-D-mannose-4,6-dehydratase, a key enzyme for fucose metabolism defective in Lec13 cells.* J Biol Chem, 1998. **273**(23): p. 14582-7.

29.   Tonetti, M., et al., *Synthesis of GDP-L-fucose by the human FX protein.* J Biol Chem, 1996. **271**(44): p. 27274-9.

30.   Smith, P.L., et al., *Conditional control of selectin ligand expression and global fucosylation events in mice with a targeted mutation at the FX locus.* J Cell Biol, 2002. **158**(4): p. 801-15.

31.   Listinsky, J.J., G.P. Siegal, and C.M. Listinsky, *Alpha-L-fucose: a potentially critical molecule in pathologic processes including neoplasia.* Am J Clin Pathol, 1998. **110**(4): p. 425-40.

32.   Staudacher, E., et al., *Fucose in N-glycans: from plant to man.* Biochim Biophys Acta, 1999. **1473**(1): p. 216-36.

33.   Lowe, J.B., *The blood group-specific human glycosyltransferases.* Baillieres Clin Haematol, 1993. **6**(2): p. 465-92.

34.   Hooper, L.V. and J.I. Gordon, *Glycans as legislators of host-microbial interactions: spanning the spectrum from symbiosis to pathogenicity.* Glycobiology, 2001. **11**(2): p. 1R-10R.

35.   Moran, A.P., et al., *Phenotypic variation in molecular mimicry between Helicobacter pylori lipopolysaccharides and human gastric epithelial cell surface glycoforms. Acid-induced phase variation in Lewis(x) and Lewis(y) expression by H. Pylori lipopolysaccharides.* J Biol Chem, 2002. **277**(8): p. 5785-95.

36.   Springer, T.A., *Traffic signals for lymphocyte recirculation and leukocyte emigration: the multistep paradigm.* Cell, 1994. **76**(2): p. 301-14.

37.   Lowe, J.B., *Glycosylation in the control of selectin counter-receptor structure and function.* Immunol Rev, 2002. **186**: p. 19-36.

38.   Smith, P.L., et al., *Expression of the alpha(1,3)fucosyltransferase Fuc-TVII in lymphoid aggregate high endothelial venules correlates with expression of L-selectin ligands.* J Biol Chem, 1996. **271**(14): p. 8250-9.

39.   Maly, P., et al., *The alpha(1,3)fucosyltransferase Fuc-TVII controls leukocyte trafficking through an essential role in L-, E-, and P-selectin ligand biosynthesis.* Cell, 1996. **86**(4): p. 643-53.

40.   Homeister, J.W., et al., *The alpha(1,3)fucosyltransferases FucT-IV and FucT-VII exert collaborative control over selectin-dependent leukocyte recruitment and lymphocyte homing.* Immunity, 2001. **15**(1): p. 115-26.

41.   Smithson, G., et al., *Fuc-TVII is required for T helper 1 and T cytotoxic 1 lymphocyte selectin ligand expression and recruitment in inflammation, and together with Fuc-TIV regulates naive T cell trafficking to lymph nodes.* J Exp Med, 2001. **194**(5): p. 601-14.

42.   Bruckner, K., et al., *Glycosyltransferase activity of Fringe modulates Notch-Delta interactions.* Nature, 2000. **406**(6794): p. 411-5.

43.   Kozma, K., et al., *Identification and characterization of abeta1,3-glucosyltransferase that synthesizes the Glc-beta1,3-Fuc disaccharide on thrombospondin type 1 repeats.* J Biol Chem, 2006. **281**(48): p. 36742-51.

44.   Shi, S. and P. Stanley, *Protein O-fucosyltransferase 1 is an essential component of Notch signaling pathways.* Proc Natl Acad Sci U S A, 2003. **100**(9): p. 5234-9.

45.   Artavanis-Tsakonas, S., M.D. Rand, and R.J. Lake, *Notch signaling: cell fate control and signal integration in development.* Science, 1999. **284**(5415): p. 770-6.

46.   Radtke, F., et al., *Notch regulation of lymphocyte development and function.* Nat Immunol, 2004. **5**(3): p. 247-53.

47.   Zhou, L., et al., *Notch-dependent control of myelopoiesis is regulated by fucosylation.* Blood, 2008. **112**(2): p. 308-19.

48.   Swiatek, P.J., et al., *Notch1 is essential for postimplantation development in mice.* Genes Dev, 1994. **8**(6): p. 707-19.

49.   Conlon, R.A., A.G. Reaume, and J. Rossant, *Notch1 is required for the coordinate segmentation of somites.* Development, 1995. **121**(5): p. 1533-45.

50.   Radtke, F., et al., *Deficient T cell fate specification in mice with an induced inactivation of Notch1.* Immunity, 1999. **10**(5): p. 547-58.

51.   Rampal, R., K.B. Luther, and R.S. Haltiwanger, *Notch signaling in normal and disease States: possible therapies related to glycosylation.* Curr Mol Med, 2007. **7**(4): p. 427-45.

52.   Ellisen, L.W., et al., *TAN-1, the human homolog of the Drosophila notch gene, is broken by chromosomal translocations in T lymphoblastic neoplasms.* Cell, 1991. **66**(4): p. 649-61.

156

53. Miyamoto, Y., et al., *Effect of erythroid differentiation factor on erythroid differentiation and proliferation of K-562 cells.* Biochem Biophys Res Commun, 1990. **168**(3): p. 1149-56.

54. Robbins, J., et al., *Mouse mammary tumor gene int-3: a member of the notch gene family transforms mammary epithelial cells.* J Virol, 1992. **66**(4): p. 2594-9.

55. Aster, J.C., W.S. Pear, and S.C. Blacklow, *Notch signaling in leukemia.* Annu Rev Pathol, 2008. **3**: p. 587-613.

56. Dufraine, J., Y. Funahashi, and J. Kitajewski, *Notch signaling regulates tumor angiogenesis by diverse mechanisms.* Oncogene, 2008. **27**(38): p. 5132-7.

57. Joutel, A., et al., *Notch3 mutations in CADASIL, a hereditary adult-onset condition causing stroke and dementia.* Nature, 1996. **383**(6602): p. 707-10.

58. Arboleda-Velasquez, J.F., et al., *CADASIL mutations impair Notch3 glycosylation by Fringe.* Hum Mol Genet, 2005. **14**(12): p. 1631-9.

59. John, G.R., et al., *Multiple sclerosis: re-expression of a developmental pathway that restricts oligodendrocyte maturation.* Nat Med, 2002. **8**(10): p. 1115-21.

60. Sparrow, D.B., et al., *Mutation of the LUNATIC FRINGE gene in humans causes spondylocostal dysostosis with a severe vertebral phenotype.* Am J Hum Genet, 2006. **78**(1): p. 28-37.

61. Spinner, N.B., et al., *Jagged1 mutations in alagille syndrome.* Hum Mutat, 2001. **17**(1): p. 18-33.

62. Niessen, K. and A. Karsan, *Notch signaling in cardiac development.* Circ Res, 2008. **102**(10): p. 1169-81.

63. Nam, Y., J.C. Aster, and S.C. Blacklow, *Notch signaling as a therapeutic target.* Curr Opin Chem Biol, 2002. **6**(4): p. 501-9.

64. Villaronga, M.A., C.L. Bevan, and B. Belandia, *Notch signaling: a potential therapeutic target in prostate cancer.* Curr Cancer Drug Targets, 2008. **8**(7): p. 566-80.

65. Parks, A.L., et al., *Structure-function analysis of delta trafficking, receptor binding and signaling in Drosophila.* Genetics, 2006. **174**(4): p. 1947-61.

66. Sturla, L., et al., *Differential terminal fucosylation of N-linked glycans versus protein O-fucosylation in leukocyte adhesion deficiency type II (CDG IIc).* J Biol Chem, 2003. **278**(29): p. 26727-33.

67.   Ishikawa, H.O., et al., *Notch deficiency implicated in the pathogenesis of congenital disorder of glycosylation IIc.* Proc Natl Acad Sci U S A, 2005. **102**(51): p. 18532-7.

68.   Shao, L., D.J. Moloney, and R. Haltiwanger, *Fringe modifies O-fucose on mouse Notch1 at epidermal growth factor-like repeats within the ligand-binding site and the Abruptex region.* J Biol Chem, 2003. **278**(10): p. 7775-82.

69.   Acar, M., et al., *Rumi is a CAP10 domain glycosyltransferase that modifies Notch and is required for Notch signaling.* Cell, 2008. **132**(2): p. 247-58.

70.   Stanley, P., *Glucose: a novel regulator of notch signaling.* ACS Chem Biol, 2008. **3**(4): p. 210-3.

71.   Moloney, D.J., et al., *Mammalian Notch1 is modified with two unusual forms of O-linked glycosylation found on epidermal growth factor-like modules.* J Biol Chem, 2000. **275**(13): p. 9604-11.

72.   Matsuura, A., et al., *O-linked N-acetylglucosamine is present on the extracellular domain of notch receptors.* J Biol Chem, 2008. **283**(51): p. 35486-95.

73.   Stahl, M., et al., *Roles of Pofut1 and O-fucose in mammalian Notch signaling.* J Biol Chem, 2008. **283**(20): p. 13638-51.

74.   Okajima, T., et al., *Chaperone activity of protein O-fucosyltransferase 1 promotes notch receptor folding.* Science, 2005. **307**(5715): p. 1599-603.

75.   Moran, J.L., et al., *Genomic structure, mapping, and expression analysis of the mammalian Lunatic, Manic, and Radical fringe genes.* Mamm Genome, 1999. **10**(6): p. 535-41.

76.   Shimizu, K., et al., *Manic fringe and lunatic fringe modify different sites of the Notch2 extracellular region, resulting in different signaling modulation.* J Biol Chem, 2001. **276**(28): p. 25753-8.

77.   Jinek, M., et al., *Structural insights into the Notch-modifying glycosyltransferase Fringe.* Nat Struct Mol Biol, 2006. **13**(10): p. 945-6.

78.   Tan, J.B., et al., *Lunatic and manic fringe cooperatively enhance marginal zone B cell precursor competition for delta-like 1 in splenic endothelial niches.* Immunity, 2009. **30**(2): p. 254-63.

79.   Chen, J., D.J. Moloney, and P. Stanley, *Fringe modulation of Jagged1-induced Notch signaling requires the action of beta 4galactosyltransferase-1.* Proc Natl Acad Sci U S A, 2001. **98**(24): p. 13716-21.

80.   Wu, J.Y., et al., *The secreted product of Xenopus gene lunatic Fringe, a vertebrate signaling molecule.* Science, 1996. **273**(5273): p. 355-8.

81.   Okajima, T., A. Xu, and K.D. Irvine, *Modulation of notch-ligand binding by protein O-fucosyltransferase 1 and fringe.* J Biol Chem, 2003. **278**(43): p. 42340-5.

82.   Hicks, C., et al., *Fringe differentially modulates Jagged1 and Delta1 signalling through Notch1 and Notch2.* Nat Cell Biol, 2000. **2**(8): p. 515-20.

83.   Jaleco, A.C., et al., *Differential effects of Notch ligands Delta-1 and Jagged-1 in human lymphoid differentiation.* J Exp Med, 2001. **194**(7): p. 991-1002.

84.   Neves, H., et al., *Effects of Delta1 and Jagged1 on early human hematopoiesis: correlation with expression of notch signaling-related genes in CD34+ cells.* Stem Cells, 2006. **24**(5): p. 1328-37.

85.   Lei, L., et al., *An O-fucose site in the ligand binding domain inhibits Notch activation.* Development, 2003. **130**(26): p. 6411-21.

86.   Ge, C. and P. Stanley, *The O-fucose glycan in the ligand-binding domain of Notch1 regulates embryogenesis and T cell development.* Proc Natl Acad Sci U S A, 2008. **105**(5): p. 1539-44.

87.   Rampal, R., et al., *Highly conserved O-fucose sites have distinct effects on Notch1 function.* J Biol Chem, 2005. **280**(37): p. 32133-40.

88.   Parks, A.L., et al., *Ligand endocytosis drives receptor dissociation and activation in the Notch pathway.* Development, 2000. **127**(7): p. 1373-85.

89.   Nichols, J.T., et al., *DSL ligand endocytosis physically dissociates Notch1 heterodimers before activating proteolysis can occur.* J Cell Biol, 2007. **176**(4): p. 445-58.

90.   Seugnet, L., P. Simpson, and M. Haenlin, *Requirement for dynamin during Notch signaling in Drosophila neurogenesis.* Dev Biol, 1997. **192**(2): p. 585-98.

91.   Chitnis, A., *Why is delta endocytosis required for effective activation of notch?* Dev Dyn, 2006. **235**(4): p. 886-94.

92.   Varnum-Finney, B., et al., *Immobilization of Notch ligand, Delta-1, is required for induction of notch signaling.* J Cell Sci, 2000. **113 Pt 23**: p. 4313-8.

93.   Dallas, M.H., et al., *Density of the Notch ligand Delta1 determines generation of B and T cell precursors from hematopoietic stem cells.* J Exp Med, 2005. **201**(9): p. 1361-6.

94.   Fehon, R.G., et al., *Complex cellular and subcellular regulation of notch expression during embryonic and imaginal development of Drosophila: implications for notch function.* J Cell Biol, 1991. **113**(3): p. 657-69.

95.   Demetriou, M., et al., *Negative regulation of T-cell activation and autoimmunity by Mgat5 N-glycosylation.* Nature, 2001. **409**(6821): p. 733-9.

96.   Rudd, P.M., M.R. Wormald, and R.A. Dwek, *Sugar-mediated ligand-receptor interactions in the immune system.* Trends Biotechnol, 2004. **22**(10): p. 524-30.

97.   Parry, S., et al., *Integrated mass spectrometric strategy for characterizing the glycans from glycosphingolipids and glycoproteins: direct identification of sialyl Le(x) in mice.* Glycobiology, 2007. **17**(6): p. 646-54.

98.   Nita-Lazar, A. and R.S. Haltiwanger, *Methods for analysis of O-linked modifications on epidermal growth factor-like and thrombospondin type 1 repeats.* Methods Enzymol, 2006. **417**: p. 93-111.

99.   Xu, A., et al., *In vitro reconstitution of the modulation of Drosophila Notch-ligand binding by Fringe.* J Biol Chem, 2007. **282**(48): p. 35153-62.

100.   Leckband, D., *Force as a probe of membrane protein structure and function.* Curr Opin Struct Biol, 2001. **11**(4): p. 433-9.

101.   Evans, E., *Probing the relation between force--lifetime--and chemistry in single molecular bonds.* Annu Rev Biophys Biomol Struct, 2001. **30**: p. 105-28.

102.   Kellermayer, M.S., et al., *Folding-unfolding transitions in single titin molecules characterized with laser tweezers.* Science, 1997. **276**(5315): p. 1112-6.

103.   Mehta, A.D., et al., *Single-molecule biomechanics with optical methods.* Science, 1999. **283**(5408): p. 1689-95.

104.   Svoboda, K., et al., *Direct observation of kinesin stepping by optical trapping interferometry.* Nature, 1993. **365**(6448): p. 721-7.

105.   Veigel, C., et al., *The motor protein myosin-I produces its working stroke in two steps.* Nature, 1999. **398**(6727): p. 530-3.

106.   Laakso, J.M., et al., *Myosin I can act as a molecular force sensor.* Science, 2008. **321**(5885): p. 133-6.

107.   Brouhard, G.J. and A.J. Hunt, *Microtubule movements on the arms of mitotic chromosomes: polar ejection forces quantified in vitro.* Proc Natl Acad Sci U S A, 2005. **102**(39): p. 13903-8.

108. Cappello, G., et al., *Myosin V stepping mechanism.* Proc Natl Acad Sci U S A, 2007. **104**(39): p. 15328-33.

109. Holland, N.B. and R.E. Marchant, *Individual plasma proteins detected on rough biomaterials by phase imaging AFM.* J Biomed Mater Res, 2000. **51**(3): p. 307-15.

110. Thormann, E., et al., *Ligand-receptor interactions and membrane structure investigated by AFM and time-resolved fluorescence microscopy.* J Mol Recognit, 2007. **20**(6): p. 554-60.

111. Madl, J., et al., *A combined optical and atomic force microscope for live cell investigations.* Ultramicroscopy, 2006. **106**(8-9): p. 645-51.

112. Xu, A., L. Lei, and K.D. Irvine, *Regions of Drosophila Notch that contribute to ligand binding and the modulatory influence of Fringe.* J Biol Chem, 2005. **280**(34): p. 30158-65.

113. Lowe, J.B., *Glycosylation, immunity, and autoimmunity.* Cell, 2001. **104**(6): p. 809-12.

114. Haltiwanger, R.S. and J.B. Lowe, *Role of glycosylation in development.* Annu Rev Biochem, 2004. **73**: p. 491-537.

115. Luther, K.B. and R.S. Haltiwanger, *Role of unusual O-glycans in intercellular signaling.* Int J Biochem Cell Biol, 2009. **41**(5): p. 1011-24.

116. Ripka, J., A. Adamany, and P. Stanley, *Two Chinese hamster ovary glycosylation mutants affected in the conversion of GDP-mannose to GDP-fucose.* Arch Biochem Biophys, 1986. **249**(2): p. 533-45.

117. Ripka, J. and P. Stanley, *Lectin-resistant CHO cells: selection of four new pea lectin-resistant phenotypes.* Somat Cell Mol Genet, 1986. **12**(1): p. 51-62.

118. Becker, D.J., *Genetic and biochemical determinants of fucosylated glycan expression*, in *Ph.D. Thesis*. 2002, The University of Michigan: Ann Arbor, MI.

119. Wang, Y., et al., *Modification of epidermal growth factor-like repeats with O-fucose. Molecular cloning and expression of a novel GDP-fucose protein O-fucosyltransferase.* J Biol Chem, 2001. **276**(43): p. 40338-45.

120. Krebs, L.T., et al., *Notch signaling is essential for vascular morphogenesis in mice.* Genes Dev, 2000. **14**(11): p. 1343-52.

121.	Kumano, K., et al., *Notch1 but not Notch2 is essential for generating hematopoietic stem cells from endothelial cells.* Immunity, 2003. **18**(5): p. 699-711.

122.	Feyerabend, T.B., et al., *Deletion of Notch1 converts pro-T cells to dendritic cells and promotes thymic B cells by cell-extrinsic and cell-intrinsic mechanisms.* Immunity, 2009. **30**(1): p. 67-79.

123.	Parrott, M.B. and M.A. Barry, *Metabolic biotinylation of secreted and cell surface proteins from mammalian cells.* Biochem Biophys Res Commun, 2001. **281**(4): p. 993-1000.

124.	Heinzel, K., et al., *Bone marrow-derived hemopoietic precursors commit to the T cell lineage only after arrival in the thymic microenvironment.* J Immunol, 2007. **178**(2): p. 858-68.

125.	Glittenberg, M., et al., *Role of conserved intracellular motifs in Serrate signalling, cis-inhibition and endocytosis.* Embo J, 2006. **25**(20): p. 4697-706.

126.	Yuan, C., et al., *Energy landscape of streptavidin-biotin complexes measured by atomic force microscopy.* Biochemistry, 2000. **39**(33): p. 10219-23.

127.	Zhang, X., D.F. Bogorin, and V.T. Moy, *Molecular basis of the dynamic strength of the sialyl Lewis X--selectin interaction.* Chemphyschem, 2004. **5**(2): p. 175-82.

128.	Chapman-Smith, A. and J.E. Cronan, Jr., *The enzymatic biotinylation of proteins: a post-translational modification of exceptional specificity.* Trends Biochem Sci, 1999. **24**(9): p. 359-63.

129.	Chapman-Smith, A. and J.E. Cronan, Jr., *In vivo enzymatic protein biotinylation.* Biomol Eng, 1999. **16**(1-4): p. 119-25.

130.	Beckett, D., E. Kovaleva, and P.J. Schatz, *A minimal peptide substrate in biotin holoenzyme synthetase-catalyzed biotinylation.* Protein Sci, 1999. **8**(4): p. 921-9.

131.	Kanda, Y., et al., *Establishment of a GDP-mannose 4,6-dehydratase (GMD) knockout host cell line: a new strategy for generating completely non-fucosylated recombinant therapeutics.* J Biotechnol, 2007. **130**(3): p. 300-10.

132.	Imai-Nishiya, H., et al., *Double knockdown of alpha1,6-fucosyltransferase (FUT8) and GDP-mannose 4,6-dehydratase (GMD) in antibody-producing cells: a new strategy for generating fully non-fucosylated therapeutic antibodies with enhanced ADCC.* BMC Biotechnol, 2007. **7**: p. 84.

133. Neuman, K.C. and A. Nagy, *Single-molecule force spectroscopy: optical tweezers, magnetic tweezers and atomic force microscopy.* Nat Methods, 2008. **5**(6): p. 491-505.

134. Ahimou, F., et al., *The adhesion force of Notch with Delta and the rate of Notch signaling.* J Cell Biol, 2004. **167**(6): p. 1217-29.

135. Gordon, W.R., et al., *Structure of the Notch1 negative regulatory region: Implications for normal activation and pathogenic signaling in T-ALL.* Blood, 2008.

136. Brouhard, G.J., H.T. Schek, 3rd, and A.J. Hunt, *Advanced optical tweezers for the study of cellular and molecular biomechanics.* IEEE Trans Biomed Eng, 2003. **50**(1): p. 121-5.

137. Peterman, E.J., F. Gittes, and C.F. Schmidt, *Laser-induced heating in optical traps.* Biophys J, 2003. **84**(2 Pt 1): p. 1308-16.

138. Schek, H.T., 3rd and A.J. Hunt, *Micropatterned structures for studying the mechanics of biological polymers.* Biomed Microdevices, 2005. **7**(1): p. 41-6.

139. Neuman, K.C. and S.M. Block, *Optical trapping.* Rev Sci Instrum, 2004. **75**(9): p. 2787-809.

140. Binnig, G., C.F. Quate, and C. Gerber, *Atomic Force Microscope.* Physical Review Letters, 1986. **56**(9): p. 930-933.

141. Bustamante, C., C. Rivetti, and D.J. Keller, *Scanning force microscopy under aqueous solutions.* Curr Opin Struct Biol, 1997. **7**(5): p. 709-16.

142. Lee, G.U., L.A. Chrisey, and R.J. Colton, *Direct measurement of the forces between complementary strands of DNA.* Science, 1994. **266**(5186): p. 771-3.

143. Ratto, T.V., et al., *Force spectroscopy of the double-tethered concanavalin-A mannose bond.* Biophys J, 2004. **86**(4): p. 2430-7.

144. Wojcikiewicz, E.P., et al., *Force spectroscopy of LFA-1 and its ligands, ICAM-1 and ICAM-2.* Biomacromolecules, 2006. **7**(11): p. 3188-95.

145. Wong, J., A. Chilkoti, and V.T. Moy, *Direct force measurements of the streptavidin-biotin interaction.* Biomol Eng, 1999. **16**(1-4): p. 45-55.

146. Idiris, A., et al., *Force measurement for antigen-antibody interaction by atomic force microscopy using a photograft-polymer spacer.* Biomacromolecules, 2005. **6**(5): p. 2776-84.

147. Neuert, G., et al., *Dynamic force spectroscopy of the digoxigenin-antibody complex.* FEBS Lett, 2006. **580**(2): p. 505-9.

148. Evans, E. and K. Ritchie, *Strength of a weak bond connecting flexible polymer chains.* Biophys J, 1999. **76**(5): p. 2439-47.

149. Ray, C. and B.B. Akhremitchev, *Conformational heterogeneity of surface-grafted amyloidogenic fragments of alpha-synuclein dimers detected by atomic force microscopy.* J Am Chem Soc, 2005. **127**(42): p. 14739-44.

150. Bouchiat, C., et al., *Estimating the persistence length of a worm-like chain molecule from force-extension measurements.* Biophysical Journal, 1999. **76**(1): p. 409-413.

151. Evans, E. and K. Ritchie, *Dynamic strength of molecular adhesion bonds.* Biophys J, 1997. **72**(4): p. 1541-55.

152. Noguera-Troise, I., et al., *Blockade of Dll4 inhibits tumour growth by promoting non-productive angiogenesis.* Nature, 2006. **444**(7122): p. 1032-7.

153. Ridgway, J., et al., *Inhibition of Dll4 signalling inhibits tumour growth by deregulating angiogenesis.* Nature, 2006. **444**(7122): p. 1083-7.

154. Le Borgne, R., *Regulation of Notch signalling by endocytosis and endosomal sorting.* Curr Opin Cell Biol, 2006. **18**(2): p. 213-22.

155. Okajima, T. and K.D. Irvine, *Regulation of notch signaling by o-linked fucose.* Cell, 2002. **111**(6): p. 893-904.

156. de Celis, J.F. and S.J. Bray, *The Abruptex domain of Notch regulates negative interactions between Notch, its ligands and Fringe.* Development, 2000. **127**(6): p. 1291-302.

157. Brennan, K., et al., *The abruptex mutations of notch disrupt the establishment of proneural clusters in Drosophila.* Dev Biol, 1999. **216**(1): p. 230-42.

158. Cordle, J., et al., *A conserved face of the Jagged/Serrate DSL domain is involved in Notch trans-activation and cis-inhibition.* Nat Struct Mol Biol, 2008. **15**(8): p. 849-57.

159. Geffers, I., et al., *Divergent functions and distinct localization of the Notch ligands DLL1 and DLL3 in vivo.* J Cell Biol, 2007. **178**(3): p. 465-76.

160. Ladi, E., et al., *The divergent DSL ligand Dll3 does not activate Notch signaling but cell autonomously attenuates signaling induced by other DSL ligands.* J Cell Biol, 2005. **170**(6): p. 983-92.

161. Dunwoodie, S.L., et al., *Axial skeletal defects caused by mutation in the spondylocostal dysplasia/pudgy gene Dll3 are associated with disruption of the segmentation clock within the presomitic mesoderm.* Development, 2002. **129**(7): p. 1795-806.

162. Hozumi, K., et al., *Delta-like 4 is indispensable in thymic environment specific for T cell development.* J Exp Med, 2008. **205**(11): p. 2507-13.

163. Koch, U., et al., *Delta-like 4 is the essential, nonredundant ligand for Notch1 during thymic T cell lineage commitment.* J Exp Med, 2008. **205**(11): p. 2515-23.

164. Besseyrias, V., et al., *Hierarchy of Notch-Delta interactions promoting T cell lineage commitment and maturation.* J Exp Med, 2007. **204**(2): p. 331-43.

165. Yang, L.T., et al., *Fringe glycosyltransferases differentially modulate Notch1 proteolysis induced by Delta1 and Jagged1.* Mol Biol Cell, 2005. **16**(2): p. 927-42.

166. Shimizu, K., et al., *Binding of Delta1, Jagged1, and Jagged2 to Notch2 rapidly induces cleavage, nuclear translocation, and hyperphosphorylation of Notch2.* Mol Cell Biol, 2000. **20**(18): p. 6913-22.

167. Hicks, C., et al., *A secreted Delta1-Fc fusion protein functions both as an activator and inhibitor of Notch1 signaling.* J Neurosci Res, 2002. **68**(6): p. 655-67.

168. Sulis, M.L., et al., *NOTCH1 extracellular juxtamembrane expansion mutations in T-ALL.* Blood, 2008. **112**(3): p. 733-40.

169. Malecki, M.J., et al., *Leukemia-associated mutations within the NOTCH1 heterodimerization domain fall into at least two distinct mechanistic classes.* Mol Cell Biol, 2006. **26**(12): p. 4642-51.

170. Kared, H., et al., *Jagged2-expressing hematopoietic progenitors promote regulatory T cell expansion in the periphery through notch signaling.* Immunity, 2006. **25**(5): p. 823-34.

171. Weikl, T.R. and C. von Deuster, *Selected-fit versus induced-fit protein binding: kinetic differences and mutational analysis.* Proteins, 2009. **75**(1): p. 104-10.

172. Man, Y., *Genetic and biochemical determinants of fucosylated glycan expression*, in *Ph.D. Thesis*. 2007, The University of Michigan: Ann Arbor, MI.

173. Hambleton, S., et al., *Structural and functional properties of the human notch-1 ligand binding region.* Structure, 2004. **12**(12): p. 2173-83.

174.   Cordle, J., et al., *Localization of the delta-like-1-binding site in human Notch-1 and its modulation by calcium affinity.* J Biol Chem, 2008. **283**(17): p. 11785-93.

175.   Kao, Y.H., et al., *The effect of O-fucosylation on the first EGF-like domain from human blood coagulation factor VII.* Biochemistry, 1999. **38**(22): p. 7097-110.

176.   Pei, Z. and N.E. Baker, *Competition between Delta and the Abruptex domain of Notch.* BMC Dev Biol, 2008. **8**: p. 4.

177.   Perez, L., et al., *Ligand-binding and signaling properties of the Ax[M1] form of Notch.* Mech Dev, 2005. **122**(4): p. 479-86.

178.   de Celis, J.F. and A. Garcia-Bellido, *Modifications of the notch function by Abruptex mutations in Drosophila melanogaster.* Genetics, 1994. **136**(1): p. 183-94.

179.   Kopan, R. and M.X. Ilagan, *The canonical Notch signaling pathway: unfolding the activation mechanism.* Cell, 2009. **137**(2): p. 216-33.

180.   Komatsu, H., et al., *OSM-11 facilitates LIN-12 Notch signaling during Caenorhabditis elegans vulval development.* PLoS Biol, 2008. **6**(8): p. e196.

181.   Weijzen, S., et al., *Activation of Notch-1 signaling maintains the neoplastic phenotype in human Ras-transformed cells.* Nat Med, 2002. **8**(9): p. 979-86.

182.   Varnum-Finney, B., et al., *Pluripotent, cytokine-dependent, hematopoietic stem cells are immortalized by constitutive Notch1 signaling.* Nat Med, 2000. **6**(11): p. 1278-81.

183.   Pratt, W.B., J.L. Kaine, and D.V. Pratt, *The kinetics of glucocorticoid binding to the soluble specific binding protein of mouse fibroblasts.* J Biol Chem, 1975. **250**(12): p. 4584-91.

184.   Rand, M.D., et al., *Calcium depletion dissociates and activates heterodimeric notch receptors.* Mol Cell Biol, 2000. **20**(5): p. 1825-35.

185.   Engler, A.J., et al., *Matrix elasticity directs stem cell lineage specification.* Cell, 2006. **126**(4): p. 677-89.

186.   Apodaca, G., *Modulation of membrane traffic by mechanical stimuli.* Am J Physiol Renal Physiol, 2002. **282**(2): p. F179-90.

187.   Raucher, D. and M.P. Sheetz, *Membrane expansion increases endocytosis rate during mitosis.* J Cell Biol, 1999. **144**(3): p. 497-506.

188. Galbraith, C.G. and M.P. Sheetz, *A micromachined device provides a new bend on fibroblast traction forces.* Proc Natl Acad Sci U S A, 1997. **94**(17): p. 9114-8.

189. Rabodzey, A., et al., *Mechanical forces induced by the transendothelial migration of human neutrophils.* Biophys J, 2008. **95**(3): p. 1428-38.

190. Munevar, S., Y. Wang, and M. Dembo, *Traction force microscopy of migrating normal and H-ras transformed 3T3 fibroblasts.* Biophys J, 2001. **80**(4): p. 1744-57.

191. Sabass, B., et al., *High resolution traction force microscopy based on experimental and computational advances.* Biophys J, 2008. **94**(1): p. 207-20.

192. Gardel, M.L., et al., *Traction stress in focal adhesions correlates biphasically with actin retrograde flow speed.* J Cell Biol, 2008. **183**(6): p. 999-1005.

193. Krieg, M., et al., *Tensile forces govern germ-layer organization in zebrafish.* Nat Cell Biol, 2008. **10**(4): p. 429-36.

194. Kosztin, I., et al., *Mechanical force generation by G proteins.* Proc Natl Acad Sci U S A, 2002. **99**(6): p. 3575-80.

195. Wu, L.C., et al., *Two-step binding mechanism for T-cell receptor recognition of peptide MHC.* Nature, 2002. **418**(6897): p. 552-6.

196. Choudhuri, K., et al., *Immunology: how do T cells recognize antigen?* Curr Biol, 2005. **15**(10): p. R382-5.

197. Davis, M.M., *A new trigger for T cells.* Cell, 2002. **110**(3): p. 285-7.

198. Minguet, S., et al., *Full activation of the T cell receptor requires both clustering and conformational changes at CD3.* Immunity, 2007. **26**(1): p. 43-54.

199. Gil, D., et al., *Recruitment of Nck by CD3 epsilon reveals a ligand-induced conformational change essential for T cell receptor signaling and synapse formation.* Cell, 2002. **109**(7): p. 901-12.

200. Guentchev, M. and R.D. McKay, *Notch controls proliferation and differentiation of stem cells in a dose-dependent manner.* Eur J Neurosci, 2006. **23**(9): p. 2289-96.

201. Vooijs, M., et al., *Ectodomain shedding and intramembrane cleavage of mammalian Notch proteins is not regulated through oligomerization.* J Biol Chem, 2004. **279**(49): p. 50864-73.

202.   Morgan, W.D., et al., *Solution structure of an EGF module pair from the Plasmodium falciparum merozoite surface protein 1*. J Mol Biol, 1999. **289**(1): p. 113-22.